3-2006

Fretting Fatigue Behavior of Shot-Peened IN 100

Jonathan L. Ng

FRETTING FATIGUE BEHAVIOR OF SHOT-PEENED IN 100

THESIS

Jonathan L. Ng, 2d Lt, USAF

AFIT/GMS/ENY/06-M01

DEPARTMENT OF THE AIR FORCE
AIR UNIVERSITY

AIR FORCE INSTITUTE OF TECHNOLOGY

Wright-Patterson Air Force Base, Ohio

AFIT/GMS/ENY/06-M01

FRETTING FATIGUE BEHAVIOR OF SHOT-PEENED IN 100

THESIS

Presented to the Faculty

Department of Systems and Engineering Management

Graduate School of Engineering and Management

Air Force Institute of Technology

Air University

Air Education and Training Command

In Partial Fulfillment of the Requirements for the

Degree of Master of Science in Engineering and Environmental Management

Jonathan L. Ng, BS

2d Lt, USAF

March 2006

AFIT/GMS/ENY/06-M01

FRETTING FATIGUE BEHAVIOR OF SHOT-PEENED IN 100

Jonathan L. Ng, BS
2d Lt, USAF

Approved:

/APPROVED/	03/07/2006
Shankar Mall (Chairman)	date
/APPROVED/	03/07/2006
Vinod K. Jain (Member)	date
/APPROVED/	03/07/2006
Theodore Nicholas (Member)	date

Abstract

The fretting fatigue behavior of shot-peened of IN 100 was investigated in this study. S-N curves were obtained for two different shot-peened intensities (7A and 12A) and were compared to those of unpeened specimens. Stress relaxation behavior under fretting fatigue was also investigated after their measurements were obtained using the X-ray diffraction method. The crack initiation location and the crack angle orientation along the surface were determined using optical and scanning electron microscopy (SEM). Cracks initiated near the trailing edge and on the contact surface for both 7A and 12A shot-peened specimens. Finite element analysis was performed using commercially available software, ABAQUS, to obtain contact region state variables such as stress, strain and displacement. These state variables were needed for the computation of fretting fatigue parameters, such as stress range, effective stress, shear stress range (SSR) and modified shear stress range (MSSR), which were further analyzed. It was found that there was relaxation of residual compressive stress during fretting fatigue up to a certain depth. The effects of shot-peening were negated relatively early in the fretting fatigue life. There was little difference in fretting fatigue life between the two intensities of shot-peening, but there was an improvement in relation to unpeened specimens. Also, the MSSR parameter, a critical plane based fatigue parameter, was effective in characterizing the fretting fatigue behavior in terms of fatigue life, crack initiation location and orientation. However, it is not applicable to both shot-peened and unpeened cases simultaneously to yield a single trend. This may be due to the peened specimens having

been plastically-deformed on the surface and the unpeened specimens remain unchanged, and hence they were two different types of material which did not to act the same way under fretting fatigue conditions.

Acknowledgements

I would like to express my sincere appreciation to my advisor, Dr. Shankar Mall, for his guidance, explanations, patience, support, and all the time spent editing and revising this thesis. I also acknowledge the financial support of Dr. Mark Blodgett, Air Force Research Laboratory (AFRL/MLLP). I thank the Watson Scholars Initiative for giving myself and my fellow Scholars the opportunity to attend AFIT and earn our Masters degree.

I would also like to thank Dr. Hyukjae Lee, Bahraini Air Force Lieutenant Salman Albinali, and all the laboratory technical support who gave me much technical support for the conduction of this project. I express my appreciation for my pseudo-partner, Moroccan Air Force Captain El Houcine Madhi, with whom I worked side-by-side on many steps of this project.

I also appreciate the moral support that all my fellow Scholars and students gave me throughout the entire time we shared at AFIT. Finally, I am grateful for my parents, family, and my fiancée without their constant encouragement, love, and support, I would not have the strength to endure the hard-times.

Jonathan L. Ng

Table of Contents

Page

List of Figures

List of Tables

List of Symbols

7A	shot-peening intensity 7 Almen
12A	shot-peening intensity 12 Almen
R	stress ratio
MSSR	modified shear stress range fatigue predictive parameter
SEM	scanning electronic microscopy
FEA	finite element analysis
Q	tangential loads
P	applied contact loads
σ_{axial}	applied axial stress
a	contact half-width
c	stick zone boundary
HCF	high cycle fatigue
$\Delta\sigma$	stress range for applied axial load
σ_{max}	maximum applied axial stress
σ_{min}	minimum applied axial stress
σ_{eff}	effective axial stress
N_f	numbers of fatigue cycles to break a specimen into two pieces
$\sigma_{1,2}$	principal normal stresses
σ_{xx}	normal stress along x-direction
σ_{yy}	normal stress along y-direction
τ_{xy}	in-plane shear stress
τ_{max}	maximum shear stress at a given point
σ	normal stresses at a given point with a specific orientation
σ_f'	fatigue strength coefficient
b_f'	fatigue strength exponenet
ε_f'	fatigue ductility coefficient
c'	fatigue ductility exponent
N_i	numbers of fatigue cycles to crack initiation
ε_a	total strain amplitude
τ	shear stress at a given point with a specific orientation
$\Delta\tau$	shear stress range
τ_{max}	maximum shear stress due to the applied maximum axial load

τ_{min}	maximum shear stress due to the applied minimum axial load
SSR	shear stress range fatigue predictive parameter
$\Delta\tau_{crit}$	shear stress range fatigue predictive parameter
R_τ	shear stress ratio at the critical plane (τ_{min}/τ_{max})
FP	Findley Parameter
τ_a	shear stress amplitude (τ_{max} - τ_{min})/2
k	Findley Parameter influence factor (= 0.35)
d	specimen thickness
b	specimen's half thickness
r	fretting pad radius
q	surface shear stress distribution
R_1	radius of fretting pad
R_2	radius of fretting specimens
E	Young's Modulus (modulus of elasticity)
ν	Poisson's Ratio
p	contact pressure distribution in the contact zone
P_0	maximum contact pressure or Hertzian Peak Pressure
c	stick zone half-width
f	coefficient of friction
$(\sigma_{xx})_{contact}$	x-direction normal stress contributed from contact load
$(\sigma_{xx})_{tangential}$	x-direction normal stress contributed from tangential load
$(\sigma_{xx})_{axial}$	x-direction normal stress contributed from axial load
h	depth of penetration
Q_{max}	maximum tangential loads
Q_{min}	minimum tangential loads
$a_{analytical}$	contact half-width carried out from analytical solution
$a_{Exp,\ max}$	maximum contact half-width measured from experiments
$a_{Ruiz,\ max}$	contact half-width at maximum load conditions from Ruiz program
$x/a_{Ruiz,max}$	Ruiz program calculated maximum σ_{xx} value location
A	a specimen's cross section area
θ	direction of stress in a material, observed angle of orientation
σ_{xy}	shear stress on x-y plane
%R	percent relaxation
f_{FEA}	coefficient of friction used in FEA

FRETTING FATIGUE BEHAVIOR OF SHOT-PEENED IN 100

1 Introduction

1.1 Fretting Fatigue

Fretting fatigue is a phenomenon that causes damage in components under oscillating load due to their localized relative motion. This motion leads to premature crack initiation and failure, thereby causing a reduction in fatigue life. Fretting fatigue is the cause of high cycle fatigue failure which is common in turbine engines. It is for this reason that studying fretting fatigue is of great interest to the United States Air Force. Fretting fatigue can occur at the interface of components such as the disk slot and blade attachment in the fan (see Figure 1), compressor or turbine section of a turbine engine and could reduce the service life of components. If the initiated cracks are not detected, they could lead to a catastrophic failure. In order to prevent such failures, severe reduction in the service life of components has to be implemented to ensure safe operation. This results in high maintenance and inspection costs, as well as reduced operation hours. Research in fretting fatigue could provide a better understanding on the crack initiation mechanism that will help to develop methods which will be able to decrease maintenance costs and increase operating hours for newly designed components. Many studies have been conducted on different aspects of fretting fatigue in an effort to better understand this phenomenon and provide answers. Researchers have also formulated different fatigue parameters to investigate and predict crack initiation

mechanisms. In Chapter 2, formulation and parameters effecting fretting fatigue will be discussed.

1.2 Shot-Peening

One of the most common cold-working processes used to enhance the plain fatigue and fretting fatigue performance in components is shot-peening. Shot- peening involves the bombardment of the material surface with small, hard steel balls. This action causes a biaxial yielding, which creates a residual compressive stress and grain distortion near the shot-peened surface. At the same time, a tensile stress within the interior is also created. The residual compressive stress plays a critical role in fretting fatigue crack initiation and crack propagation retardation [36]. There are several factors or variables in the shot-peening process which can have considerable effect on the fatigue performance. One of these is the shot-peening intensity. It was observed that increasing the intensity from 4A to 10A leads to higher level of tensile stress and moves the boundary between negative and positive stress to a greater depth inside the material. It was also observed that an increase in intensity practically did not affect the maximum value of residual compressive stress on the contact surface. Moreover, it has been reported that the residual stress is subject to relaxation during fretting fatigue cycles [15]. Original residual stress along with stress relaxation phenomenon modifies contact stress profiles and causes different operating performance in fretting fatigue life.

1.3 Purpose and Objectives

As mentioned earlier fretting fatigue life is significantly reduced when compared to plain fatigue enforcing a high cost for operation and maintenance inspections and repairs. In order to reduce this cost and improve performance of components undergoing

fretting fatigue, an extensive number of studies have been conducted to analyze different variables such as environmental corrosion, elevated temperature, shot-peening process, fretting pad geometry, axial load frequency, and contact load frequency [35,2,16,15,22,29,36,14]. Most of the previous studies focused more or less on one of the previously mentioned variables. This study is focused on the effect of shot-peening versus no cold-working treatment. This investigation was conducted to determine the usefulness of shot-peening on a nickel based super alloy, which has received very little attention in spite of their wide -spread use in gas turbine engines. Recently, titanium alloys have been investigated extensively for their fretting fatigue behavior. However, titanium alloys are not the best choice for high temperature environments as elaborated in the next chapter. Therefore, other options for material selection must be explored.

The primary purpose of this study was to investigate the fretting fatigue behavior of IN 100. The study also covered the effect of two shot-peening intensities (7A and 12A). Constant amplitude fretting fatigue tests were conducted over a wide range of maximum applied axial stresses σ_{max} = 650 to 1000 MPa with stress ratio of R = 0.03. A cylindrical-end shape with 50.8 mm radius was chosen as the fretting pad geometry which was pressed against the specimen surface with a constant normal load of 1335 N (900 lb_f). Experiments were conducted at room temperature. Also, shot-peening intensity effects on the crack initiation location, and crack propagation behavior will be investigated in this study. Two magnitudes of shot-peening intensity (Almen) were investigated in this study (7A and 12A) all with 100% surface coverage of the specimens. The data for non-peened samples undergoing fretting fatigue was obtained from a

concurrent study by Madhi [19]. In the present study S-N curves for the unpeened, 7A, and 12A shot-peened intensity were developed.

The emphasis of the present study was to determine the effect of shot-peening and fretting fatigue mechanisms in terms of fatigue life, crack initiation location, and crack initiation orientation. In addition, effects of shot-peening intensity were also investigated. Shot-peening induced residual stress profiles which were analyzed with different relaxation rates to investigate a critical plane based fatigue parameter, the modified shear stress range (MSSR) fretting predictive parameter, for its effectiveness in predicting fretting fatigue behavior in terms of fatigue life, crack initiation location, and crack initiation orientation.

1.4 Methodology

The complexity introduced by real component geometry and load bearing condition of turbine engines might make replicating the exact configuration as a turbine engine a complex, time consuming and an expensive task. Therefore, a simplified cylinder-on-flat model (see Figure 2) was adopted as the experimental setup in this study for the sake of investigating fretting fatigue behavior. A uni-axial servo-hydraulic machine was used to apply desired load conditions and record experimental results. The fatigue life diagrams, i.e. S-N curves were developed to investigate the effects introduced by shot-peening intensity. Optical and scanning electron microscopy (SEM) was used to examine the fracture surface, contact half-width, crack initiation location, crack initiation orientation. Finite element analysis (FEA) was conducted to compute local fretting variables such as stress, strain, and displacement. The X-ray diffraction technique was applied to measure the shot-peening induced residual stress on the surface, which

accompanied with stress relaxation which was superimposed into FEA stress solutions for the development of fatigue predictive parameters. The stress evolution, stress concentration, contact half-width, and other variables were also analyzed.

Figure 1. Blade/Disc Dovetail Joint in a Turbine Engine.

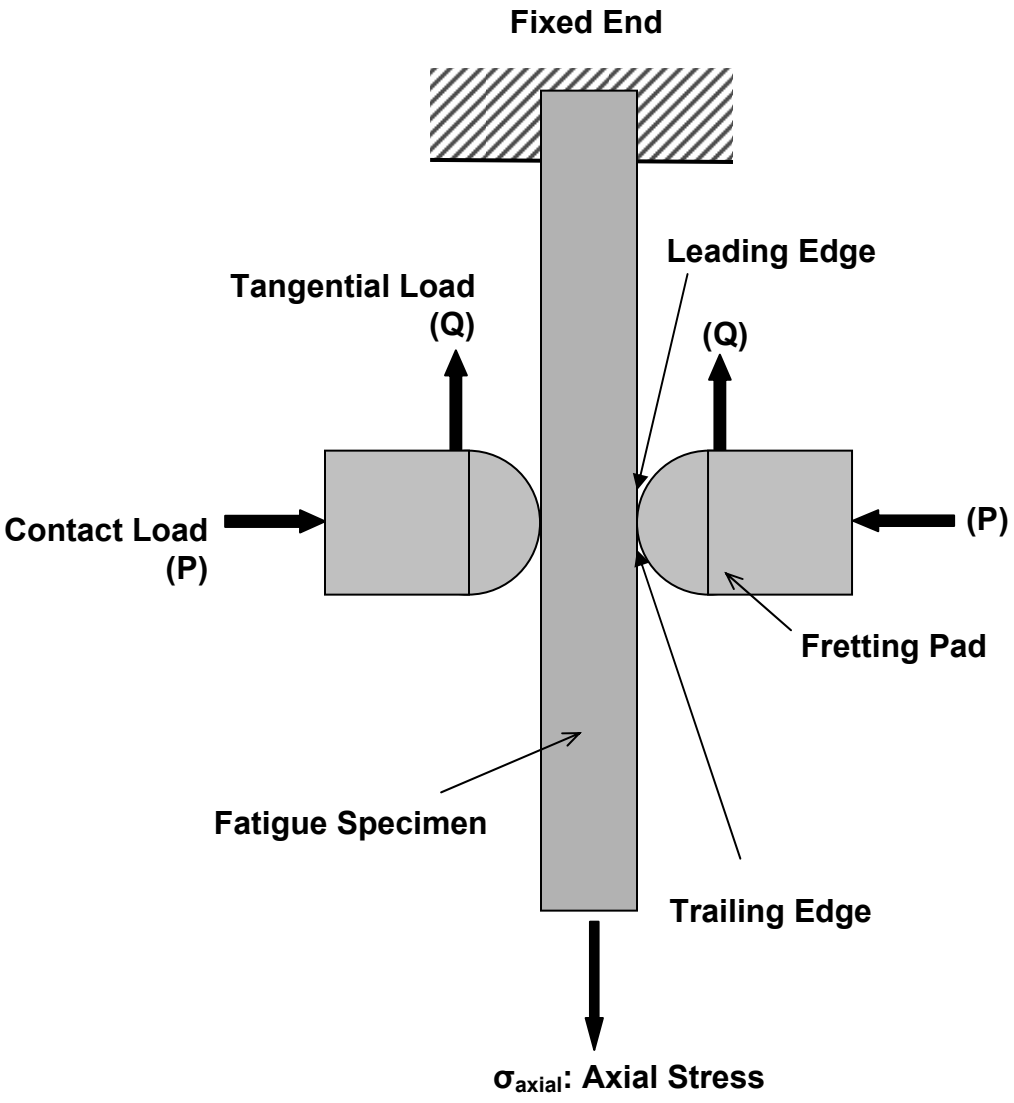

Figure 2. Simplified Fretting Configuration

2 Background

This study involves the nickel-based super-alloy, IN 100. Nickel alloys have been used for a wide variety of applications. Many studies have been conducted to understand the mechanism of fretting fatigue. This chapter is devoted to the background of nickel alloys and nickel-based super-alloys, and the analyses of contact mechanics in terms of contact width, Hertzian peak pressure, etc. The effect of shot-peening and intensity is also covered. Stress relaxation behavior of shot-peened specimens under fretting fatigue is discussed as well. Fatigue parameters are also presented and elaborated in this chapter.

2.1 Nickel Alloys and Super-Alloys

Nickel and nickel alloys are primarily used for applications where corrosion resistance and/or heat resistance are major factors in material selection. They also offer relatively high stress tolerance. Currently, they are being used in aircraft gas turbines, steam turbine power plants, medical applications, nuclear power systems, and in the chemical petrochemical industries [28]. Nickel superalloys are used in the manufacture of McDonnell Douglas F-15 and General Dynamics F-16 fighters for combustor, flameholder, afterburner, inner liners and nozzles [27].

A superalloy is a metal-based alloy which can withstand high temperatures, often in excess of 70% of the absolute melting temperature. The essential components in nickel-based superalloys are aluminum and/or titanium. These solutes "generate a two-phase equilibrium microstructure, which is largely responsible for the elevated-temperature strength of the material." [3] "Superalloy blades are used in aero-engines and gas turbines in regions where the temperature is in excess of about 400^{o}C, with titanium blades in the colder regions. This is because there is a danger of titanium igniting in

special circumstances if its temperature exceeds 400°C."[3] Currently, high-performance blades and parts for turbine engines are being made of single-crystal nickel alloys, however, it is a highly expensive and control-intensive process. The benefit of the single-crystal components is an increase in melting temperature; this is due to the elimination of localized melting due to chemical segregation.[3] However, polycrystalline parts still have very good physical properties and melting temperatures, which can be useful, especially in the less heat-intensive areas of engines, like the blade/disc dovetail joint as mentioned in Section 1.1. In this study, a poly-crystalline form of IN100 is being analyzed.

2.2 Typical Fretting Fatigue Configuration

Previous studies have developed a general and simple test scheme to improve the understanding of the fretting fatigue phenomenon and isolate its controlling variables which would lead to simplifying analysis. In this general fretting fatigue configuration, fretting specimen and pads are presented as two mechanical components in contact with each other. Axial stress, σ_{axial}, is typically applied by a hydraulic test machine at one end of a specimen that is gripped and fixed at the other end. The applied axial load can be controlled to produce fatigue loads with different frequency, waveform, magnitude, and stress ratio to simulate the load condition of interest. At the same time, the fretting pads are pressed against the specimen by a constant contact load P in the direction perpendicular to the applied axial load.

A tangential load known as shear load (Q) is induced along the contact surface when an axial load and a contact load are applied. This tangential load forces pads and specimens to move relative to each other in a partial slip condition. The tangential load is defined as half of the difference between the applied axial load and the load measured at

the gripped end of specimens. A contact region along the contact surface of a pad and specimen is created by fretting fatigue. The edge of the contact region near the fixed end is called the leading edge and the edge of the contact region near the applied axial loads is defined as the trailing edge. Contact half-width (a) incorporates both stick-zone (c) and partial slip zones and the center of contact width is defined as the origin of x-direction (see Figures 3 and 4). In this study a similar fretting fatigue configuration were cylindrical-end pads in contact with a flat specimen was used.

2.3 Shot-peening Surface Treatment

2.3.1 Introduction to Shot-peening

Surface treatments, such as shot-peening, are widely known to improve material strength under fatigue conditions and are commonly used in aerospace industries where most of the main structural components are subjected to cyclic loading. Fretting fatigue can damage the microstructure on the highly stressed contact surface. This fosters crack initiation. In the shot-peening process, a high velocity spherical projectile, called shot, made of materials such as iron, glass or ceramic beads, are used to bombard the material surface. This creates a plastically deformed surface layer constrained by an un-deformed interior underneath. This action introduces a biaxial residual stress profile on the peened material, which is compressive near the peened surface and tensile away from the peened surface.

The shot-peening induced compressive stress plays a critical role in crack initiation and propagation retardation mechanisms under plain and fretting fatigue conditions. This residual compressive stress can close a pre-existing crack tip at the early

stages of fatigue life and can reduce crack propagation rate by compensating detrimental tensile stress applied by global loads [21].

In order to optimize shot-peening induced fatigue strength, shot-peening controlling parameters should be manipulated carefully including shot-peening media, shot velocity or pressure, angle of impingement, shot hardness and shape and intensity. In this study, 7A and 12A shot-peened specimens were used to investigate the shot peening effect on fretting fatigue behavior. Also, shot-peening induced residual stress was superimposed into results from finite element.

2.3.2 Shot-Peening Intensity

Shot-peening intensity, known as Almen intensity (A), is a measurement of the shot-peening stream energy; it is directly related to the induced residual stress magnitude and distribution. To increase Almen intensity, use larger beads and/or increase shot velocity of the shot stream. Sebalkin et al.[26] and Martinez [21] investigated fretting fatigue behavior under shot-peening intensities of 4A, 7A, and 10A. They showed that the residual stress on a peened surface was not significantly different under the different intensities. However, underneath the peened surface, significant differences in the residual stress profiles were observed. Also, as peening intensity increased, the greater the compressive magnitude and depth became. It was also shown that the crack initiation location occurred on the specimen surface under 4A and 7A, and in the interior under 10A. This was due to the greater residual stress magnitude caused by the greater intensity. In this study, all shot-peened specimens were peened under 7A and 12A to investigate the effects of shot-peening under fretting fatigue.

2.3.3 Residual Stress Relaxation Behavior

Relaxation behavior has been reported to be a result of the cyclic loading conditions. This relaxation effect reduced the improvement on material fatigue strength under fretting fatigue conditions [16,20,24]. Martinez et al. [21,22] used specimens peened with intensity 7A±1 with 100% surface coverage to investigate the contribution of fretting fatigue on residual stress relaxation behavior. It was shown that before a specimen failed due to fretting fatigue, the residual stress profile became non-uniform and anisotropic within a fretting scar on the contact surface. Additionally, stress relaxation increased with the increase of fretting fatigue cycles until a specimen failed. After failure occurred, full relaxation of residual stress was measured at crack location, accompanied with no relaxation far away from the contact region. As a fretting region was approached, residual stress was observed under some degree of relaxation on the contact surface.

In other reports,[16,23,29,36] it was found that residual stress relaxation due to fretting fatigue cycles affected fatigue life and crack initiation location significantly. Larger relaxation caused more fatigue life reduction and might shift crack initiation location from the interior of specimens to the contact surface.

2.3.4 Shot-peening Effect on Fretting Fatigue Life

Due to the introduction of residual compressive stress induced by shot-peening process in the substrate specimens, both plain and fretting fatigue strength under laboratory environment was improved for shot-peened Ti-6Al-4V specimens when compared with un-peened ones [15,21,22,34,36]. In addition, crack initiation locations for shot-peened specimens may occur either on the contact surface or far away from contact surface at a depth of 200-300 microns. These initiation locations were close to the

location where maximum tensile residual stress which also depends on the residual stress profile gradient, the depth of compressive residual stress, microstructure crack on the contact surface and specimen thickness. In order to get the most beneficial effects from residual compressive stresses the depth of the compressive regime must be greater than the depth where cracks may initiate such that pre-existing crack tips could be closed and crack initiation and propagation can be retarded.

2.4 Fatigue Parameters

Crack initiation models and predictive parameters are developed on the basis of stress or strain history of the plain fatigue configuration. These techniques can be extended to fretting fatigue data. Attention has been drawn to the use of multi-axial fatigue parameters, such as a critical plane approach, to describe fretting fatigue behavior. Critical plane fatigue parameters were generated based on the maximum damage plane which is formulated during fatigue.

Fatigue life of mechanical components under fretting fatigue conditions has been demonstrated to be significantly reduced as compared to fatigue life under plain fatigue conditions [13,17,36]. A fretting fatigue condition is associated with high cycle fatigue (HCF) where a large fraction of fatigue life is spent in crack nucleation and growth to a detectable size while only a small fraction of life is spent in the crack propagation from detectable size to a critical size. Therefore, unlike using a damage-tolerant approach for predicting fatigue life under low cycle fatigue regime, an alternative approach is needed to predict HCF crack initiation behavior.

2.4.1 Stress range and Effective Stress

Fretting fatigue conditions are affected by local interfacial mechanistic parameters such as peak contact pressure, local cyclic bulk stress, local cyclic shear stress, and slip amplitude and contact semi-width [10]. However, predictive parameters based on global boundary conditions (contact load, tangential load, far field stresses) are still favored in some areas of study because global boundary conditions are more easily controlled in experiments and are the most obvious variables in a practical situation. Consequently, predictive models relating global mechanistic variables are most desirable in terms of applicability; two such parameters are stress range and effective stress.

Stress range for applied axial load can be described as:

$$\Delta\sigma = \sigma_{\max} - \sigma_{\min} \tag{1}$$

Equation (1) does not include the effect from mean stress or stress ratio, which were well documented in fatigue literature to be relevant to fatigue strength. Walker [32] proposed an alternative method using effective stress to account for the effects from the stress ratio:

$$\sigma_{eff} = \sigma_{\max}(1-R)^m \tag{2}$$

where σ_{eff} is the effective stress taking into account the effect from the stress ratio and residual stress, and m was found to be 0.45 by Lykins [16] for titanium.

When evaluating effectiveness of Equation (2) for un-peened Ti-6Al-4V specimens in fatigue life prediction under fretting fatigue conditions, Mall et al.[20,25] found that this equation could only effectively collapse fretting fatigue life data into a single curve under specific pad geometries.

In order to fit the experimental data on a curve, the applied stress range can be described as:

$$\Delta\sigma = C_1(N_f)^{C_2} + C_3(N_f)^{C_4} \tag{3}$$

where C_1, C_2, C_3, and C_4 can be found using a curve fitting technique with Kaleidagraph for each curve. Also, effective stress can be described as:

$$\sigma_{eff} = C_1(N_f)^{C_2} + C_3(N_f)^{C_4} \tag{4}$$

Different C coefficients can also be found for effective stress values.

Equations (1) and (2) worked well for correlating fatigue life with global load conditions under certain circumstances. However, it should be noted that these equations only provide a crude representation on a mechanic basis. They do not include the stress concentrations effects occurring at the trailing edge of the contact region or multi-axial loading conditions induced by fretting fatigue. This explains why critical plane-based predictive parameters formulated on local stress distributions are needed.

2.4.2 Critical Plane Based Fatigue Approach

The maximum or minimum in-plane principal stresses acting at a specific point can be expressed as:

$$\sigma_{1,2} = \frac{\sigma_{xx} - \sigma_{yy}}{2} \pm \sqrt{\left(\frac{\sigma_{xx} - \sigma_{yy}}{2}\right)^2 + \tau_{xy}^2} \tag{5}$$

$$\tau_{\max} = \sqrt{\left(\frac{\sigma_{xx} - \sigma_{yy}}{2}\right)^2 + \tau_{xy}^2} \tag{6}$$

where σ_1 and σ_2 are principal normal stresses and the planes on which they act are called principal planes. σ_{xx}, σ_{yy}, τ_{xy} are stress components at a local point. τ_{max} is the maximum

shear stress at a given point, and it always acts on a plane with 45^o from the orientation of principal planes.

The critical plane is defined as the plane where a fatigue parameter has its maximum value. In order to evaluate critical plane-based fatigue parameters, local normal and shear stresses are computed as follows

$$\sigma = \frac{\sigma_{xx} + \sigma_{yy}}{2} + \frac{\sigma_{xx} - \sigma_{yy}}{2}\cos(2\theta) + \tau_{xy}\cos(2\theta) \tag{7}$$

$$\tau = -\frac{\sigma_{xx} - \sigma_{yy}}{2}\sin(2\theta) + \tau_{xy}\cos(2\theta) \tag{8}$$

where θ is evaluated from -90^o to +90^o. A good critical plane fatigue parameter formulated from Equations (7) and (8) should be able to predict fatigue life, crack initiation location, and crack initiation orientation. These requirements will be adopted to examine the validity of fatigue parameters.

2.4.3 Smith-Watson-Topper Parameter (SWT)

Smith, Watson, and Topper [30] proposed a fatigue parameter shown below:

$$SWT = \frac{\left(\sigma_f^{'}\right)^2}{E} \bullet \left(2N_i\right)^{2b_f{'}} + \sigma_f^{'}\varepsilon_f^{'}\left(2N_i\right)^{b_f{'}+c'} \tag{9}$$

where $\sigma_f^{'}$ is the fatigue strength coefficient, b_f' is fatigue strength exponent, ε_f' is fatigue ductility coefficient, c' is fatigue ductility exponent, E is the elasticity modulus, and N_i is cycles to crack initiation. This equation is widely known as Smith-Watson-Topper (SWT) parameter.

Szolwinski and Farris [31] made modifications to SWT parameter using critical plane approach as follows:

$$SWT = \sigma_{\max}\varepsilon_a \quad or \quad \max(\sigma_{\max}\varepsilon_a) \tag{10}$$

where σ_{max} is the stress normal to a critical plane, and ε_a is the normal strain amplitude to a critical plane. This parameter affirms crack initiation occurs on the plane where the product of σ_{max} and ε_a is maximized. Using the computed local stress and strain from finite element analysis of the fretting fatigue experiments, this parameter was calculated at all planes ranging from $-90^o \leq \theta \leq +90^o$, which provided this parameter's maximum value.

The SWT parameter, for un-peened specimens, was found to be effective in predicting the number of cycles to crack initiation and crack initiation location with strong dependence on pad geometry [20,25,26,31]. However, it did not provide good concurrence with crack initiation orientation. Also, the maximum shear strain amplitude did not coincide with the crack initiation location under fretting fatigue conditions for un-peened specimens, as is shown under plain fatigue tests [25]. For shot-peened specimens, Yuksel [36] found that this parameter was effective in crack initiation location prediction, but failed in predicting either fatigue life or crack initiation orientation.

2.4.4 Shear Stress Range Parameter (SSR)

SSR parameter considers only maximum and minimum shear stress on the critical plane. This parameter is computed by first finding the shear stress at all points along all planes ranging from $-90^o \leq \theta \leq 90^o$ from the state of stress (σ_{xx}, σ_{yy}, τ_{xy}), as computed from FEA by applying the following equation:

$$\tau = -\frac{\sigma_{xx} - \sigma_{yy}}{2}\sin 2\theta + \tau_{xy}\cos 2\theta \qquad (11)$$

Then the shear stress range (SSR) $\Delta\tau = \tau_{max} - \tau_{min}$ was computed at all planes and at all points in the contact region, where τ_{max} and τ_{min} are shear stresses due to the applied maximum and minimum axial load, respectively. Since the mean stress and stress ratio

also affect fretting fatigue behavior, they are accounted by incorporating a technique proposed by Walker [33]. Thus the SSR parameter is expressed as:

$$(SSR = \Delta\tau_{crit}) = \tau_{\max}(1 - R_{\tau})^{m} \tag{12}$$

where τ_{max} is the maximum shear stress and R_{τ} is the shear stress ratio (τ_{min} / τ_{max}) at the critical plane, respectively, and *m* is a fitting parameter found to be 0.45 from a previous study [18].

It was shown that the SSR, for un-peened specimens with different pad geometry, was useful in conjunction fretting fatigue life with plain fatigue life [20,25]. In addition, this parameter can also correlate crack initiation location and orientation with experimental observations. On the other hand, for shot-peened specimens, Yuksel [36] showed that under fretting fatigue conditions, this parameter is only effective in crack initiation orientation prediction but failed in predicting both fatigue life and crack initiation location.

2.4.5 Findley Parameter (FP)

Crack initiation mechanism in multi-axial loading fatigue conditions should be influenced by both normal and shear stresses. Since SSR only accounts for the effect from shear stress, another multi-axial fatigue parameter involved the effect from normal stress on a critical plane in addition to shear stress amplitude can be found in Findley's study as follows [7]

$$FP = \tau_{a} + k\sigma_{\max} \tag{13}$$

where k is an influence factor determined to be 0.35 from plain fatigue data [25], and τ_a is stress amplitude defined as $\tau_a = (\tau_{max} - \tau_{min})/2$. FP was calculated at all planes ranging from $-90^{o} \le \theta \le +90^{o}$ from computed stresses and strains obtained from finite element

analysis. These calculations provided the critical plane, where this parameter is the maximum.

For un-peened specimens with different geometry pads under fretting fatigue conditions, FP could predict crack initiation location well but was not able to predict fretting fatigue life from plain fatigue data. In addition, the predicted crack orientations were different from experimental observations as was found by Mall et al. [24,25]. For shot-peened specimens under fretting fatigue conditions it was found that this parameter was most effective in crack initiation location prediction but failed to predict fatigue life and crack initiation orientation [36].

2.4.6 Modified Shear Stress Range Parameter (MSSR)

This parameter is formed by combining the maximum normal stress, which generally aids in opening the crack surface, on a critical plane of maximum SSR into the original SSR as follows:

$$MSSR = A\Delta\tau_{crit}^{B} + C\sigma_{\max}^{D} \tag{14}$$

where $\Delta\tau_{crit}$ is same as Equation (12) and σ_{max} is the maximum normal stress on the critical plane of the SSR parameter. A, B, C, D are fitting constants determined by curve fitting approach. These constants are determined empirically [25]. MSSR was calculated at all planes ranging from $-90^{o} \leq \theta \leq +90^{o}$ from the computed stresses and strains obtained from finite element analysis. These calculations provided the critical plane, where this parameter is maximized.

MSSR was the only critical plane-based parameter available in predicting fatigue life, crack initiation location, and crack initiation orientation along with their experimental counterparts for both shot-peened and un-peened Ti-6Al-4V specimens

with little dependency on pad geometry under fretting fatigue conditions [20,25,33]. Therefore, the MSSR parameter was determined to be an appropriate fatigue predictive parameter while investigating crack initiation behavior of both shot-peened and un-peened Ti-6Al-4V under fretting fatigue conditions. Since MSSR was so successful for Ti-6Al-4V, a similar analysis was attempted for IN100.

MSSR was also able to adequately characterize fretting crack initiation orientation and location independent of contact geometry for two values of friction coefficients, 0.5 and 0.8 [36] for Ti-6Al-4V. Sabelkin et al.[29] showed that MSSR could predict fretting fatigue life as well as crack initiation location consistent with experimental counterparts for specimens shot-peened under 4A, 7A, and 10A intensities with 100% surface coverage.

2.5 Contact Mechanics

A cylindrical-end body in contact with a flat body setup is adopted as the fretting fatigue configuration and is incorporated in this study. Contact mechanics and analytical solutions associated with this configuration are discussed in detail in this section. A diagram of two bodies in contact under fretting fatigue loads is shown in Figure 3. Here, A represents the cross sectional area of the fretting specimen, σ_{axial} represents the applied axial stress, P is the applied contact load, Q is the reacted tangential load, d is the thickness of a specimen, b indicates half thickness of a specimen, and a represents the contact half width. The constant radius of fretting pads in the cross sectional plane is r, and the radius of the fretting fatigue specimen is infinite in the cross sectional plane, that is, a flat surface of specimens is used in this study. For analytical solutions, an assumption was made that the two contact bodies have infinite boundaries, and analytical

equations were formulated based on the displacement relationships of the two contact bodies.

Assume that given points in the contact zone are displaced in the *y*-direction by $v_1(x) - v_2(x)$ and invoke the displacement relationship developed by Hills and Nowell [6]; the relationships in the contact region was obtained:

$$\frac{1}{A^*}\frac{\delta h(x)}{\delta x} = \frac{1}{\pi}\int \frac{p(\xi)}{x-\xi} d\xi - \beta q(x) \tag{15}$$

where $h(x) = v_1(x) - v_2(x)$ is the amount of overlap that will occur if the contacting bodies could penetrate each other freely, p is the pressure in the contact zone and q is the surface shear stress. The other parameters of Equation (15) are:

$$A^* = 2\left(\frac{1-\nu_1^2}{E_1} - \frac{1-\nu_2^2}{E_2}\right) \tag{16}$$

$$\beta = \frac{1}{2A^*}\left(\frac{1-2\nu_1}{E_1} - \frac{1-2\nu_2}{E_2}\right) \tag{17}$$

where E is modulus of elasticity and ν is Poisson's ratio for the contact bodies, respectively.

Assuming that the tangential displacement can be defined by $g(x) = u_1(x) - u_2(x)$, a similar equation can be formulated as follows:

$$\frac{1}{A^*}\frac{\delta g(x)}{\delta x} = \frac{1}{\pi}\int \frac{q(\xi)}{x-\xi} d\xi - \beta p(x) \tag{18}$$

In this study, since the contact bodies are made of the same material, $\beta = 0$, and Equations (15) and (18) can be further simplified.

When fretting bodies are brought into contact with each other by applying a contact load, the displacement of adjoining points on the contact surface within the stick

zone will be the same. Furthermore, a pressure distribution *p(x,y)* will be introduced by the contact load. The solution of the pressure distribution from the contact load is usually called the Hertz solution. In order to solve the pressure distribution, two primary assumptions are made. First, the radii of both bodies are large in comparison to the contact dimension. Second, the contacting bodies have infinite boundaries. The infinite boundary assumption is commonly referred to as the half-space assumption. A half-space exists if one half of the specimen thickness ($b = d/2$) matches the requirement $b/a > 10$. Fellows et al.[5] found the violation of the infinite half-space assumption will introduce significant deviation into analytical solutions when compared to solutions from finite element analysis.

If one simplifies the profile of contact surfaces as a parabola, a weight function can then be achieved as:

$$w(x) = \sqrt{a^2 - x^2} \tag{19}$$

where a is the contact half-width. Solving Equations (18) and (19) yields:

$$p(x) = -\frac{k}{a}\sqrt{a^2 - x^2} \tag{20}$$

where k is termed the radius of curvature. $k = 1/R_1 + 1/R_2$, where R_1 and R_2 are the radii of fretting pad and specimen, respectively. Equilibrium in the contact surface between the applied contact load and the pressure distribution can then be defined as

$$P = -\int_{-a}^{a} P(\xi)d\xi = \frac{\pi k a^2}{2A^*} \tag{21}$$

From Equations (20) and (21), one can write with the following:

$$p(x) = -P_0\sqrt{1 - \left(\frac{x}{a}\right)^2} \tag{22}$$

where P_0 is the maximum pressure (Hertzian Peak Pressure) defined as:

$$P_0 = \frac{2P}{\pi a} \tag{23}$$

Contact half-width, a, can be found from Equation (21) as follows:

$$a^2 = \frac{2PA^*}{\pi k} \tag{24}$$

In this study, since the fretting specimen has a flat surface ($R_1 = \infty$), Equation (24) can be simplified as:

$$a = \sqrt{\frac{8PR_2}{\pi}\frac{1-\nu^2}{E}} \tag{25}$$

The axial stress resulting from the applied contact load P can be expressed in Cartesian coordinates as:

$$(\sigma_{xx})_{contact} = -P_0\left(\frac{\sqrt{a^2 - x^2}}{a}\right) \tag{26}$$

As shown in Figure 4, after applying a contact load, P, and the accompanying tangential load, Q, there will be a stick zone in the middle portion of the contact surface and slip zones at both sides. The portion ($-c < x < c$) defines the stick zone, while the portion between ($-a < x < -c$) and ($c < x < a$) are the slip zones. The stick zone is a section where the contact points of the fretting bodies, the specimen and the pad, move together. On the other hand, the contact points can move freely with each other within the slip zones. The stick zone in the fretting fatigue configuration is determined by factoring the contact geometry, contact pressure, and coefficient of friction. The formation of the stick zone leads to an amplification of remotely applied stresses in the vicinity of the contact surface and also leads to premature crack initiation.

Shear stress distribution along the contact surface can be expressed as:

$$q(x) = \frac{C}{\sqrt{a^2 - x^2}} \tag{27}$$

where $C = Q/\pi$. Q is the total shear stress along the contact length which is obtained by integrating the shear stress distribution as:

$$Q = \frac{fp_0\pi}{2a}(a^2 - c^2) \tag{28}$$

where f is the coefficient of friction. The stick zone size is calculated as:

$$\frac{c}{a} = \sqrt{1 - \left|\frac{Q}{fP}\right|} \tag{29}$$

The stress distribution cased by the tangential load in the x-direction is found to be:

$$(\sigma_{xx})_{Tangential} = 2fp_0 - \frac{2}{\pi}\int_{-a}^{a}\frac{q'(x)}{x+a}dx \tag{30}$$

where:

$$q'(x) = -\frac{fp_0 c}{a}\sqrt{1 - \left(\frac{x-e}{c}\right)^2} \tag{31}$$

and

$$e = \frac{\sigma a}{4fp_0} \tag{32}$$

$$\sigma = \frac{E\varepsilon_{xx}}{1-\nu^2} \tag{33}$$

where ε_{xx} is the corresponding strain induced by the axial tensile stress (σ_{axial}) under plane strain.

Total axial stress along the contact surface between the fretting specimen and the fretting pad can then be expressed as:

$$\sigma_{xx} = (\sigma_{xx})_{contact} + (\sigma_{xx})_{tangential} + (\sigma_{xx})_{axial} \quad (34)$$

Chan and Lee [13] wrote a FORTRAN program named "Ruiz program" to calculate the numerical solutions required by analytical analyses for variables such as Hertzian Peak Pressure in Equation (23), contact half-width in Equation (25), σ_{xx} in Equation (34), etc. These solutions from both analytical equations and Ruiz program are computed to verify the finite element model used in this study and then was compared to experimental results.

2.6 Summary

Fretting fatigue occurs between two contact components under relative motion and reduces fatigue life in comparison with plain fatigue. Shot-peening, on the other hand, improves material fatigue strength. In order to better understand fretting fatigue mechanisms, analytical solutions have been developed and comprehensive studies have been conducted to analyze different contributing variables, such as shot-peening intensity. Predictive parameters using both a plain fatigue technique and a critical plane-based approach were also investigated for the effectiveness in fretting fatigue mechanism predictions. Most of the previous studies focused on the effect of varying one contributing factor to fretting fatigue. This primary objective of this study was to investigate the effect of shot-peening and shot-peening intensity on the fretting fatigue of IN 100.

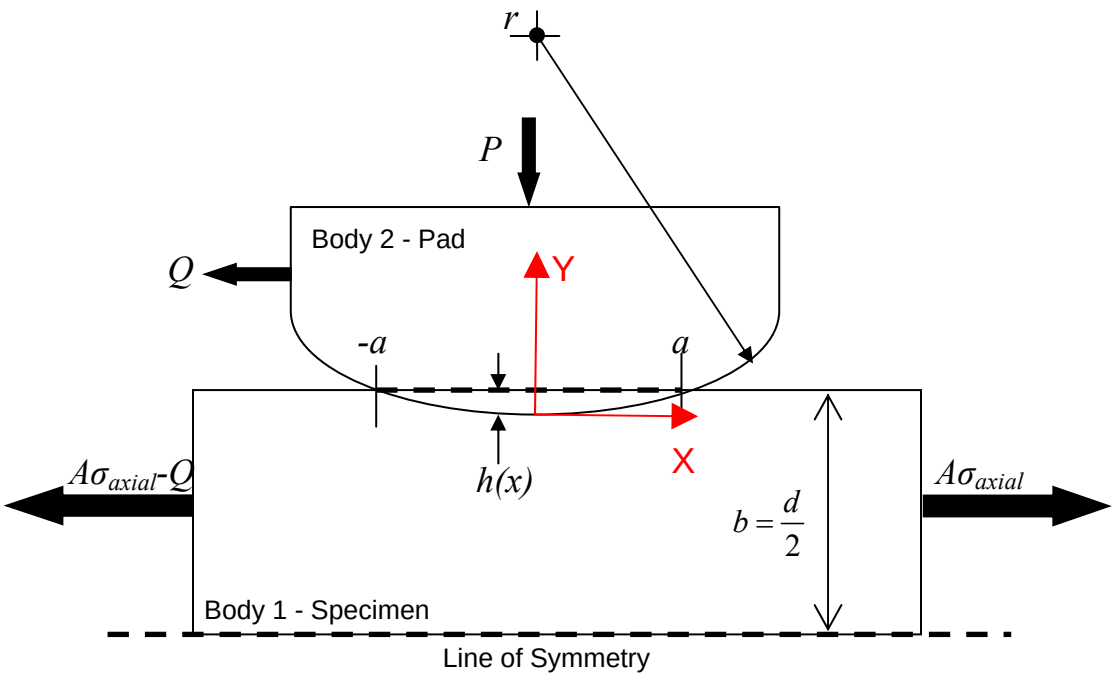

Figure 3. Free Body Diagram of Two Bodies under Fretting Fatigue Loads [1]

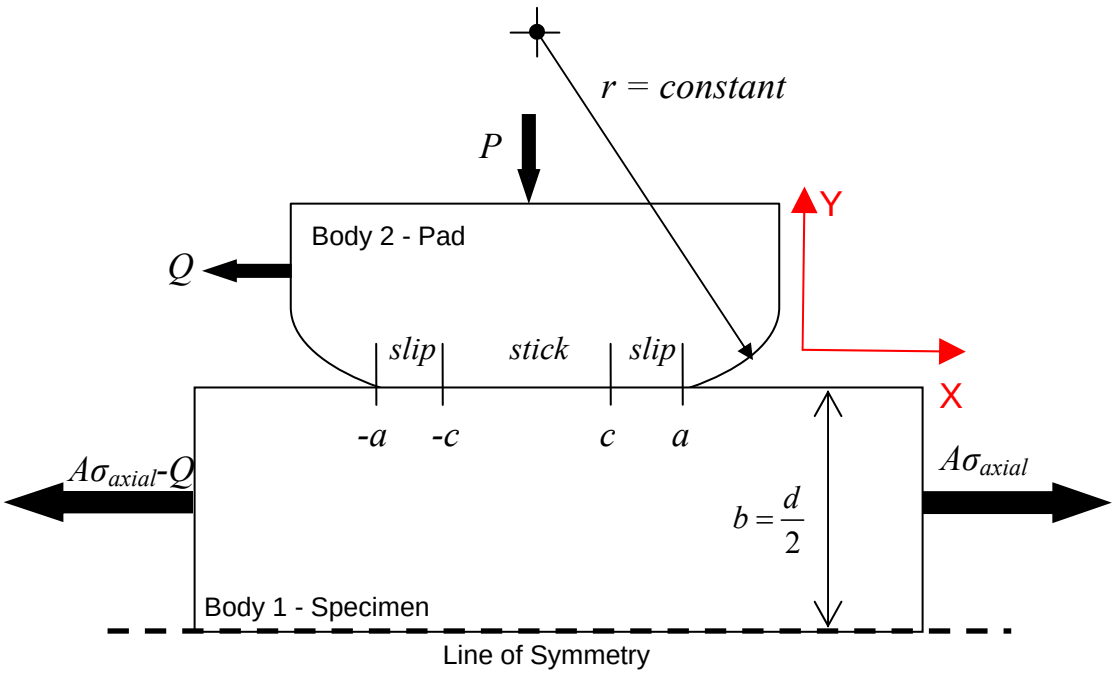

Figure 4. Partial Slip Condition for Deformed Bodies [1]

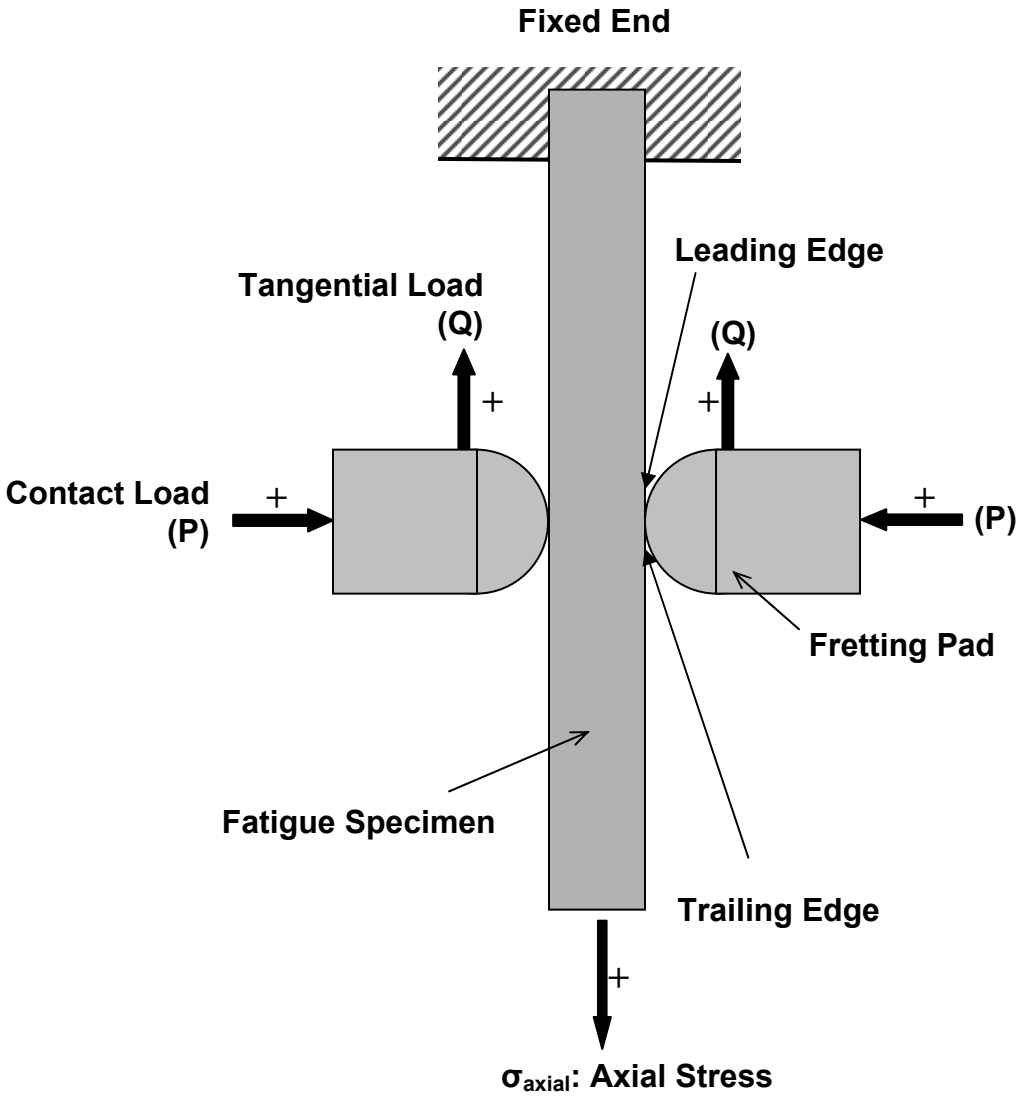

Figure 5. Typical Fretting Fatigue Configuration [1]

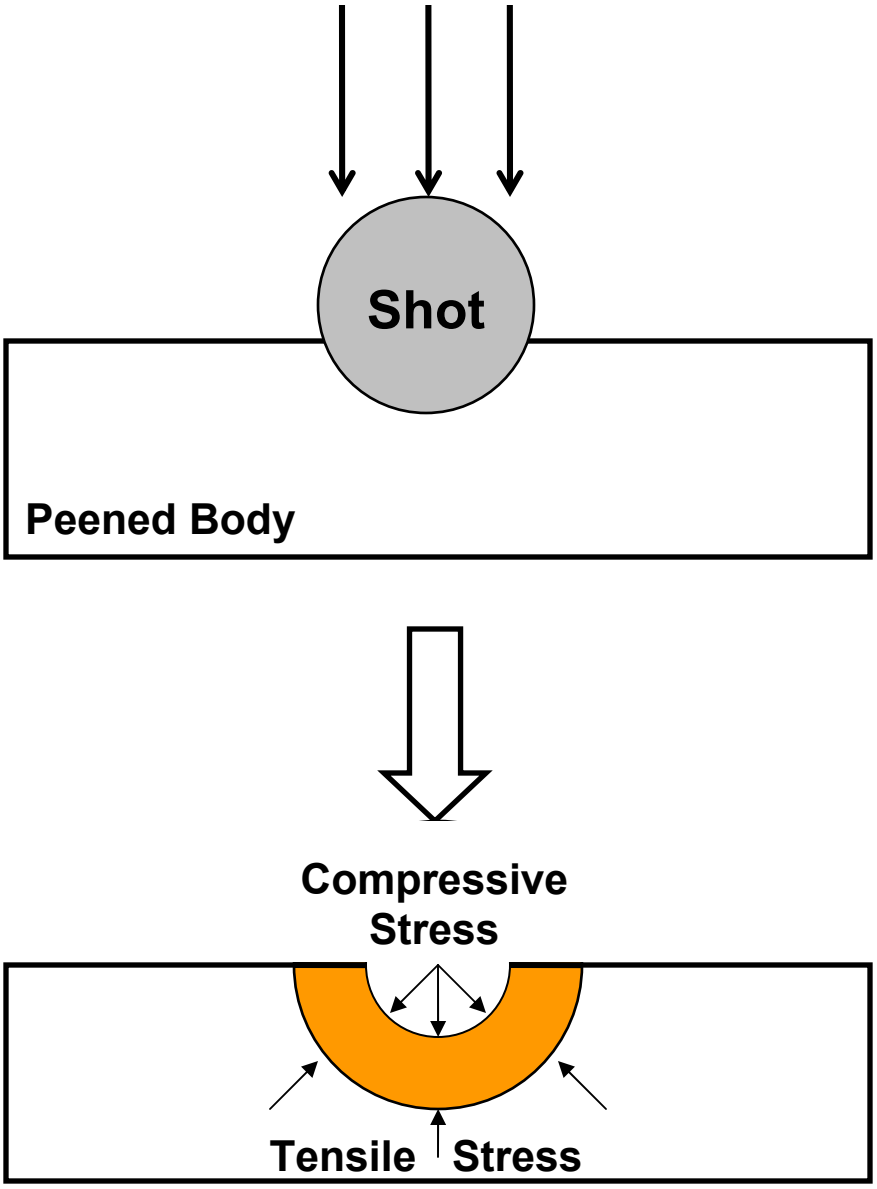

Figure 6. Schematic of Shot-Peening Process

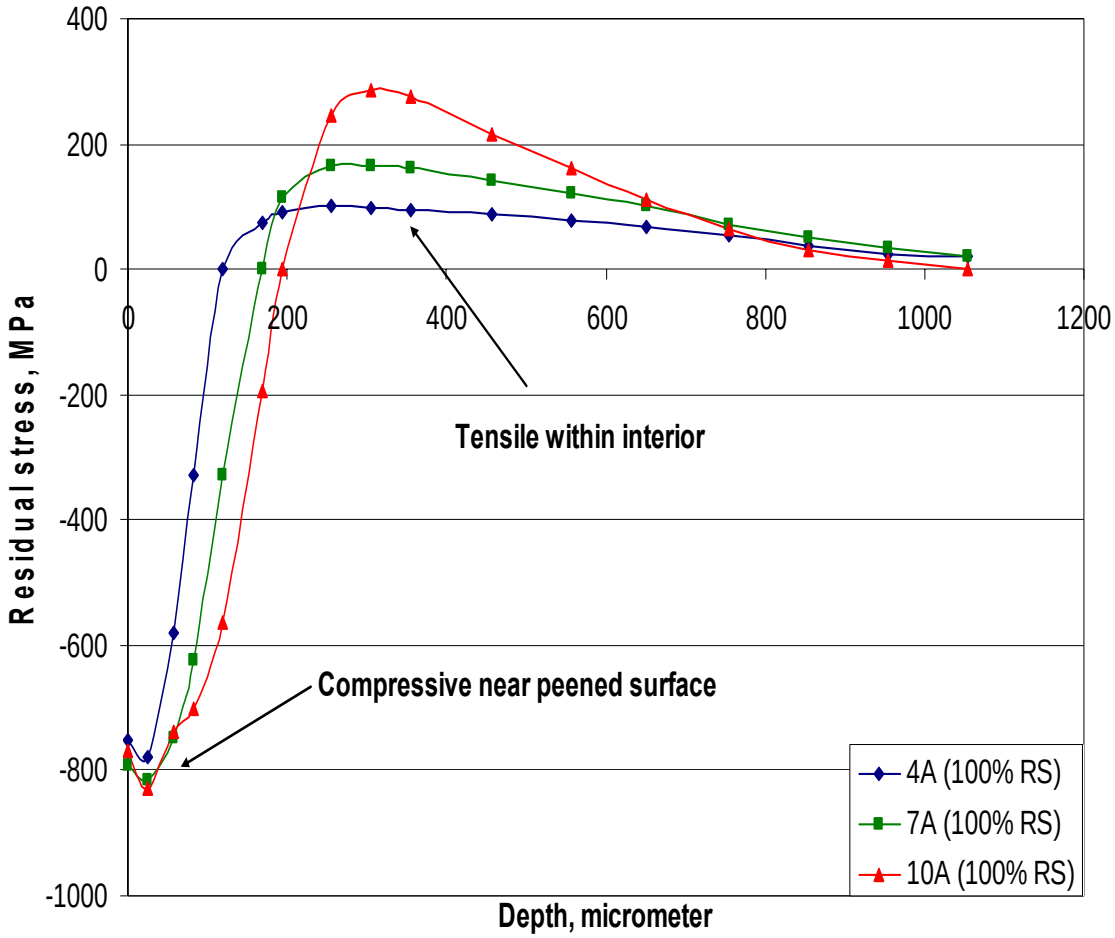

Figure 7. Typical Residual Stress Profile Induced by Shot-peening ($\sigma_{xx}=\sigma_{yy}$, $\tau_{xy} = 0$) for 4A, 7A and 10A specimens [29]

3 Experimental Configuration

This chapter documents the experimental configuration used in this study to investigate the effect of shot-peening intensity on the fretting fatigue behavior of IN 100. Experimental test details such as test apparatus, specimen and pad geometry, material property, load determination, and test procedure are covered in this chapter.

3.1 Test Apparatus

The experimental setup in this study incorporated a 22.2 kN servo-hydraulic uni-axial test machine. A photograph showing the complete test machine is presented in Figure 8. This test machine, as demonstrated schematically in Figure 9, has a fretting fixture capable of keeping the normal load constant via lateral springs through out the test. The axial load can be varied with the help of the 22.2 kN servo-hydraulic load frame. The axial load variation that the test specimen experiences during the fatigue test were controlled by load cells attached to the servo-hydraulic load frame. This actuator was controlled by Multi-Purpose Test Software (MPT) which allowed users to vary the magnitude, frequency, and waveform of the axial load. When a cycle load is applied to the specimen, the contact pads move relative to the specimen and cause fretting fatigue action on the face of the specimen. Due to this alignment becomes a big concern, therefore testing and alignment should be checked before every test.

3.2 Specimen and Pad Geometry

The dimensions of the dog-bone specimens are illustrated in Figure 10. Both shot-peened intensities (7A and 12A) specimens have the same dimensions. The thickness ($2b$) of the gauge section is 6.35 mm, width (w) is 6.36 mm, having a gauge cross-sectional area (A) of 40.3225 mm^2, and overall length (L) is 60 mm. The geometry

of the fretting pad is also displayed in Figure 10. These cylindrically-tipped pads are not shot-peened and have a radius (r) = 50.8 mm at the contact ends. The thickness of the pads is 9.525 mm and the width is 9.525 mm.

3.3 Material Property

Both shot-peened intensities specimens and the pads used in this study were made up of the nickel alloy, IN 100. The metal is a polycrystalline alloy. The material had a modulus of elasticity of 207.1 GPa, and Poisson's ratio of 0.275.

Dog-bone specimens were machined by the wire electrical discharged method. However, when machined, the specimens tended to bow to a significant degree. Therefore, specimens were originally cut thicker to account for the bowing, then ground flat to the proper dimensions. In addition, the shot-peened specimens were shot-peened per SAE Aerospace Material Specification (AMS) 2432 standard, using computer controlled equipment with 7 and 12 Almen intensity. The process was accomplished with ASR 110 cast steel shot with 100% surface coverage in the gage section.

Residual stress on the surface for the shot-peened specimen was measured via X-ray diffraction technique before and after fretting fatigue cycles were determined in a commercial facility, Lambda Technologies, (Cincinnati, Ohio). Its value was determined to be about -923 MPa for 7A specimens and -831 MPa for 12A specimens. The X-ray diffraction measurements of residual stress were conducted using a two-angle sine-squared technique, in accordance with SAE J784. The surface area irradiated in these measurements was 0.5mm × 5mm.

The coefficient of friction has to be determined for use in finite element analysis covered in Chapter 4. In previous studies[13] it was shown that after cycling the specimen,

the coefficient of friction increases. Due to that the coefficient of friction in this study is measured after the cycling of the specimen reach a constant value approximately 10,000 cycles as observed by Lee [15]. In this study the coefficient of friction ranged from 0.41 to 0.72. Also the difference in coefficients of friction between 7A and 12A shot-peened specimens was not significant. Therefore, a constant value of 0.75 was designated as the static coefficient of friction for all tests.

3.4 Determination of Applied Load

The main goal of this study is to investigate the effects shot-peening intensity on the fretting fatigue behavior. For both fretting tests, an axial stress, σ_{axial} ranging from 650 to 1000 MPa was applied at a frequency of 10 Hz with stress ratio, $R = 0.03$ to produce tension-tension condition. A constant contact load of 4003 N was applied via lateral springs, followed by maximum σ_{axial} as the second step. After maximum normal and axial loads were applied at Step 2, subsequent load steps were then applied as a sinusoidal function, using peak/valley load and frequency until specimens broke into two pieces.

3.5 Test Procedure

One pair of fretting pads was mounted individually into the holding blocks that were fixed to the apparatus frame. The pads were aligned to ensure the contact surfaces of pads were orthogonal to the specimen and perpendicular to the applied axial load. This was ensured using the pressure sensitive tape, which was put between specimen and pad. Afterwards, specimens were then taken out from hydraulic machine, and a warm-up procedure programmed in MPT was executed to warm up the test machine for at least 30 minutes. This warm-up procedure was programmed using the displacement control for

the axial load actuator. Next, a test specimen was mounted and clamped into test machine by the upper and the lower grips. Contact loads were then applied manually as Step 1 with an increment of 111.2 N to each side of the pads until a maximum value of 4003 N was reached. Axial loads followed as Step 2 in increments until a maximum load was met. After Step 2, the applied loads were then imposed using a sinusoidal function with maximum/minimum load and frequency until specimens broke into two pieces.

During the tests, peak-valley compensator (PVC) was activated for axial loads to reduce variation between command and feedback signals sensed by the test machine. The induced tangential load was determined by half of the difference between the lower axial load and upper axial load after tests were executed for 10,000 fretting fatigue cycles. Axial loads and tangential loads were monitored and recorded continuously during tests until an experiment was ended due to specimen failure. After a specimen failed, the fretting fatigue cycles were recorded as its fretting fatigue life. These previously mentioned fretting variables were then used as the load inputs for FEA modeling and MSSR prediction to be discussed in latter chapters.

Figure 8. Uni-axial Servo-Hydraulic Material Test Machine with Fretting Fixture

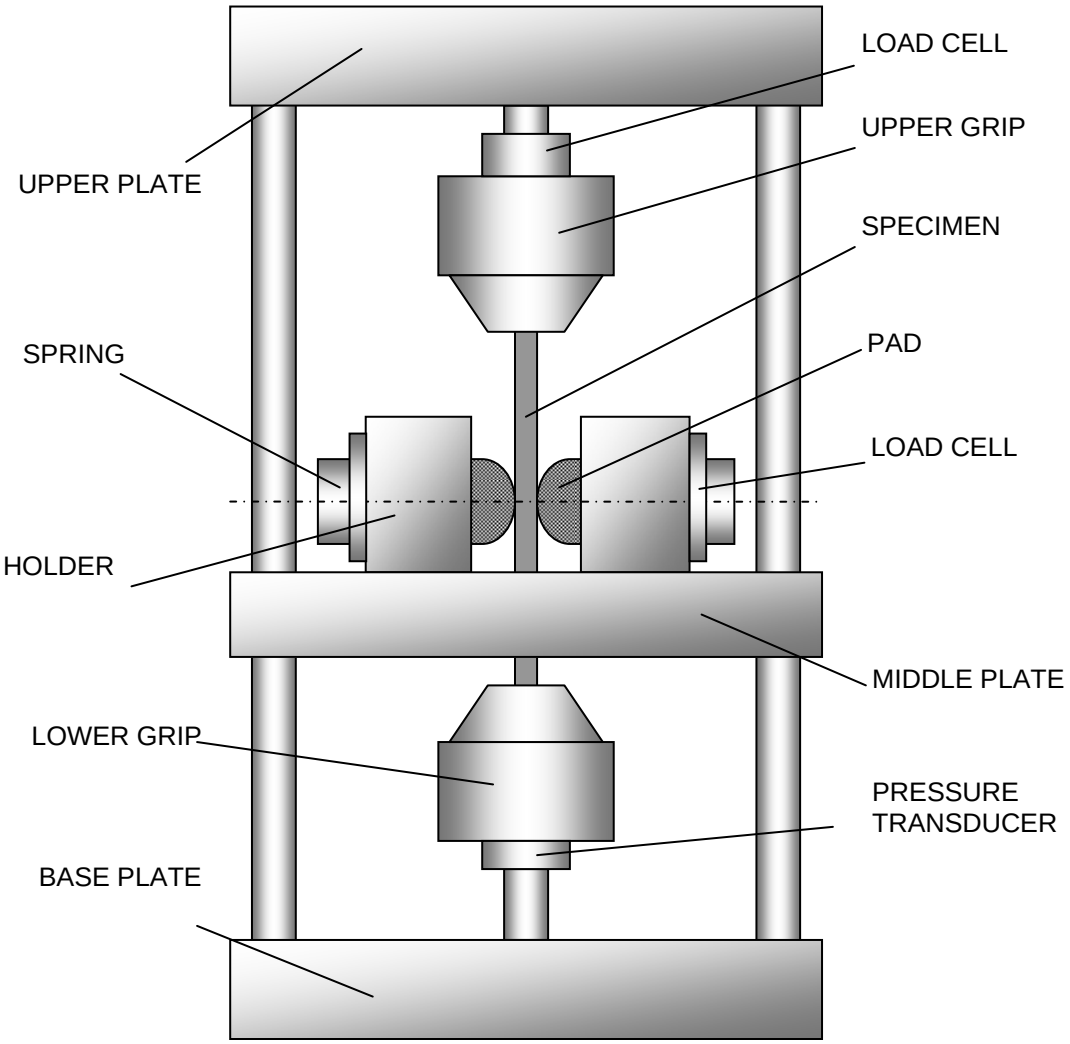

Figure 9. Schematic of Uni-axial Fretting Fatigue Set-up Configuration

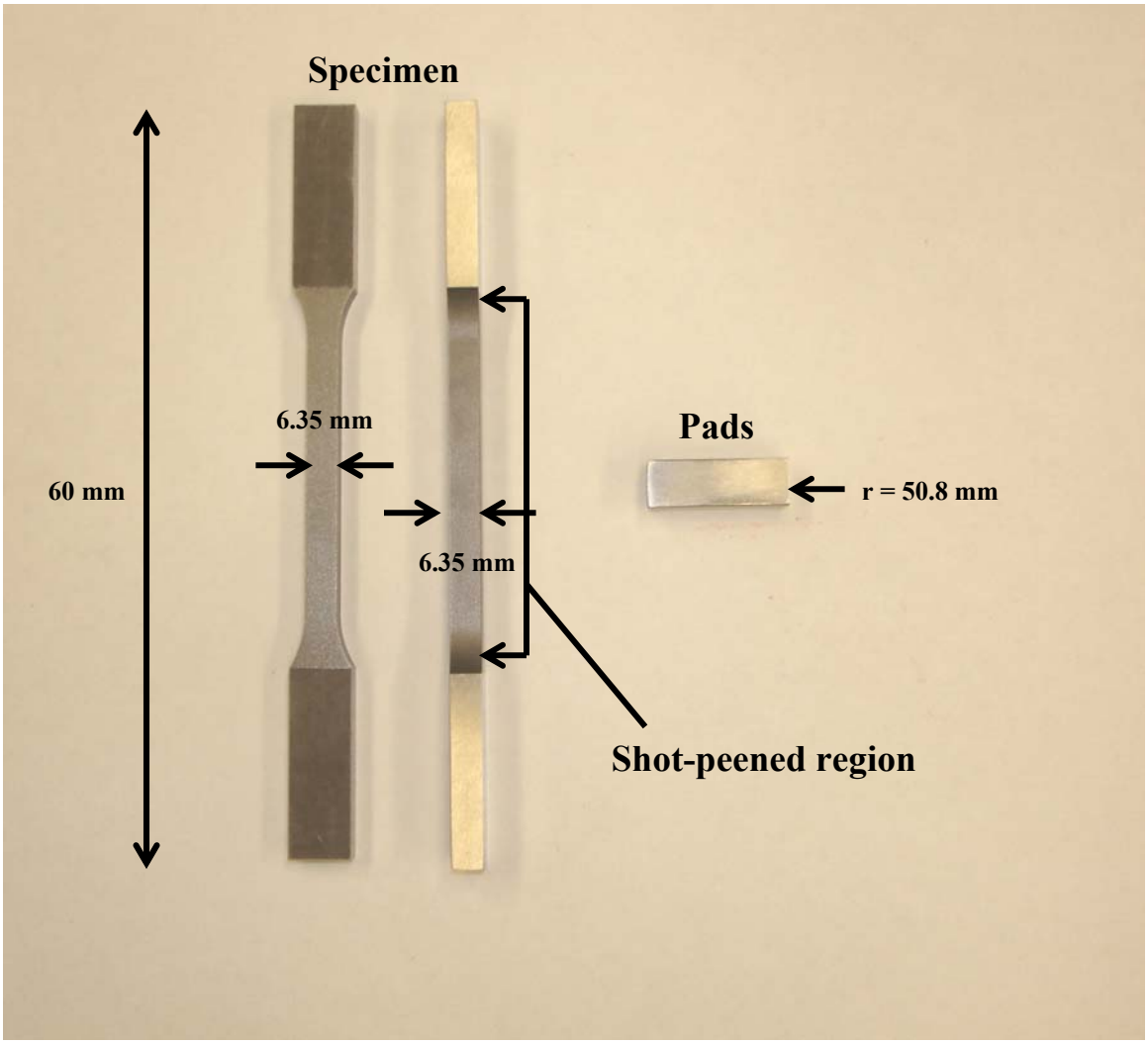

Figure 10. Specimen and Pad Geometry

4 Finite Element Analysis

In this chapter the reason why finite element analysis (FEA) was needed for conducting analysis of fretting fatigue tests will be discussed. FEA analysis such as model development, load inputs, coefficient of friction, model validation and cyclic load effects will also be addressed.

4.1 Requirement for Finite Element Analysis

Finite element analysis segregates a continuum body into a finite number of elements. The basic premise is to formulate the governing equations at the discrete points, the nodes, which make up the elements, and then solve the equations as well as unknowns simultaneously to obtain the solution.

An infinite half-space assumption in fretting fatigue analysis is defined as specimen thickness (b) / contact half-width (a) > 10. Finite specimen half-thickness can affect substrate compliance, and the stress components may differ for specimens with finite half-thickness. There is significant inconsistency between finite specimen half-thickness models and infinite half-space cases with respect to stress distribution within contact zone [4,6]. The infinite half-space assumption is necessary for the FEA result to match the analytical solution retrieved from a FORTRAN based "Ruiz" program. As mentioned in Section 2.5, analytical solutions were developed based on an infinite half-space assumption. However, in all the tests of this study, b/a = 5.27, therefore the infinite half-space assumption was violated. For this reason, FEA, a numerical analysis technique that does not require an infinite half-space assumption, was necessary for conducting an effective quantitative analysis in this study. In addition, FEA can be used to determine the governing variables of fretting fatigue, such as contact stress, strain and

displacement. These variables, as well as residual stress profiles and stress relaxation phenomenon can then be adopted to develop fretting fatigue predictive parameters which are addressed in Chapter 5 and 6.

4.2 Finite Element Model

A commercially available software package, ABAQUS, was used to model the fretting fatigue configuration of this study, as shown in Figure 11. In this study, a four-node, plain-strain quadrilateral element was employed instead of an eight-node element. This was to eliminate the oscillation in the stress state along the contact interface, which is present due to the mid-edge node of the eight-node element. The contact condition was developed by using a "master-slave" interfacial algorithm for modeling the finite element model of both shot-peened and un-peened experimental configuration. The model consisted of three parts: rigid body constraint, fretting pad, and fretting specimen. The fretting pad was constrained in the *x*- and *y*- direction by the rigid body constraint. Multi-point constraint (MPC) was applied to the pad and specimen to keep it from rotating due to the application of loads as presented in Figure 11. Only one half of the fretting specimen was used in FEA model to increase the computational efficiency of the analyses and to save memory resources. This was possible because of its symmetric nature. The half-space of fretting specimen was constrained in the *x*- and *y*-direction along its boundary. The stiffness of the rigid body constraint was set very low for improved convergence of the finite element analysis. Moreover, very little load was transmitted from rigid body constraint to fretting pad. The main purpose of this rigid body constraint was to restrict the rotation of fretting pad in the *x*- and *y*-direction before the load steps were applied to the FEA model. The contact load was applied at the top of

the pad, the tangential load was applied on the left hand side of the fretting pad, and the axial stress was applied to the right hand side of half space of the specimen. A small sliding contact condition was used between the fretting specimen and fretting pad.

The mesh of the pad and the specimen were refined incrementally from the center of contact surface by changing certain geometric coordinates in the ABAQUS input file. The mesh near the contact surface was refined to increase the accuracy of the stress, strain, and displacement distribution profile. On the other hand, coarse mesh far away from contact surface was used to reduce computation time and save system resources. The half specimen thickness was equal to 3.175 mm for all specimens. The modulus of elasticity for both the fretting pad and specimen was 207.1 GPa. A Poisson's ratio of 0.275, and a static coefficient of friction (f) of 0.75 were used for all models.

4.3 Load Inputs

For all FEA analysis, a maximum contact load was always applied as Step 1 and then kept constant until Step 2 to avoid gross slip condition. The maximum axial and tangential loads then followed as the second step. For all tests, the axial load frequency was held constant at 10 Hz. The stress range and stress ratio were adjusted to achieve tension-tension configuration. After Step 2, applied loads were simulated as predetermined peak/valley values for axial (σ_{max}, σ_{min}), and measured tangential loads (Q_{max}, Q_{min}) as documented in Table 1 on page 97. A detailed explanation for the applied load sequence is illustrated in Figure 12.

4.4 Coefficient of Friction

As mentioned earlier, the difference between the coefficients of friction for specimens shot-peened at 7A intensity and 12A intensity was not significant. In addition,

Iyer [10] showed that increasing friction from 0.37 to 0.5 (25% increase) caused no effect in contact half-width, a 7% elevation on peak local cyclic stress range, and a 15% increase in peak local cyclic shear stress range. Lykins [17] also observed that increasing the coefficient of friction from 0.45 to 0.7 (66% increase) caused a 20% increase in strain amplitude. Lee [14] showed that increasing coefficients of friction from 0.4 to 1.0 (250% increase) only produced, at most, 27% variation in σ_{xx} stress profile and a 16% increase in the MSSR parameter. In all these studies, a slight difference in a coefficient of friction did not generate much change in the stress profile, contact half-width, and so forth. Previous studies also found that the experimentally stabilized static coefficient of friction ranged between 0.37 - 0.46 for un-peened Ti-6Al-4V specimens [11] and 0.33 - 0.46 for shot-peened Ti-6Al-4V specimens [23,36]. From these measurements, the shot-peening process did not modify the coefficient of friction significantly, and the value of a static coefficient of friction could be treated as the same for both shot-peened and un-peened specimens. For this study, a constant value of 0.75 was used as the static coefficient of friction for all tests. The detailed values for coefficients of friction used in FEA are listed in Table 1.

4.5 Model Validation

Although the FORTRAN program, "Ruiz", was developed on the basis of infinite half-space assumption under static applied contact and axial loads, and the half-space assumption was violated in this study, it is still a useful tool for to quickly validate the ABAQUS model by comparing their outputs. For this check, results from ABAQUS (Test #9) were chosen to compare with their counterparts calculated from Ruiz Program

under the same load conditions. This check was conducted by checking the contact half-width, the stress profile, Hertzian peak pressure, and nominal stress.

4.5.1 Contact Half-Width

Contact half-width can be found analytically using Equation (25). Using this equation, contact half-width ($a_{analytical}$) was calculated to be 0.602 mm, identical to the value from the Ruiz program. From discussions above, contact half-width calculated from Equation (25) and the Ruiz program were identical to each other. Therefore, only the ($a_{Ruiz,max}$) contact half width was chosen in the rest of this study.

4.5.2 Stress State and Hertzian Peak Pressure

The Ruiz program is based upon the conditions that both contact and axial loads are applied statically, and the infinite half-space criterion is met. In order to obtain these conditions, Step 2 of Test #9 along the contact surface was chosen to validate stress profiles from ABAQUS.

Figure 13 shows that the stress curves from ABAQUS approach those from the Ruiz program. The maximum value of σ_{xx} from ABAQUS was calculated to be 1650 MPa at $x/a_{Ruiz,max} = 0.948$. Comparing the ABAQUS outputs with those from the Ruiz program, the deviation was only 6.06% in magnitude and 1.27% along the *x*-direction. Hertzian Peak Pressure (P_o) from ABAQUS (see Figure 14), was 669 MPa at $x/a_{Ruiz,max} = -0.052$. Comparing the ABAQUS outputs with those from the Ruiz program, the deviation was only 0.30% in magnitude and negligible deviation in the *x*-direction.

4.5.3 Applied Nominal Stress

The final criterion to validate the FEA model is the nominal stress (σ_{xx}) far away from the contact zone along the *x*-direction. In principle, σ_{xx}, from FEA analysis, far

away from the contact region should be consistent with the applied axial stress. Figure 15 presents that at the location where $x/a_{Ruiz,max}$ = 14.01, the value from σ_{xx} from FEA calculation reached 700 MPa, which is the same as the applied axial stress.

4.6 Maximum and Minimum Load Conditions

As illustrated in Figure 12, axial loads and tangential loads were subjected to continuously changing magnitude during fretting fatigue cycles. Therefore, clarifying and defining maximum and minimum load conditions are helpful to improve the readability and comprehension for the subsequent discussions. The maximum load condition is defined as a load step at which the maximum axial and tangential loads occur simultaneously under a variable loading condition. Also, the minimum load condition means a load step at which minimum axial and tangential loads happen at the same time under a variable loading condition. The contact load stays constant throughout the test.

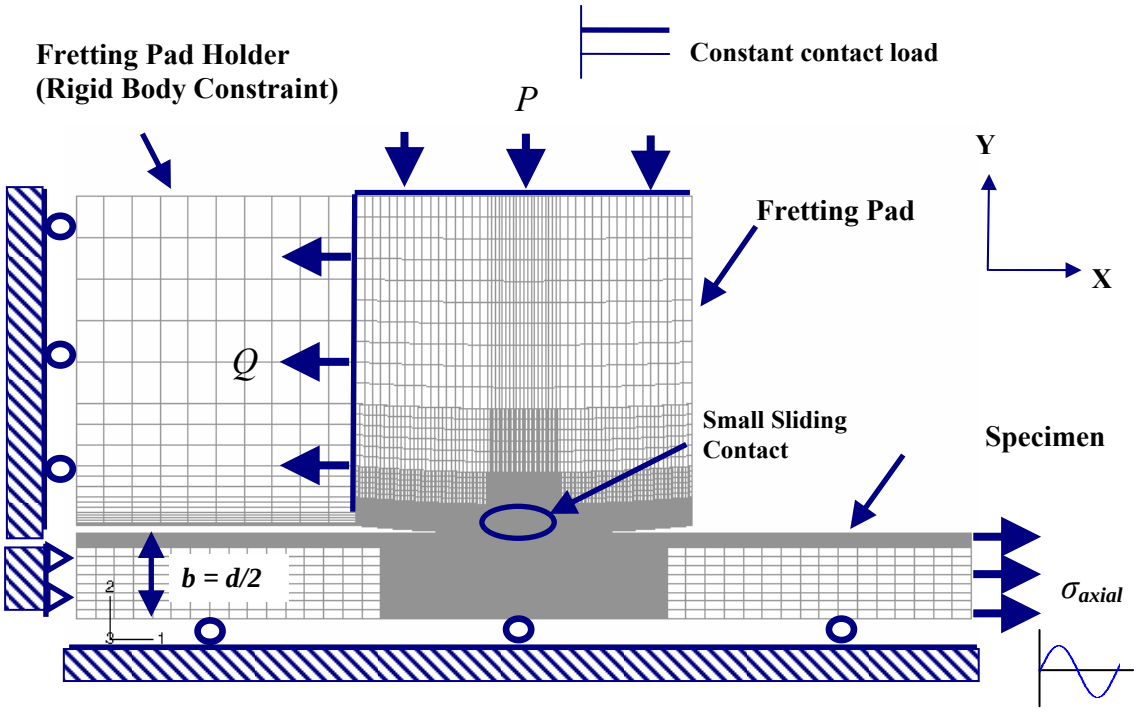

d = 6.35 mm

Figure 11. FEA Model with Load and Boundary Conditions [1]

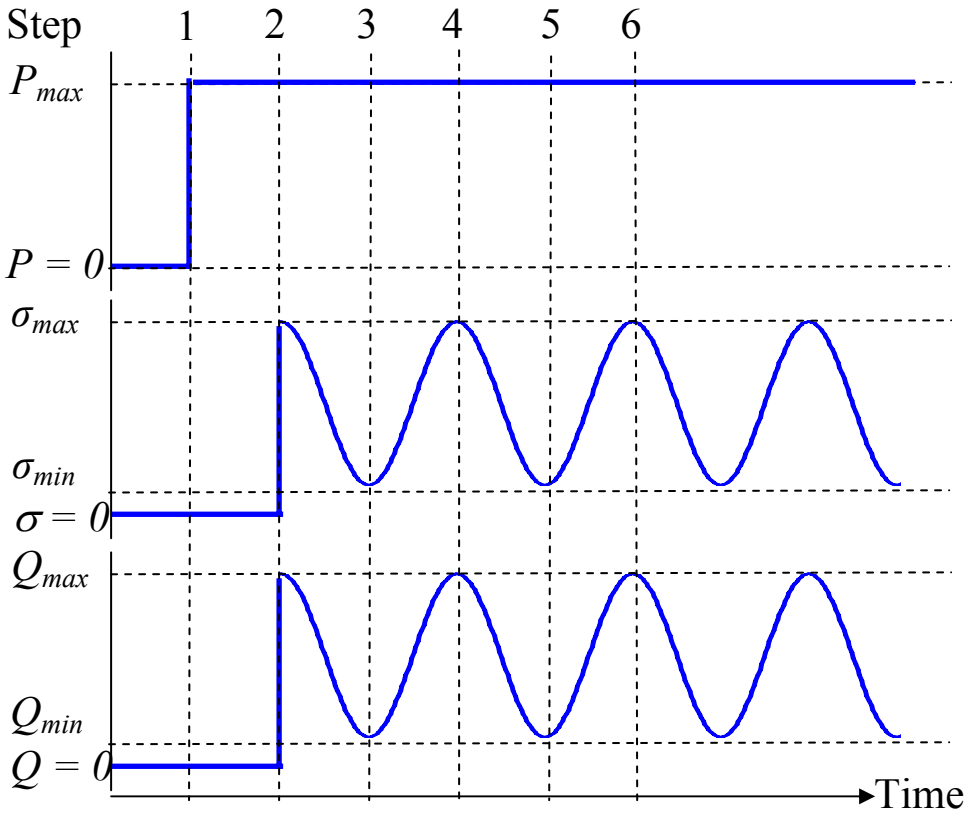

Figure 12. Load Sequences and Configurations

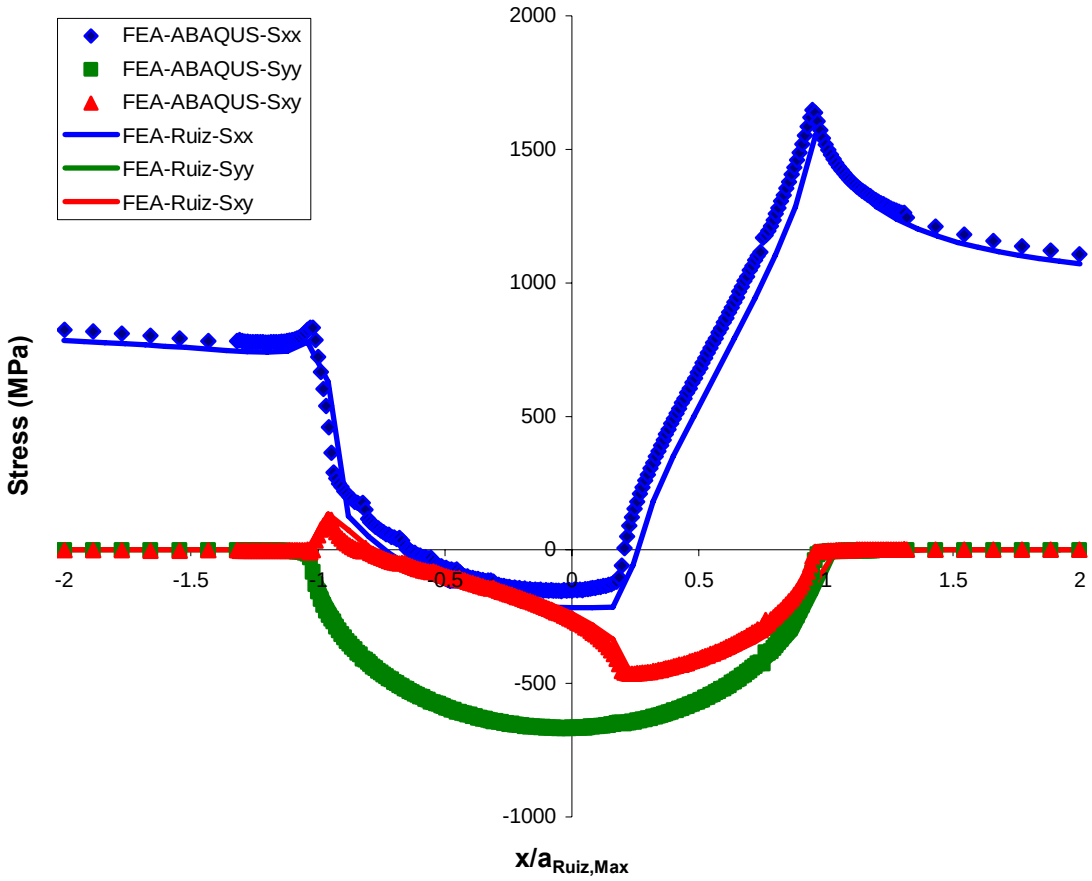

Figure 13. Stress Profiles Calculated from ABAQUS and Ruiz Program along Contact Surface at Step 2 (Test #9)

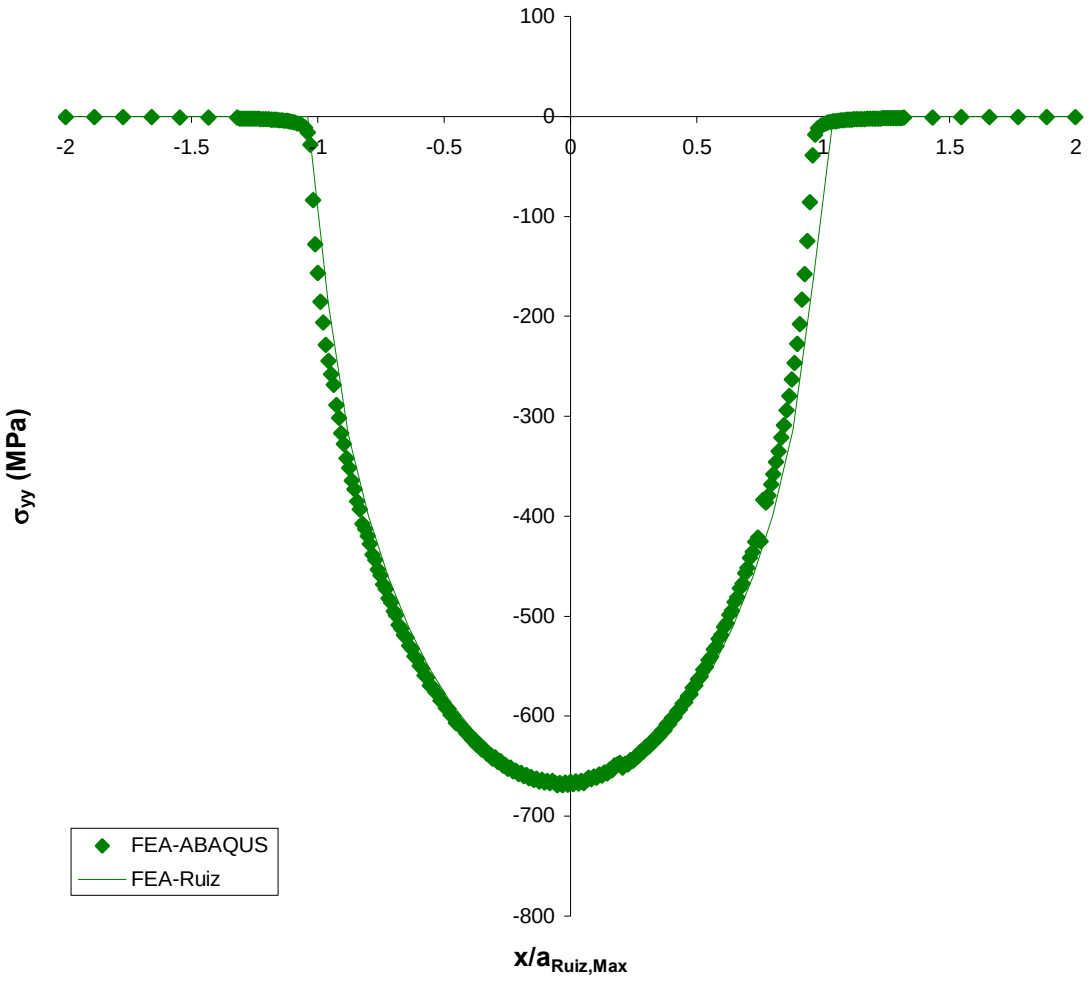

Figure 14. Stress Profile Calculated from ABAQUS and Ruiz Program along Contact Surface at Step 2 for Hertzian Peak Pressure (Test #9)

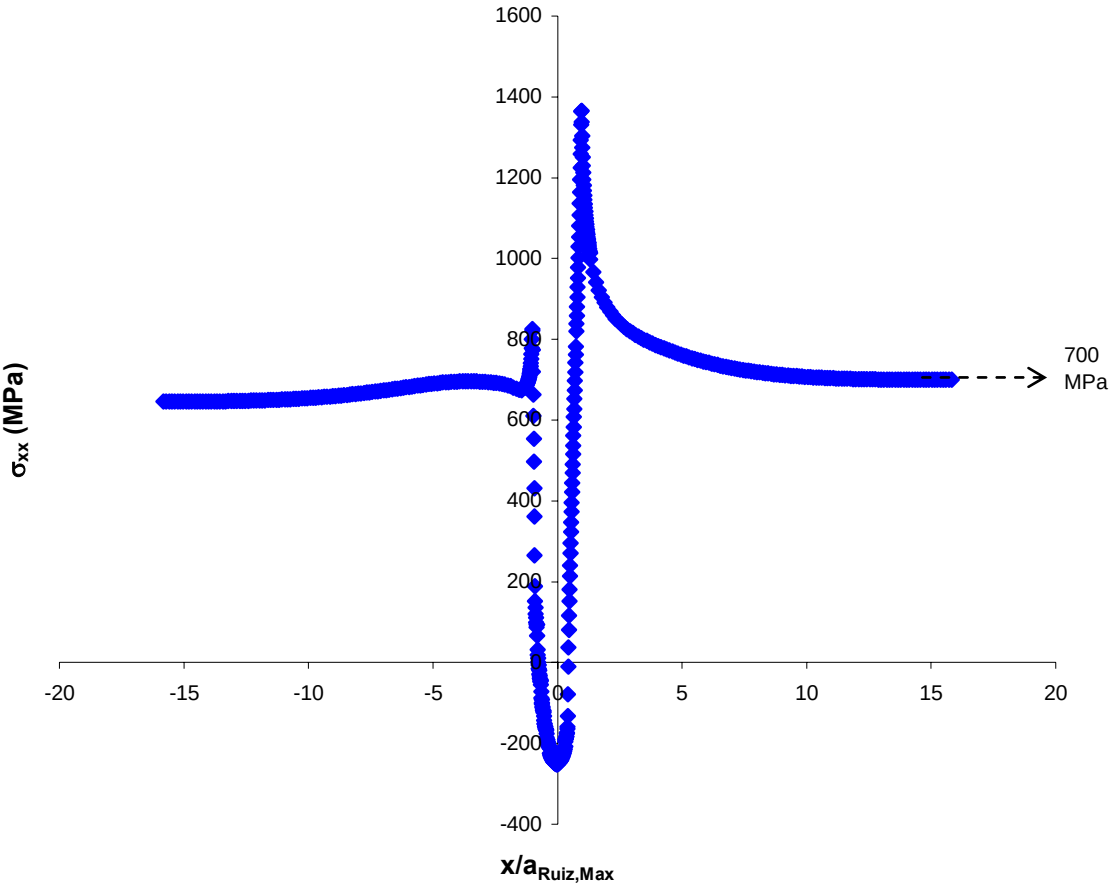

Figure 15. Stress Profile Calculated from FEA for σ_{xx} far away from the Contact Region at Step 2 (Test #9)

5 Analysis

This chapter discusses the two critical plane based parameters to characterize the fretting fatigue behavior of IN100: the SSR and MSSR parameters. Additionally, the method used in this study to account for shot-peening induced residual stress along with stress relaxation on the SSR and MSSR determination for shot-peened specimens is also elaborated.

5.1 SSR Parameter

From the discussion in Section 2.4.4, the SSR parameter was a parameter that only considers maximum and minimum shear stress on the critical plane. It was shown that the SSR was useful in associating fretting fatigue life with plain fatigue life. However, for shot-peened specimens it was shown that under fretting fatigue conditions, this parameter was only effective in crack initiation orientation and failed in predicting fatigue life and crack initiation location.

The formula defining the SSR parameter was expressed in Equation (12). In this study, thorough SSR calculations were performed using FEA stress outputs superimposed with the corresponding residual stress value along all planes from $-90^{o} \leq \theta \leq +90^{o}$ in 0.1° increments throughout the whole specimen, where θ is the orientation at which stress state in material is observed. Since two load steps are needed in the finite element analysis for the determination of MSSR, these steps were computed at the peak and valley of axial loads within the test as shown in Figure 12. After the steps were completed, the outputs were then analyzed in latter sections for its location, orientation, and correlation with fretting fatigue life under cyclic axial load conditions.

5.2 MSSR Parameter

Based on the discussion presented in Section 2.4.6, the MSSR parameter was the only critical plane-based parameter which was very effective in predicting fretting fatigue life, crack initiation location, and crack initiation orientation simultaneously in the titanium alloys. Also, MSSR can also take into consideration the effects from multi-axial loading in the contact region, as is the case of a fretting fatigue condition. Based on these observations, the MSSR parameter was looked into in this study as a critical plane-based parameter to be used for predicting fretting fatigue behavior for nickel alloys.

The formula defining the fatigue predictive parameter, MSSR, is explained in section 2.4.6, and is expressed in Equation (14). In this study, comprehensive MSSR calculation was conducted in the same manner as the SSR parameter, which is detailed in Section 5.1.

5.3 Residual Stress

For shot-peened specimens, the determination of shot-peening induced residual stress is crucial because this residual stress must be superimposed to FEA stress solutions to carry out the SSR and MSSR parameter calculations. Residual stress is considered as a bi-axial stress tensor, that is, $\sigma_{xx} = \sigma_{yy}$ and $\sigma_{xy} = 0$. But we know that $\sigma_{yy} = 0$ at a free surface and we measure $\sigma_{xx} \neq 0$ at the surface with XRD. Thus, $\sigma_{xx} \neq \sigma_{yy}$. In addition, the residual stress profile can be distinguished into two portions, compressive stress near the peened surface and tensile stress in the interior of specimens after a specific depth. The compressive residual stress profile may be susceptible to shot-peening specifications. Readers can refer to Section 2.3 for a comprehensive discussion on shot-peening process and the nature of the induced residual stress.

In this study with shot-peened specimens, the original compressive stress along the specimen surface was chosen to be -920 MPa for the 7A specimens and -830 MPa for the 12A specimens which was found using X-ray diffraction technique.

5.4 Stress Relaxation

From the Martinez study [21], after specimens failed due to fretting fatigue cycles, residual stress within the contact zone was subjected to a complete (100%) relaxation. Additionally, Lee et al. [14,15] found that for specimens shot-peened under 7A specification, residual stress relaxation occurred evenly at different depths of specimens. Martinez [21] also observed that for specimens that were shot-peened under 4A and 10A specifications, these specimens, before failure occurred, were subjected to 20% and 40% stress relaxation within the contact region after 25,000 and 2 million fretting fatigue cycles, respectively.

In summary, residual stress within the contact zone relaxed with the increasing fretting fatigue cycles, and the relaxation increased from 0% relaxation before applying fretting fatigue cycles until a complete (100%) relaxation happened at specimen failure. This relaxation phenomenon occurs evenly at locations with the same depth in a specimen [15]. However, the exact correlation between fretting fatigue cycles and residual stress relaxation rate is still unclear.

In order to investigate the effects from residual stress and stress relaxation on the MSSR parameter, this study used the initial residual stress profile as presented in Figure 16 and assumed stress relaxation occurred uniformly at different depths of specimens. Further, 0% and 100% stress relaxation were applied during the SSR and MSSR computations, to be discussed in Chapter 6.

This previously mentioned assumption accompanied with uniform relaxation rate at different depths was used to determine the residual stress profile, which was then superimposed to the ABAQUS stress solution for SSR and MSSR determination. The MSSR calculation results under stress relaxation are discussed in further detail in Chapter 6.

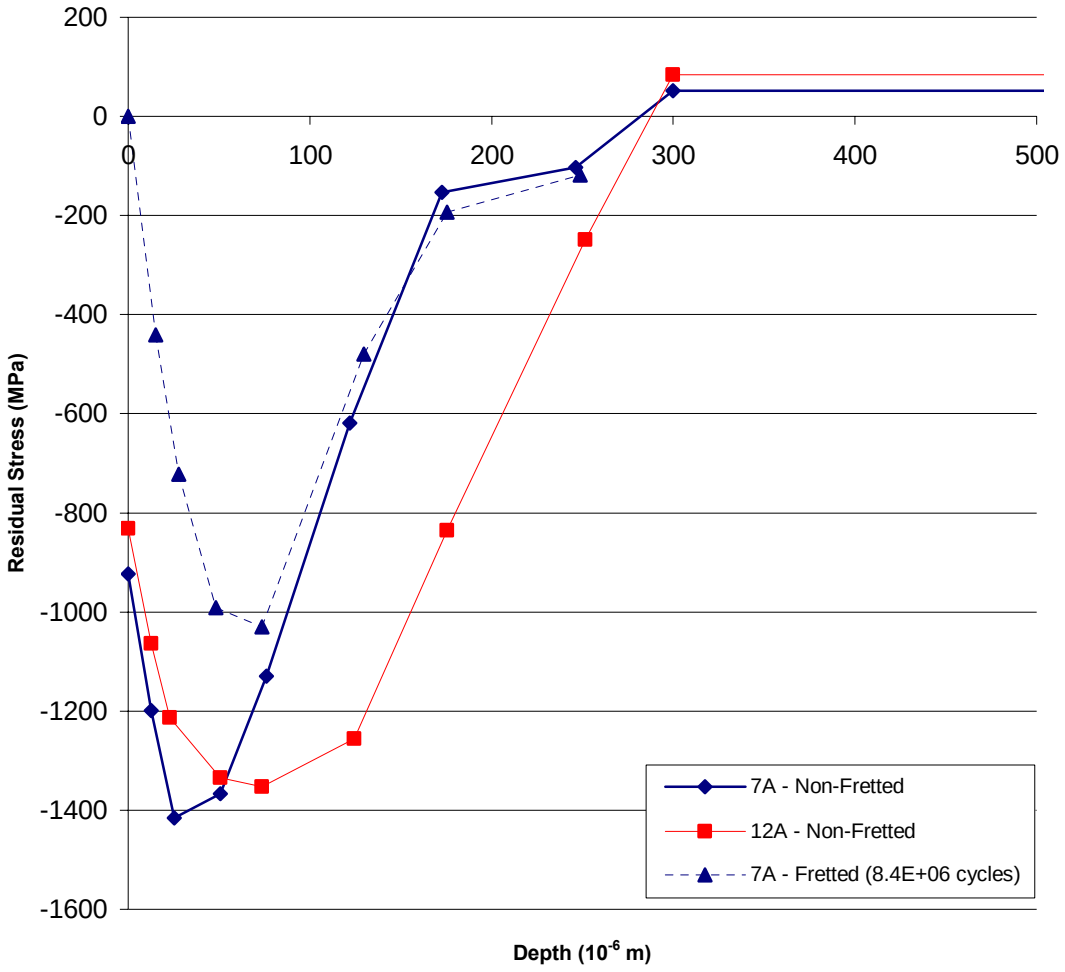

Figure 16. Residual Stress Profile Used in this Study for Shot-Peened Specimens

6 Results and Discussion

This chapter addresses the results from experimental tests, finite element analysis (FEA), and analysis of fatigue life data using two critical plane based fatigue parameters (SSR, MSSR). The analysis of fracture surface, crack initiation mechanism, fatigue life, stress solutions from FEA, SSR and MSSR prediction, and the effects of exposure to shot-peening intensity are also summarized and discussed in this chapter.

6.1 Experimental Results

Eleven fretting fatigue tests were accomplished in this study, and the experimental results for the fretting fatigue tests are summarized in Table 1 which also includes results from earlier studies [18] for comparison. Among the fretting fatigue tests, four tests were of specimens with shot-peening intensity 7A and seven tests were of specimens shot-peened at 12A.

6.1.1 Determination of Fretting Fatigue Condition

Fretting fatigue conditions were determined from the hysteresis loops between the tangential load and the axial load of the test as shown in Figure 17. This figure shows a partial slip fretting condition was achieved just after 10 cycles. Figure 18 shows that after a steady fretting fatigue configuration was reached, tangential loads remained stabilized until the end of the test. Considering Figures 17 – 19 together, it was clear that for this study, a partial slip fretting fatigue condition was met within a few hundred fretting fatigue cycles and continued until the final cycles of the experiments. Basically, a steady-state fretting fatigue configuration was quickly met among all good tests after relatively few fretting fatigue cycles, and after that, all fretting variables (coefficient of

friction, contact load, tangential load, and axial load) remained in a stable condition throughout the majority of the fatigue life until the specimen broke into two pieces.

6.1.2 Q/P Ratio

The *Q/P* ratio was determined by dividing the tangential load (*Q*) by the contact load (*P*). The maximum *Q/P*, $(Q/P)_{max}$, ratio is considered as the lower boundary of the static coefficient of friction between a fretting specimen and pads in order to prevent gross slip condition. The maximum *Q/P* ratio for all tests was less than 0.75 therefore this value was used as a constant coefficient of friction for the finite element analysis as shown in Table 1. Figure 20 illustrates that under fretting fatigue, *Q/P* was proportional to axial load and was subjected to variation in value the cycling. In other words, *Q/P* was changing dynamically all the time under fretting fatigue tests, but $(Q/P)_{max}$ presented much smaller variation among different tests.

6.1.3 Characteristics of Tangential Load

Typical characteristics of tangential load were presented in Figure 21. The tangential loads always demonstrated a sinusoidal wave pattern and were in-phase with the corresponding axial load. Contact loads only played a role in affecting the magnitude of tangential loads but had no effect on their waveform, frequency, or phase lag. This plot also provided the information about how to discretize a continuous load condition from experimental tests into discrete load steps for FEA modeling as mentioned before in Figure 12. Comparison between Figure 12 and Figure 21, shows that they both have the same pattern and features in terms of load conditions, and hence the load inputs for FEA model were verified by these experimental outputs.

6.1.4 Fracture Surface

Fracture surfaces of specimens were examined with optical and scanning electron microscopes (SEM). Due to the magnetic nature of nickel alloys, no high-resolution, high-magnification pictures could be taken with the SEM. It is therefore impossible to see any fine details, like striations or microstructure. However, from low magnification pictures, four distinguishable regions are present (see Figure 22), as seen in previous studies [1]. There is debris in Region 1; there are probably striations in Region 2; there are dimples in Region 3, and catastrophic fracture in Region 4. Figure 23 explains the pattern observed in Region 1, where the crack initiated and grew in its early stages. Figure 24 shows the magnified view of Region 3. Figure 25 shows a closer view of the region of crack initiation; note the river marks (highlighted by the dashed lines) which all point to the region of initiation. Further, these river marks point out that the crack initiated on the contact surface. Region 2 would probably show fine striations with grain boundary; this was the main region for crack propagation. Large dimples with grain boundary definition were found in Region 3 as presented in Figure 24. In Region 4, ultimate unstable crack growth occurred which was characterized by the ductile tearing and shear lip, resulting in catastrophic failure.

6.1.5 Fatigue Life Diagrams

To determine the fatigue life for both shot-peened and unpeened specimens, S-N curves were developed using both stress range, Equation (1), and effective stress, Equation (2). Figure 26 was plotted using stress range and shows that all specimens where 7A and 12A shot-peened, and unpeened, exhibited the same fatigue life trend, despite the differences in shot-peening induced residual stress. Figure 27 was plotted

using effective stress and shows a similar trend as Figure 26. From these, it can be concluded that the effects from shot-peening were negated very early in the fatigue life. The reason for this behavior was the stress relaxation phenomenon, which will be discussed in future sections.

6.1.6 Contact Half-Width

On the fretting pads, there is a visible stick zone with partial slip regions on either side just as the deformed contact model demonstrated in Figure 4. A contact region, termed as $2a_{Exp,max}$ was defined by incorporating both the stick zone and partial slip regions. Figure 28 shows the scar pattern on a fretting pad from Test #9. From the fretted region of Test sample #2, $2a_{Exp,max} = 0.6985$ mm (see Figure 29). Contact half-widths were calculated from the Ruiz program, for example Test #2: $2a_{Ruiz,max} = 0.602$ mm. The percent error between the experimental and analytical half-widths was 16%. These measurements also confirmed that contact half-widths were only affected by the magnitude of the constant contact load and independent upon the axial load conditions as predicted by Equation (25).

6.1.7 Crack Initiation Location and Orientation

In general, crack initiation location in all tests, as shown in Figure 29, always occurred at the trailing edge, at a location where $x/a_{Exp,max} \approx +1$ along x-direction. This matches the location where σ_{xx} is a maximum based on FEA outputs (see Figure 34) and where SSR and MSSR values are also maximized. It can be concluded that the crack did initiate at the point of maximum stress, which matches expectations.

In a previous study [36] of a 7A shot-peened specimens of titanium alloy tested at room temperature, the orientation of crack initiation ranged from -37° to -54° and was

reported that crack orientation for shot-peened specimens could fall within the angle 45°± 15°. Figure 30 shows the crack orientation for a 12A specimen (Test #9). As shown, the crack orientation is approximately -46^{o}, which falls well within the predicted crack orientation range.

6.2 Finite Element Analysis

Using the load details discussed in Section 4.3, the experimental load values shown in Table 1 were applied to a FEA model to determine the stresses, strains, and displacements within the entire specimen. The issues discussed in this section include σ_{xx} stress concentration, asymmetric distribution of σ_{yy}, evolution of stress state at different depths within the specimen, and the influence of residual stress on stress profile.

6.2.1 Stress Profile with Residual Stress

In the rest of the text, samples with 100% relaxation (i.e.: 0% residual stress) will be referred to as (100%R), and samples with 0% relaxation (100% residual stress) will be referred to as (0%R). The stress relaxation phenomenon is explained in detail in Section 5.4.

Figure 31 (Test #9) shows stress profiles at different depths for a shot-peened specimen with 100%R, which is identical to the case of an unpeened specimen. As depth increased, σ_{xx} at the trailing edge decreased and the profile, in general, flattened out. The corresponding graphs for σ_{yy} and σ_{xy} are shown in Figures 32 and 33. To investigate the effect of residual stress on stress states in the contact region during fretting, residual stress profiles in Figure 16 were superimposed onto the calculated stresses from FEA.

The influence on stress profiles from the stress relaxation on the contact surface (depth = 0 μm) at Step 2 of Test #9 is shown in Figures 34 - 36. Figure 34 shows the

peak σ_{xx} reduced from 1650 MPa (100%R) at $x/a_{Ruiz,max}$ = 0.948 to 790 MPa (0%R). Hertzian peak pressure was also lowered from -669 MPa at $x/a_{Ruiz,max}$ = -0.031 (100%R) under, to -1500 MPa (0%R). No effect on σ_{xy} stress distribution from stress relaxations was found as expected since residual stress was assumed as bi-axial distribution, $\sigma_{xx} = \sigma_{yy}$ and $\tau_{xy} = 0$, and resulted in no contribution on σ_{xy} stress profile.

At a depth = 300 μm below the contact surface, the induced compressive stress, from shot-peening, transitions to the resultant tensile stress. It was assumed that the tensile stress distribution was uniform along the remaining 2.895 mm of the half-space. This corresponds to a uniform tensile stress of 51.2 MPa in the 7A shot-peened case, and a tensile stress of 83.5 MPa in the 12A shot-peened case. The influence of this compensatory tensile stress for Test #9 (12A shot-peened) is demonstrated in Figures 37 - 39. The maximum σ_{xx} increased form 990 MPa to 1073 MPa at $x/a_{Ruiz,max}$ = 2.0. Hertzian Peak Pressure increased from -679 MPa to -596 MPa at $x/a_{Ruiz,max}$ = -0.093. No effect was seen on σ_{xy} profile from different relaxation rates, just like the case observed along the contact surface.

Comparing the stress profiles on the contact surface without residual stress (100%R) to those at depth = 300 μm, the maximum σ_{xx} decreased from 1637 MPa to 990 MPa (see Figures 34 and 37). The slope of the σ_{xx} profile became flatter with increasing depth. However, comparing stress profiles on the contact surface with 0%R (100% residual stress) with those at depth = 300 μm, maximum σ_{xx} increased from 817 MPa to 1073 MPa (see Figures 34 and 37). It is clear that different amounts of stress relaxation changes the location of the maximum value of σ_{xx}, thus changing the crack initiation

location. As more and more relaxation occurs, the location of crack initiation will move from the interior of the specimen towards the contact surface.

6.3 SSR and MSSR

SSR and MSSR calculations were performed in this study for all tests at the surface and subsurface levels. The maximum SSR and MSSR values for each test were found. The correlation between SSR and MSSR values and fretting fatigue life were investigated, and the effects from stress relaxation are also discussed. The effectiveness of SSR and MSSR were also investigated in terms of fatigue life, crack initiation location, and orientation.

6.3.1 Determination of the Maximum SSR

The fatigue predictive parameter, SSR, was defined in Equation (12), and a detailed discussion for SSR is presented in Section 2.4.4. As mentioned in Section 5.2, the values of MSSR parameter were symmetric with respect to a full load cycle; therefore, SSR must also be symmetric with respect to a full load cycle. In addition, two load steps were needed for the SSR determination. In this study, the peak and valley of axial loads were sampled and numbered into discrete steps as shown in Figure 12. The SSR with the greatest value was chosen as the maximum SSR of that test and is further summarized in Table 2.

6.3.2 SSR under Residual Stress Relaxation

It should be mentioned that full relaxation (100%R) is equivalent to 0% residual stress imposed, which defines a condition where no residual stress is superimposed onto stress profiles and SSR calculation. The maximum SSR with 100%R had the larger value and decreased with depth. Once relaxations other than 100% was imposed, which was

0% (100% Residual Stress) in this study, the SSR parameter decreased with depth. This will be referred to as 0%R. Figure 40 compares SSR versus depth for 7A specimen (Test #1). Figure 41 compares SSR versus depth for 12A specimen (Test #9). It was noticed that the trends, 100%R and 0%R, lie within a scatter band. In both cases, the maximum SSR always occurred at the contact surface.

6.3.3 Determination of Maximum MSSR

The fatigue predictive parameter, MSSR, was defined in Equation (14), and a detailed discussion for MSSR is presented in Section 2.4.6. Since no fitting constants (A, B, C, D) have been established for IN100, the coefficients from Ti-6Al-4V (A = 0.75, B = 0.50, C = 0.75, D = 0.50) were used initially. As mentioned in Section 5.2 the values of MSSR parameter were symmetric with respect to a full load cycle. In addition, two load steps were needed for the MSSR determination. In this study, the peak and valley of axial loads were sampled and numbered into discrete steps as shown in Figure 12. The MSSR with the greatest value was chosen as the maximum MSSR of that test and is further summarized in Table 2.

6.3.4 MSSR under Residual Stress Relaxation

As mentioned, full relaxation (100%R) is equivalent to 0% residual stress imposed, which defines a condition where no residual stress is superimposed onto stress profiles and MSSR calculation. The maximum MSSR with 100%R had the highest value. Once relaxations other than 100% was imposed, which was 0% (100% Residual Stress) in this study, the MSSR parameter varied in depth. This will be referred to as 0%R. Figure 42 compares MSSR versus depth for 7A specimen (Test #1). Figure 43 compares MSSR versus depth for 12A specimen (Test #9). It was noticed that the

100%R trends were very similar to the SSR graphs (see Figures 40 and 41). However, when residual stresses were included (0%R), the trends looked like the residual stress profiles (see Figure 16), which was due to the significant difference between 100%R and 0%R stress values. The residual stress values clearly had a considerable effect on the MSSR values compared to the SSR values.

6.3.5 Crack Initiation Details

All tests showed crack initiation at the surface based on the SSR and MSSR calculations for the 7A and 12A specimens from this study. As discussed in Section 6.3.2, for all tests, the maximum SSR value occurred at the contact surface for both 100%R and 0%R cases. This would predict that the cracks initiated at the contact surface of the specimens.

SSR and MSSR predictions for crack initiation locations and orientations are summarized in Table 2. For example in Test 4 the maximum MSSR was found near the trailing edge at locations where $x/a_{Ruiz,max} = 0.95$. Another example was MSSR prediction of crack orientation in Test 6 were the angle was 38.3˚ which is close to what is expected experimentally, between 30^o - 50^o. It can be seen that the MSSR parameter was good in predicting the crack initiation location, and orientation.

6.3.6 Fatigue Life (SSR and MSSR)

Figure 44 shows a comparison between the SSR versus fatigue life, N_f, relationships for 7A specimens with different relaxation percentages (100%R, 0%R). Figure 45 shows a comparison between the SSR versus fatigue life, N_f, relationships for 12A specimens with different relaxation percentages (100%R, 0%R). Note how, for both shot-peening intensities, the trends lie practically on top of each other. Figure 46 shows a

comparison between SSR versus fatigue life for unpeened samples. Figure 47 shows SSR versus N_f for all three cases. Notice how both trends for 7A and 12A are almost identical. From this data, the author concluded that different shot-peening intensities did not have a significant effect on the fretting fatigue life of IN100 samples. However, shot-peening, in general, did seem to change the effect on SSR versus N_f in this study.

The SSR parameter did seem to be a good predictive tool for predicting fretting fatigue life. The data for unpeened, 7A, and 12A specimens all exhibited similar trends. Also, the locations for crack initiation were in the region of $x/a_{Ruiz,max} \approx 1$ (ranged from 0.92 - 0.96), which indicates that the cracks initiated around the trailing edge. It also output crack orientations between 38^o and 49^o. These values are consistent with what is expected in fretting fatigue.

Figure 48 shows a comparison between the MSSR versus fatigue life, N_f, relationships for 7A specimens with different relaxation percentages (100%R, 0%R). Figure 49 shows a comparison between the MSSR versus fatigue life, N_f, relationships for 12A specimens with different relaxation percentages (100%R, 0%R). The trends seemed be shifted to lower values by the incorporation of residual stresses (100%R to 0%R) into the MSSR calculations, but they remain similar. Figure 50 shows a comparison between MSSR versus fatigue life for unpeened samples. Figure 51 shows MSSR versus N_f for all cases. Notice how the 100%R and 0%R points follow respective trends (denoted by the solid line for 100%R and dashed for 0%R). Contrary to the SSR parameter, there is a significant difference between the 100%R and 0%R cases. However, the trends are merely displaced down to lower MSSR values; the order or general trend was not changed. From this observation, the author confirmed his earlier conclusion that different

shot-peening intensities did not have a significant effect on the fretting fatigue life of IN100 samples. However, shot-peening, in general, did seem to change the effect on SSR and MSSR versus N_f in this study.

6.3.7 SSR versus MSSR

Studying the difference between the SSR versus depth and MSSR versus depth graphs (Figures 40 and 41 and Figures 42 and 43, respectively), it is clear that residual stresses played a greater role on the MSSR parameter than on the SSR parameter. It is also clear from these results that normal stress played a role in determining fretting life in IN100. In SSR, the residual stresses had no effect on the parameter's value. The 100%R cases lay almost completely on top of the 0%R cases. In the MSSR case, the 100%R cases had a similar trend to the 100%R SSR cases. However, when residual stresses were introduced to the σ_{xx} and σ_{yy} values, the 0%R MSSR cases had significantly different trends. This is due to the basic difference in the SSR and MSSR parameters: the MSSR parameter includes the normal stress on the critical plane.

Based on this analysis, the author concluded that MSSR was a better parameter for evaluating fretting fatigue life. While both maximum SSR and maximum MSSR were good predictors of fatigue life, crack initiation location, and crack orientation, only MSSR was sensitive to residual stress effects. This is an important factor to include when working with cold-worked substances. Also, MSSR includes the fitting constants (A, B, C, D) to allow trends to be effectively related. This provides for more versatile usage and extrapolation to similar substance. The effects of the fitting coefficients will be further discussed in Section 6.3.9.

6.3.8 Mixed Relaxation

Figure 16 shows the residual stress profiles for the shot-peened specimens used in this study. Notice that the residual stress profiles of the initial-7A and fretted-7A specimens merge at (*depth* > 75μm). Therefore, it is not unreasonable to assume that the relaxation at (*depth* > 75μm) is practically zero (0%R). For simplification, it was also assumed that for (0μm < *depth* < 75μm), the relaxation was complete (100%R). This relaxation case will be called the "mixed relaxation case." Figure 52 shows the MSSR versus N_f for the mixed relaxation case and unpeened case. Note that when compared to the maximum MSSR values for the 100%R case, the mixed relaxation case's values are the same. Table 3 summarizes the maximum MSSR values, crack initiation locations, and crack orientations for the mixed relaxation case. For the mixed relaxation case, the maximum MSSR values occur at the contact surface, and thus, crack initiation is also predicted at the surface with this more-accurate relaxation case.

6.3.9 MSSR Fitting Coefficients

As mentioned in Section 2.4.6, MSSR incorporates four fitting constants (A, B, C, D), which are determined empirically through curve-fitting. Clearly, any use of such fitting constants must be studied prior to application. It would be useless to the user if adjustments to these constants affected the trends in any drastic manner (i.e.: changed the order of points, changed the slope of the trend to be nearly horizontal or vertical, eliminated any sort of trend, etc.). Figure 53 shows the effects of changing the fitting constants on the mixed relaxation case. "Mixed – Original" shows the trend when the original coefficients from Ti-6Al-4V were applied. For the other trends, the corresponding constant was increased by 0.25. For instance, the "Mixed – A" trend

shows the effect of A increasing from 0.75 to 1.00 and "Mixed – B" shows the trend of increasing B from 0.50 to 0.75. As shown, adjustments will not significantly affect the general trends of the MSSR values, as long as one constant does not get drastically larger or smaller than the others. (Note: Making one of the constants drastically larger or smaller will effectively negate the contribution of one of the main terms of Equation (12) ($\Delta\tau_{crit}$ and σ_{max}). For instance, if A or B was made to a value approaching zero, that would effectively eliminate the contribution of $\Delta\tau_{crit}$ to the MSSR value.)

Increasing A or C has a similar effect; the slopes are not changed much, but the values have almost uniformly increased. Increasing B or D has a more significant effect by significantly changing the slopes; however, this makes sense, since B and D are exponents. However, the trends still remain, as shown by lining up the MSSR values at the same N_f. MSSR values still decrease with increasing fretting fatigue life in all cases and the slopes are not near either extreme (m = 0 or ∞). Therefore, the author concluded that changing the coefficients does not have any adverse effects on the MSSR versus N_f trends. Knowing this, it would be allowable to adjust the fitting constants to plot unpeened and peened cases to a single trend.

The goal was to bring the trends to converge to a single trend while keeping its slope not less than the slopes of the original trends. A flat slope is not acceptable because it relates that a small change in MSSR value correlates to a difference in the millions of cycles in fretting fatigue life. Figures 54 and 55 show iterations of the MSSR fitting coefficients. As shown in Figure 52, increasing the exponential coefficients, B and D, causes the curves to diverge since the slopes become more different from each other. In Figure 54, the exponential coefficients (B and D) were reduced to try to make the two

trends converge. As shown, this caused the slopes to become too flat. To remedy this, the multiplier coefficients (A and C) were increased (see Figure 55). However, once the slopes were at an acceptable grade, divergence had occurred again. Numerous iterations were performed, all leading to divergence of the trends.

One reason why trends could not converge is that the specimens are different due to the shot-peening induced compressive residual stresses. The surface of the shot-peened specimen has been plastically deformed while the unpeened specimen remains unchanged. Since MSSR predicts fretting fatigue life, crack initiation location, and orientation of one type of material at a time, and the peened and unpeened specimens are now of two different types of material, it cannot be expected that MSSR can unify these two types of materials. Two different types of material do not act the same way under fretting fatigue conditions.

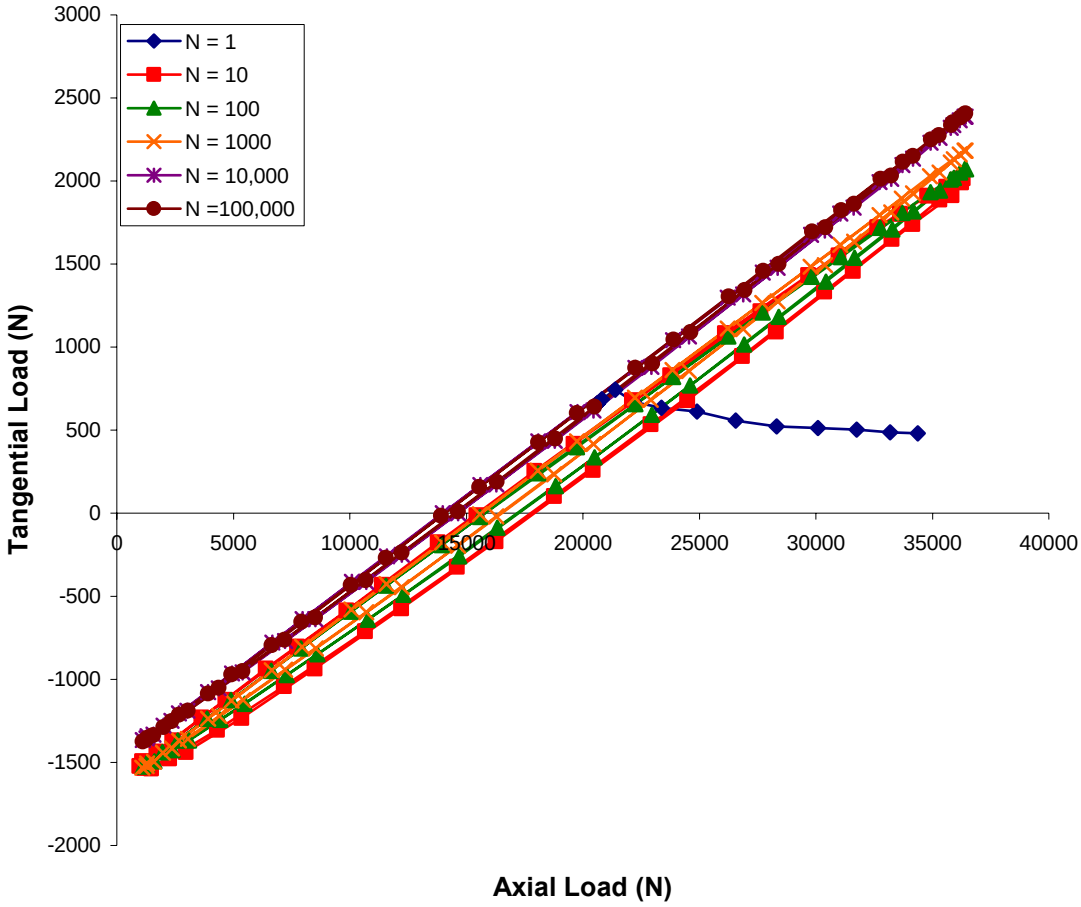

Figure 17. Typical Hysteresis Look of Tangential Load versus Axial Load (Test #1)

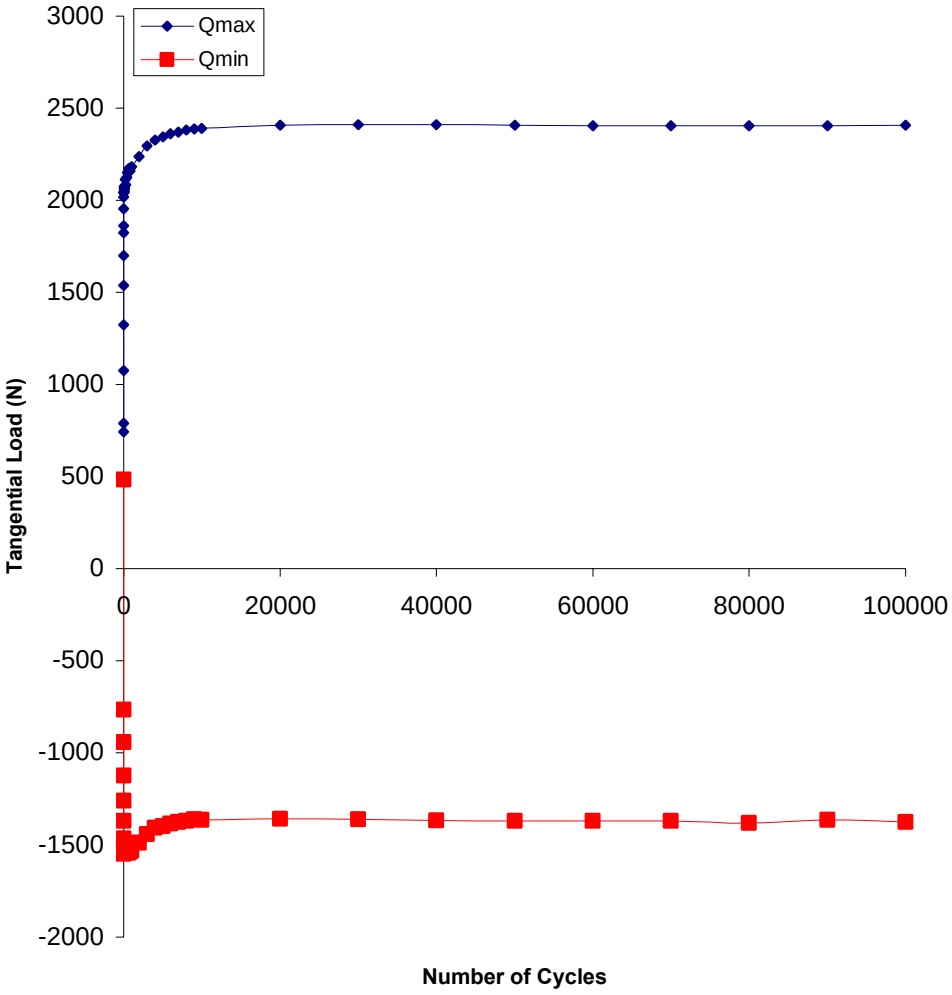

Figure 18. Q_{max} and Q_{min} versus Number of Cycles (Test #1)

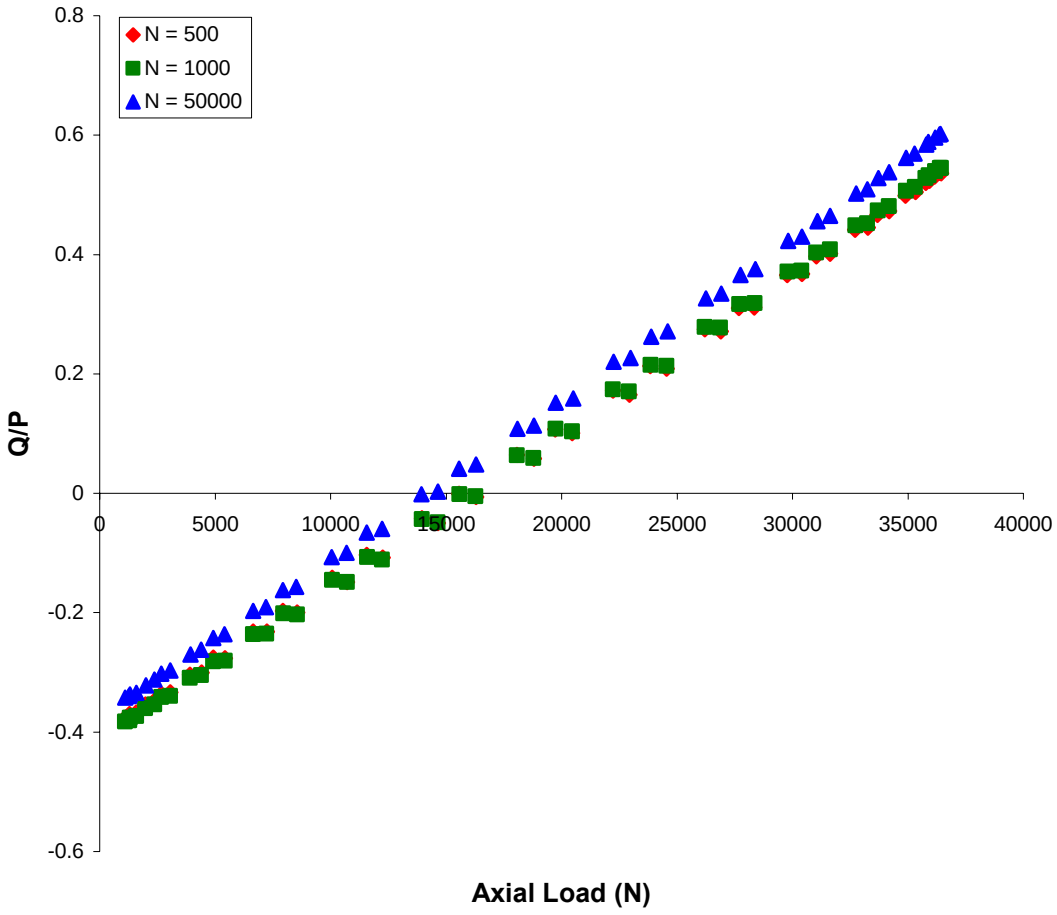

Figure 19. Q/P versus Axial Load (Test #1)

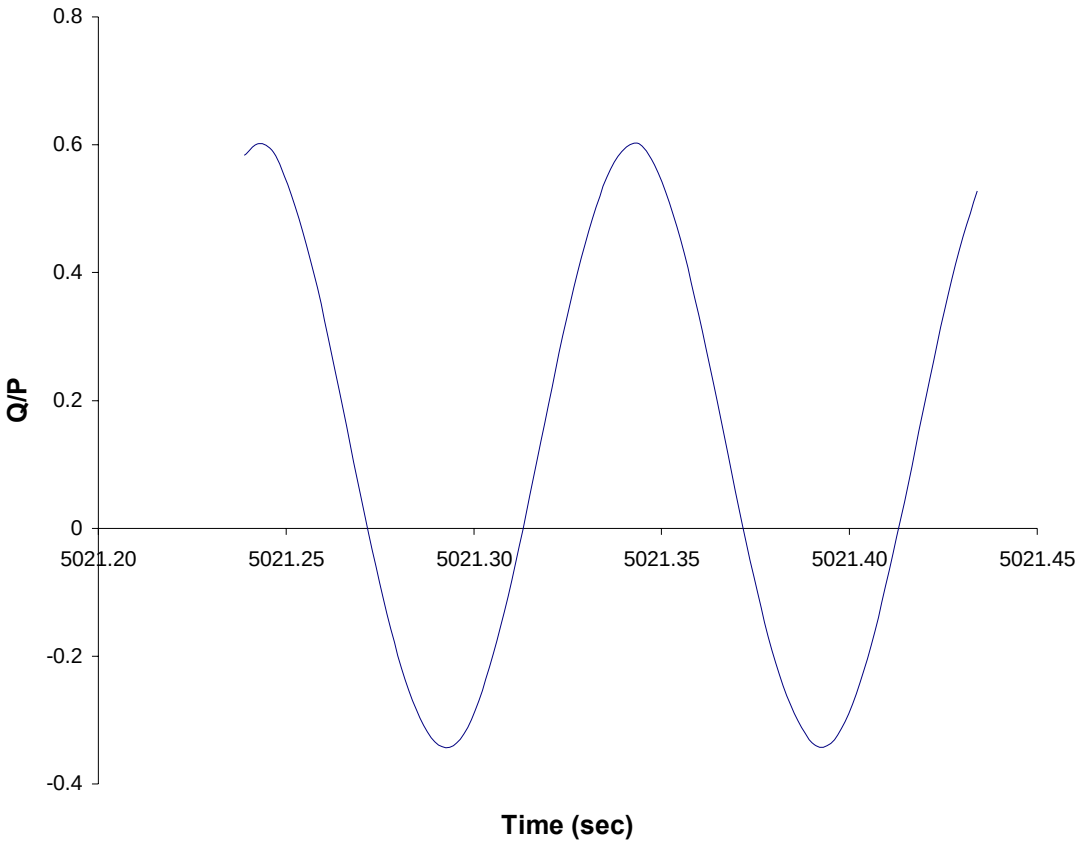

Figure 20. Q/P versus Time at N = 50,000 (Test #1)

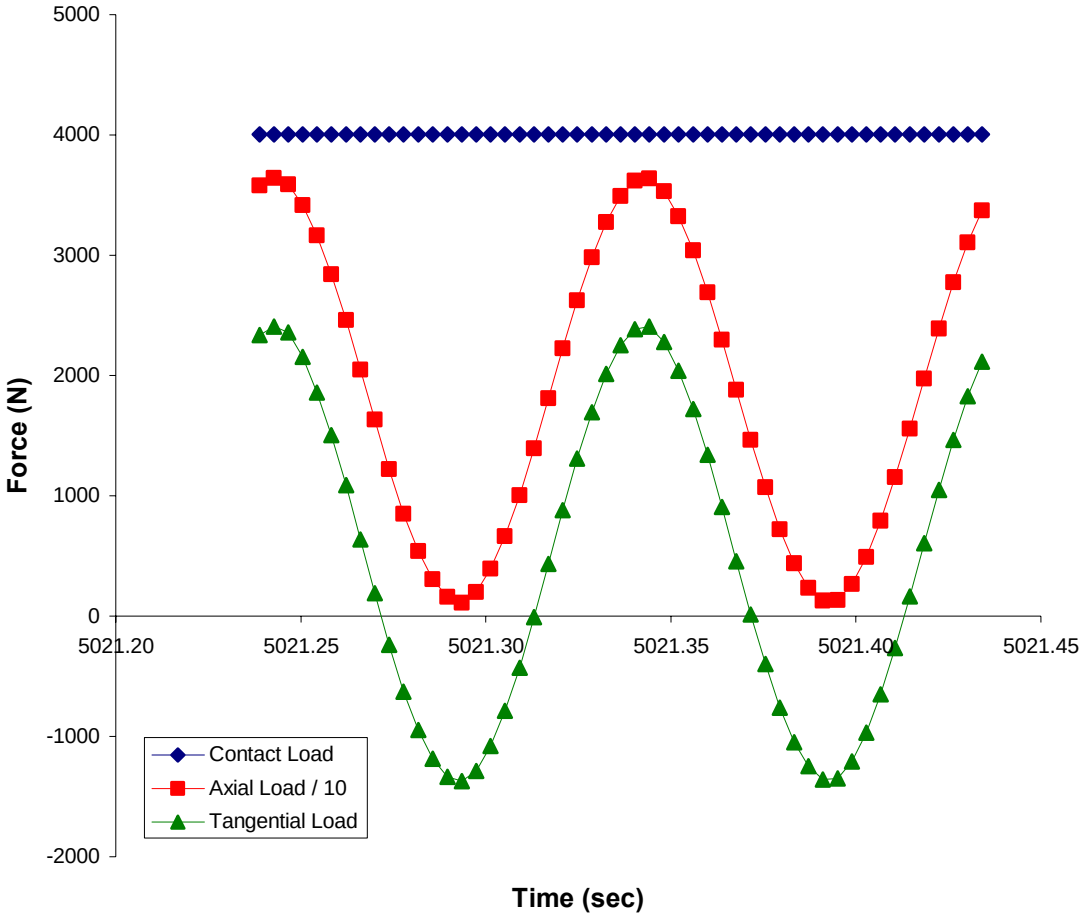

Figure 21. Relations between Axial Load, Contact Load, Tangential Load at N = 50,000 (Test #1)

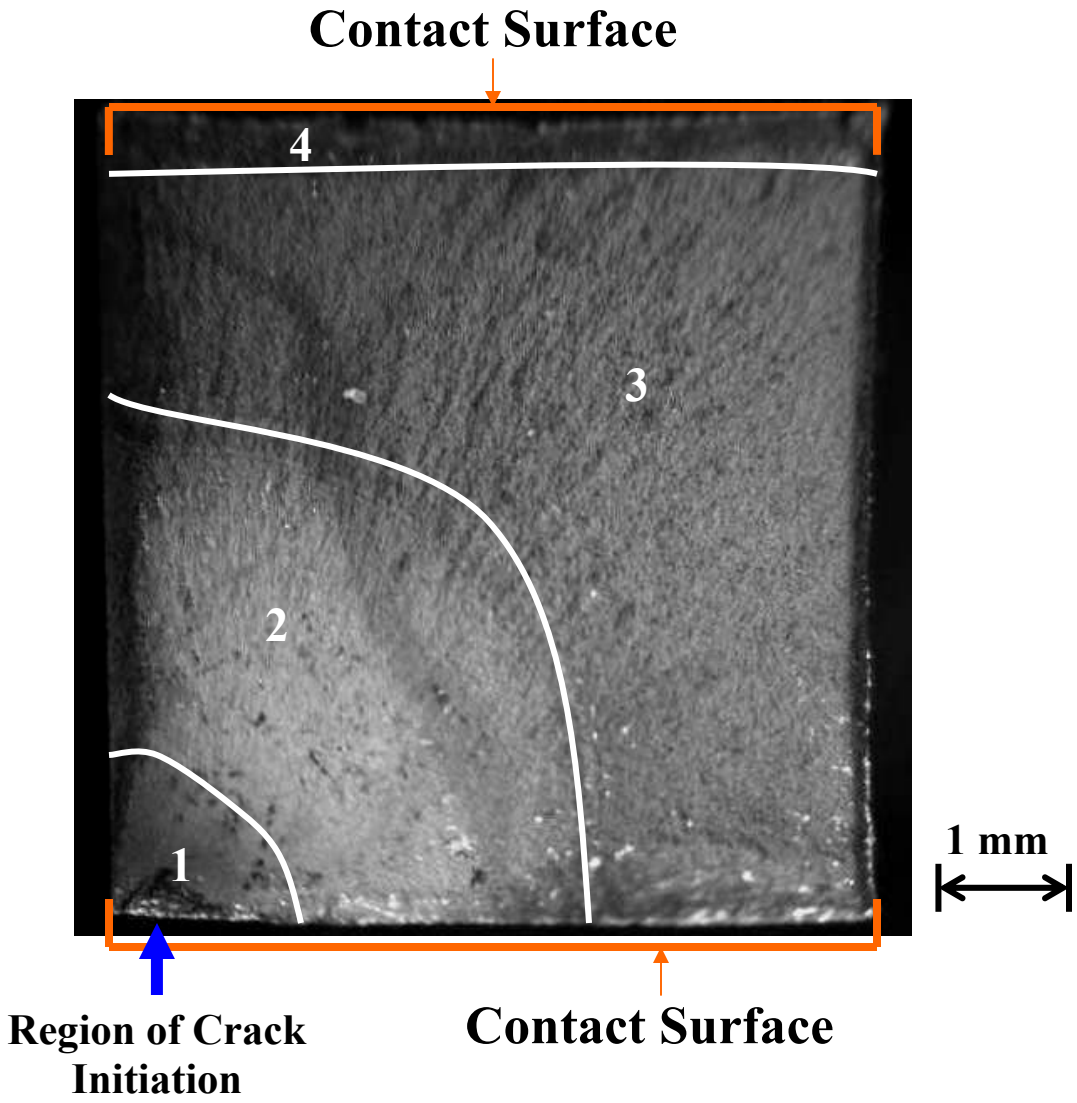

Figure 22. Typical Fracture Surface (Test #2)

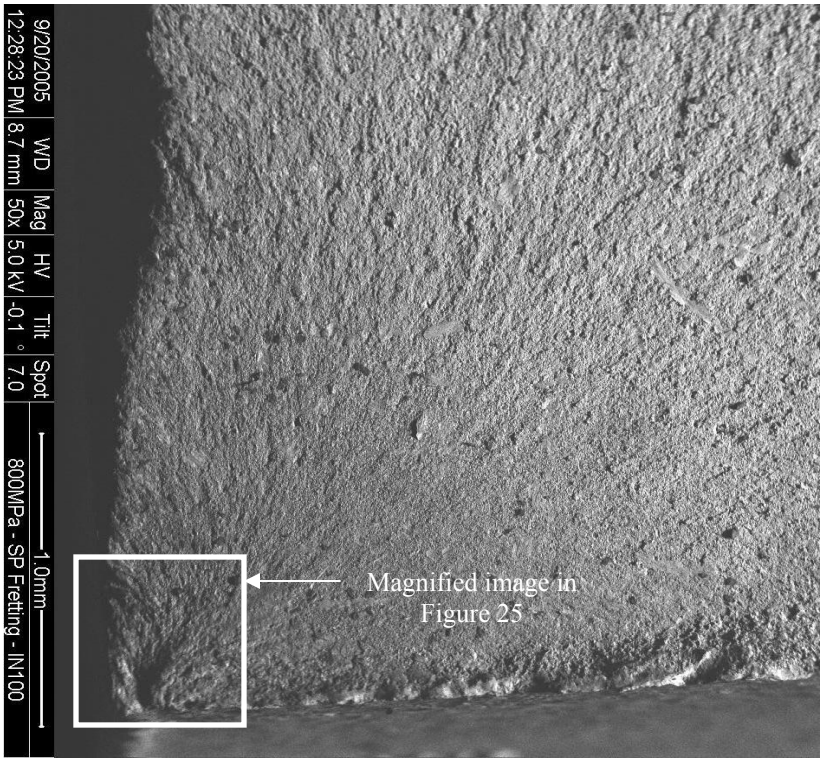

Figure 23. Debris at Region 1 (see Figure 22)

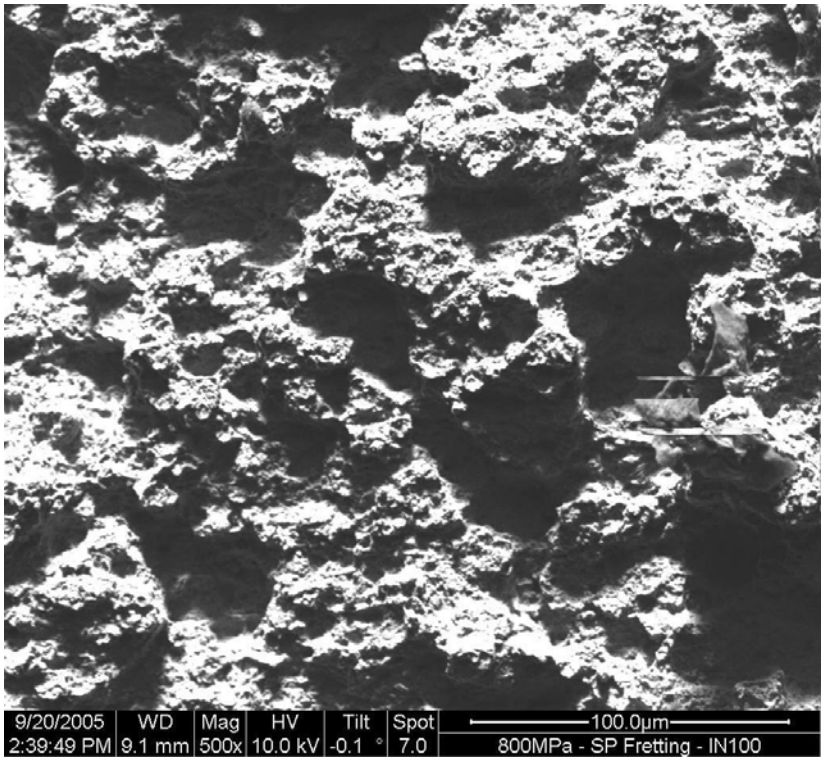

Figure 24. Large Dimples at Region 3 (see Figure 22)

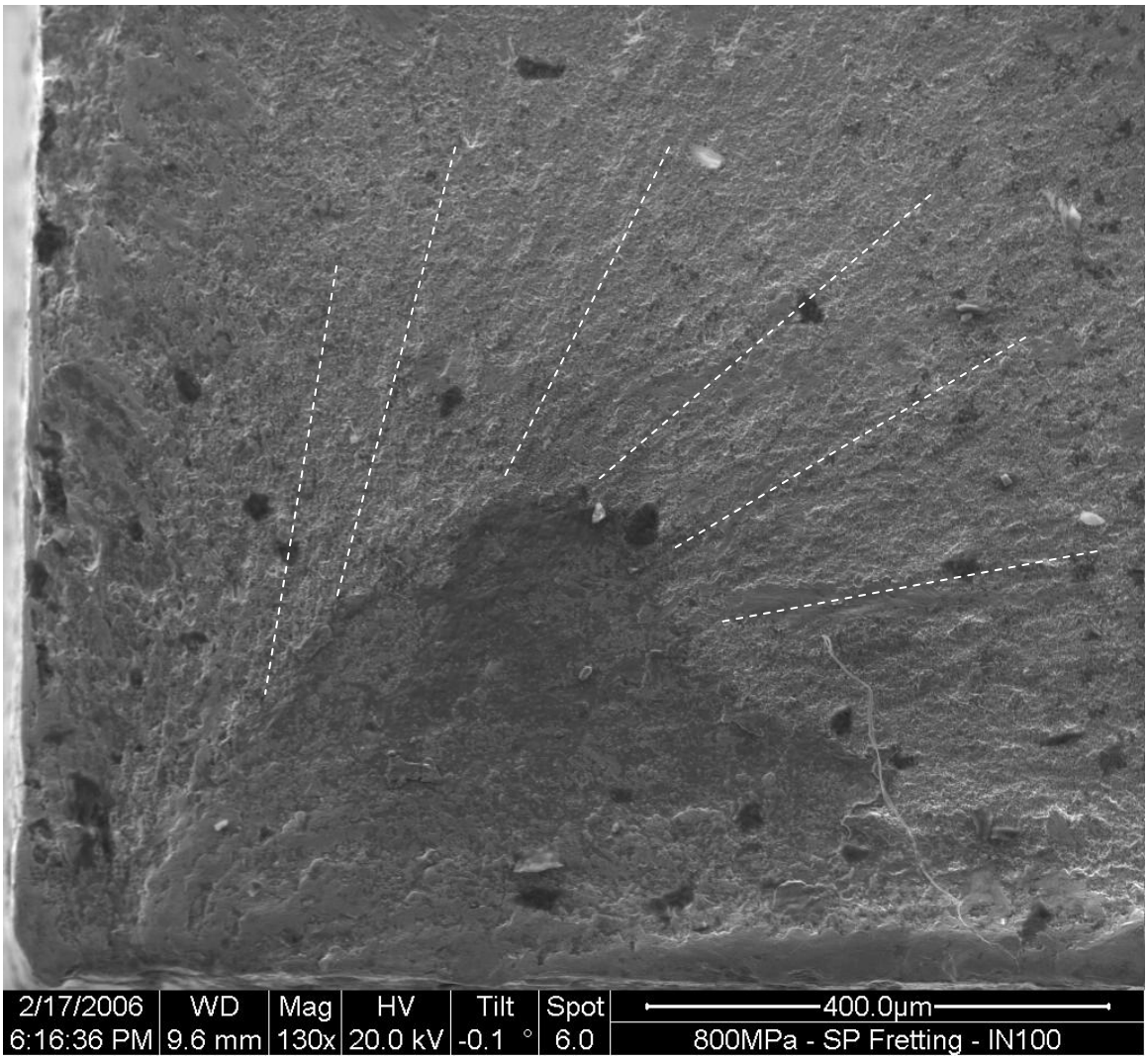

Figure 25. River marks leading to point of crack initiation

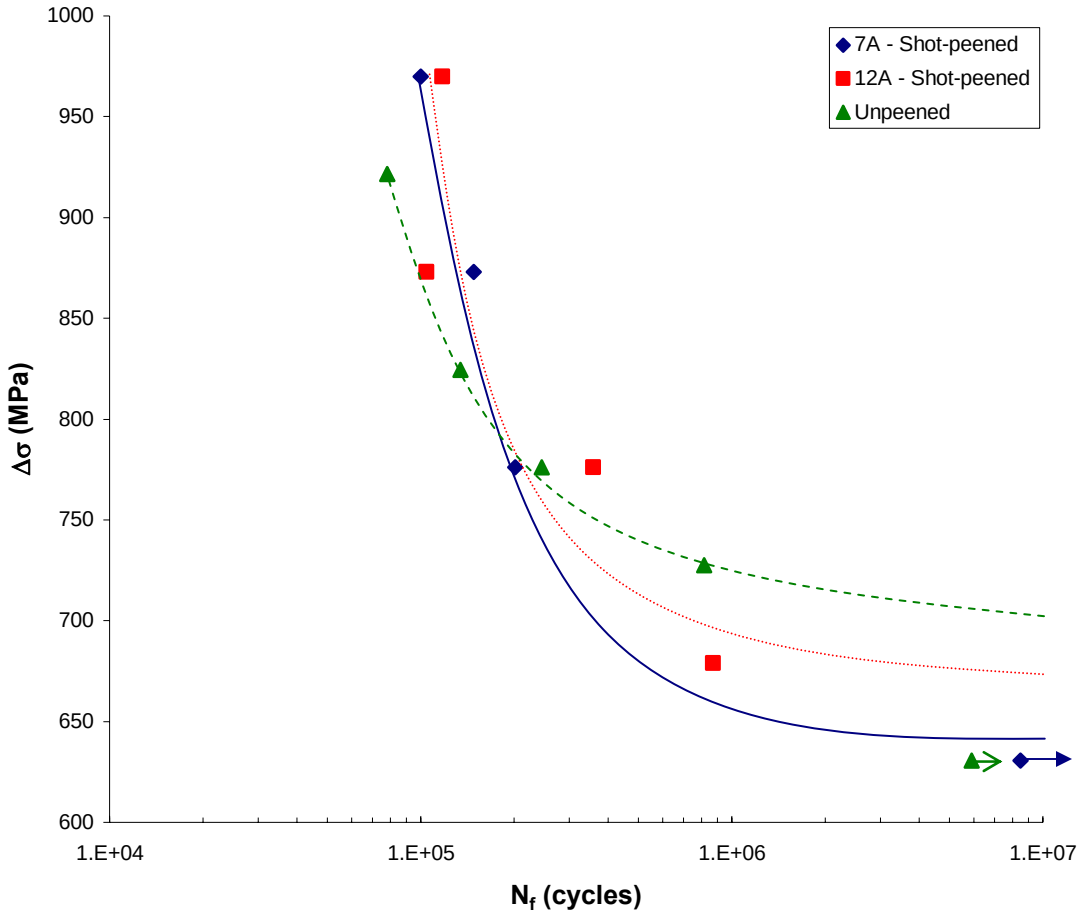

Figure 26. Stress Range versus Cycles to Failure for unpeened [7], 7A, and 12A shot-peened specimens

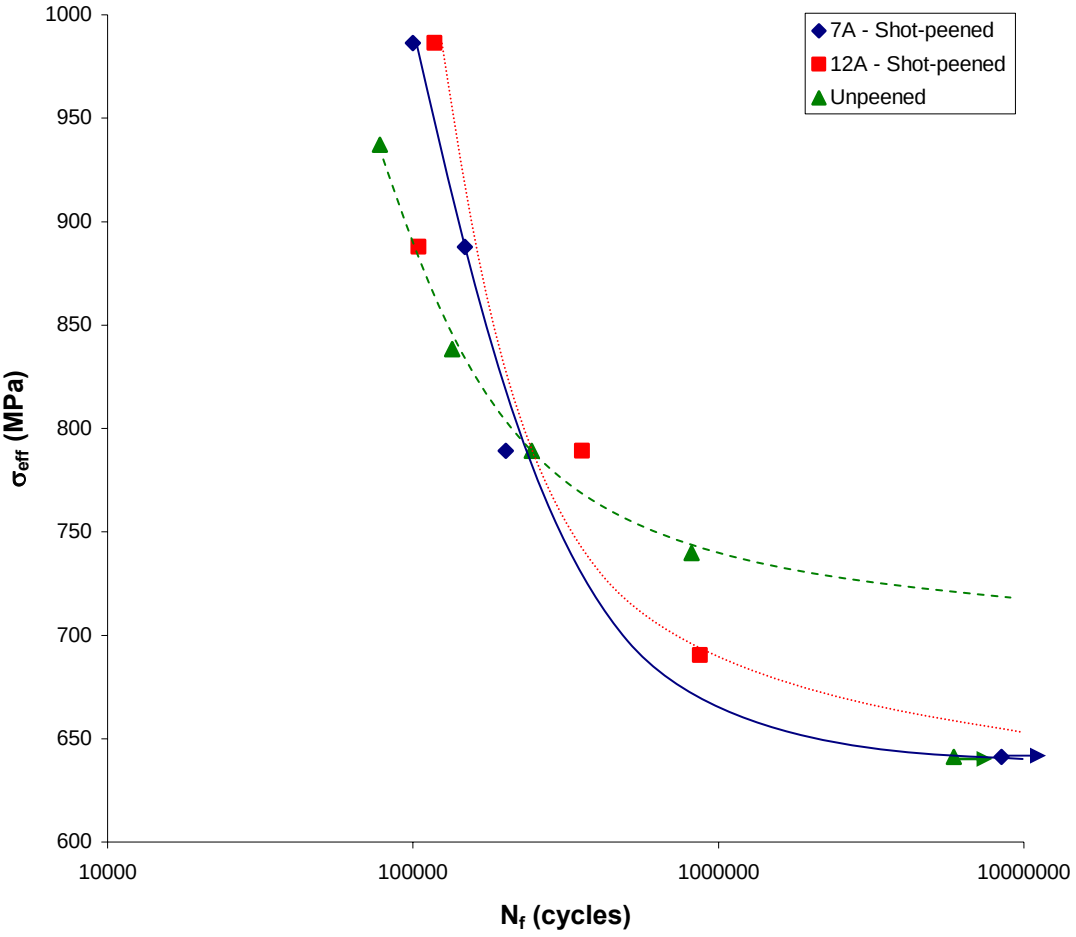

Figure 27. Effective Stress versus Cycles of Failure for unpeened [7], 7A, and 12A Shot-peened Specimens

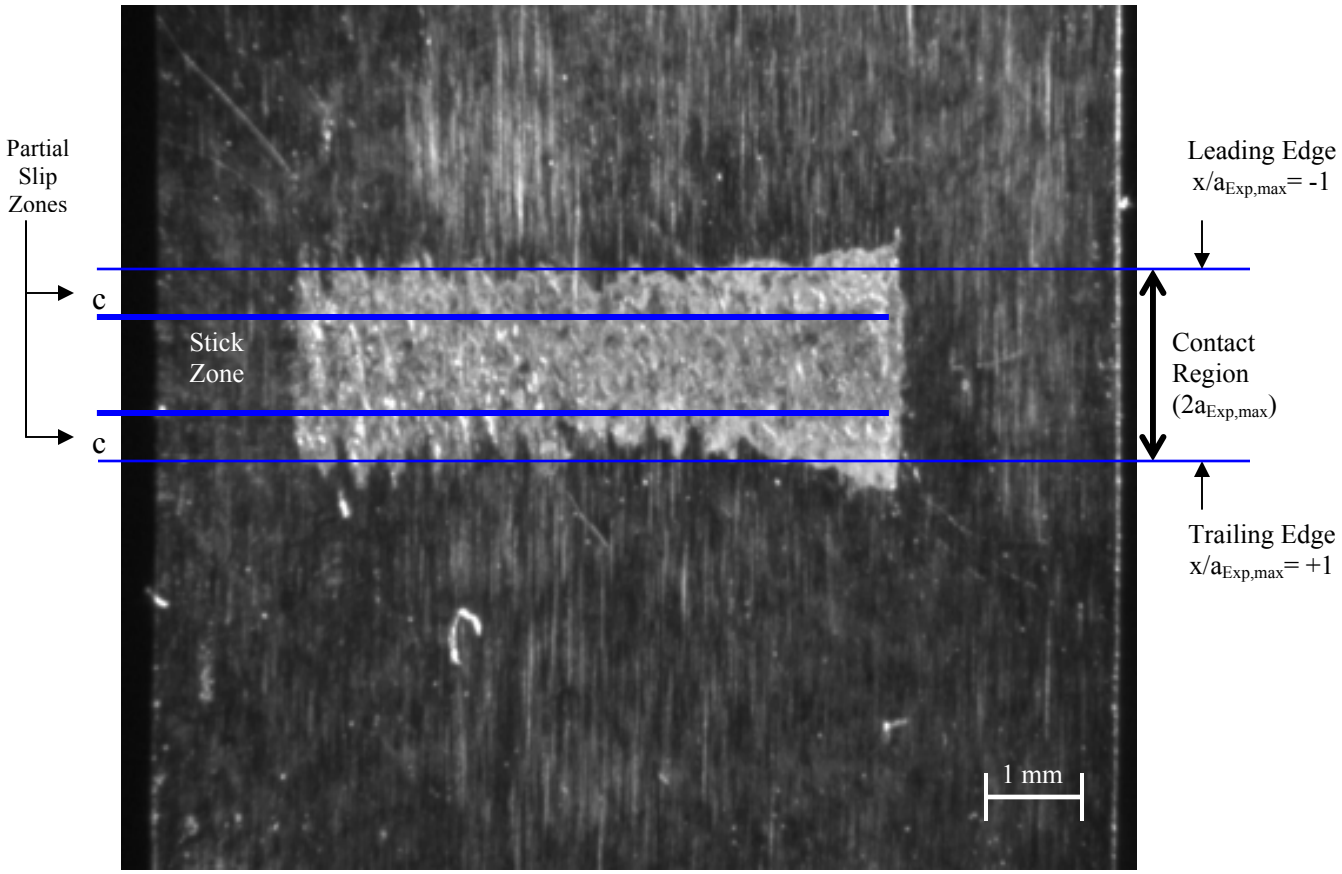

Figure 28. Scar Pattern from Test#9 specimen

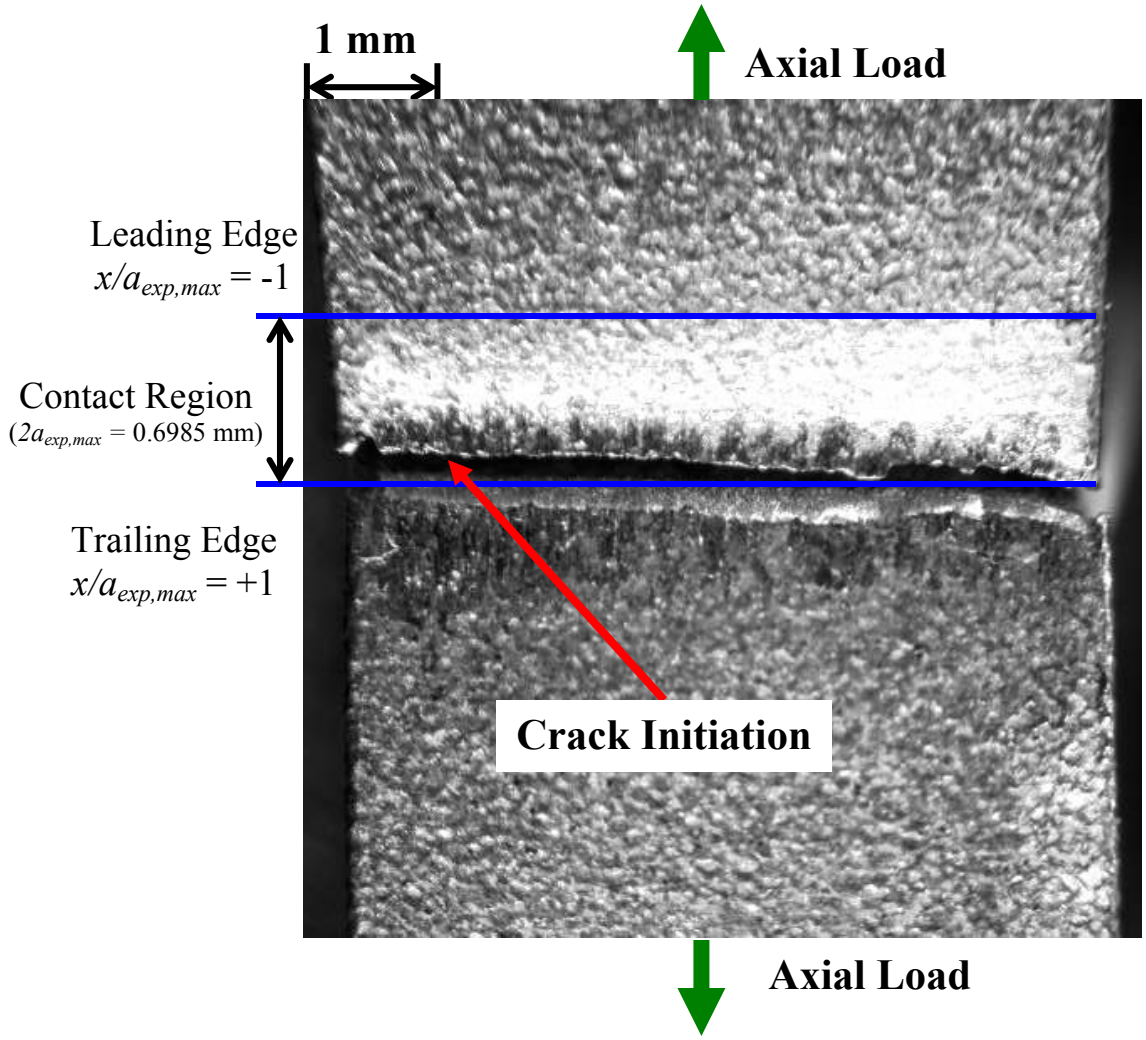

Figure 29. Crack Initiation Location (Test #2)

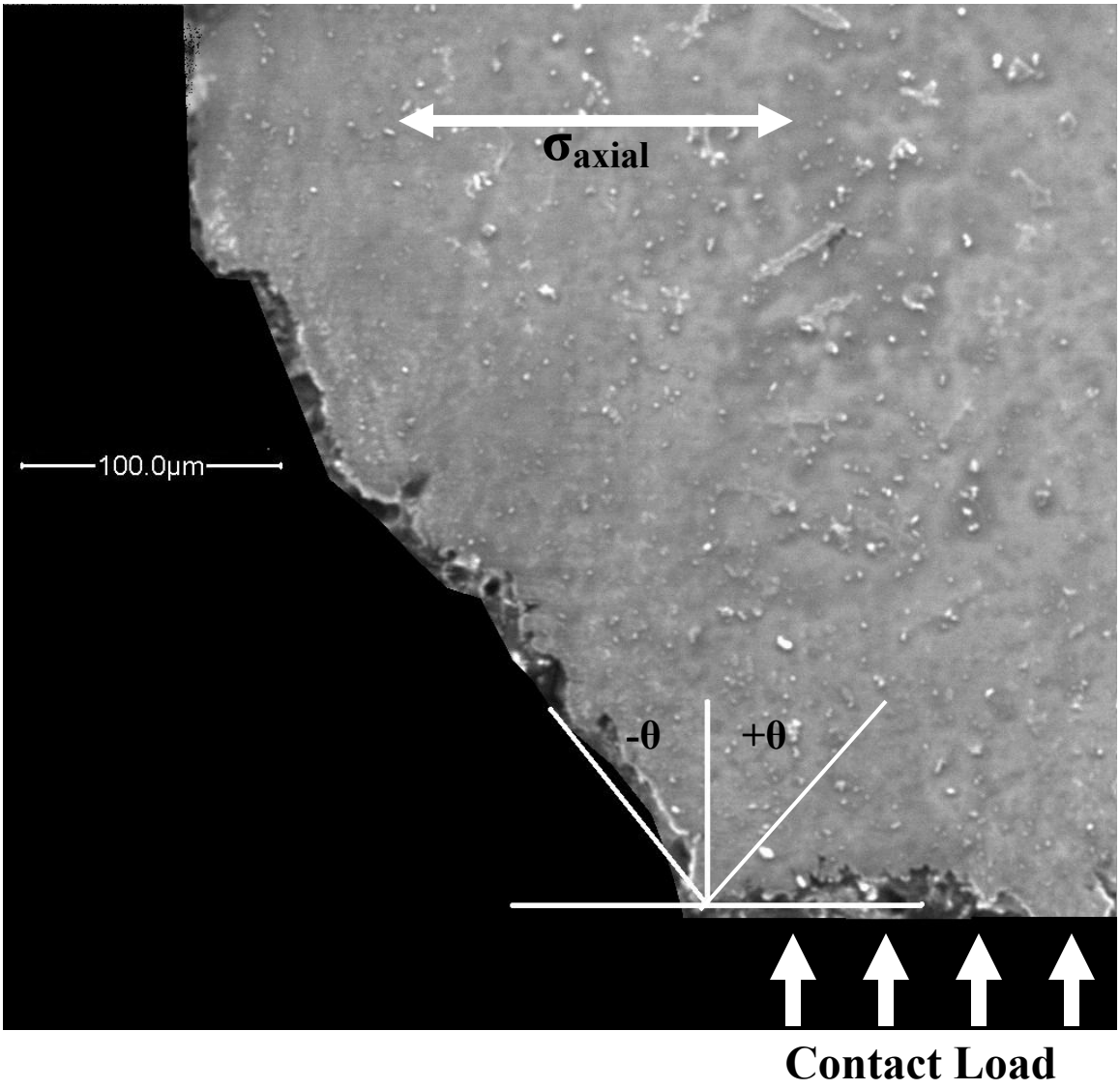

Figure 30. Crack Orientation for a 12A Specimen, Test #9; $\theta = -46^{o}$ (equivalent to $\theta = 44^{o}$)

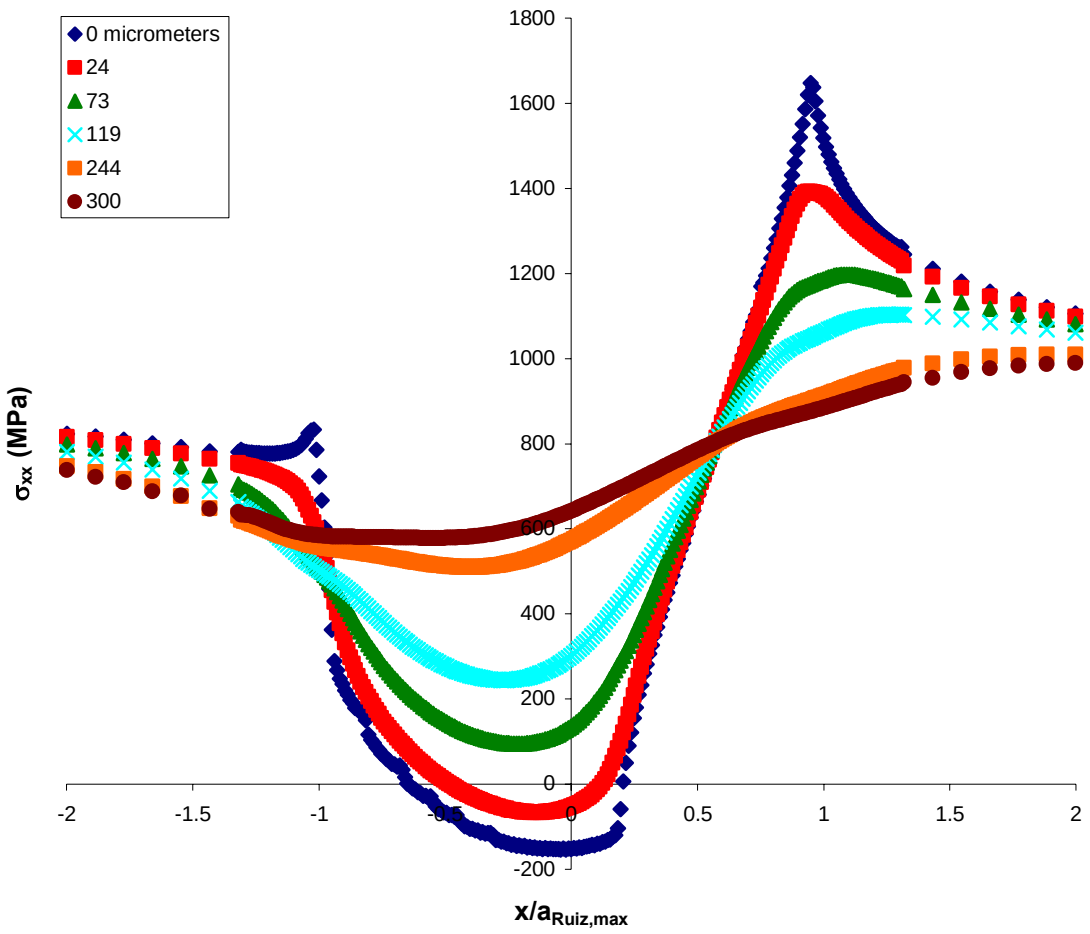

Figure 31. σ_{xx} Profile at Different Depths with 100%R (0% Residual Stress) (Test #9)

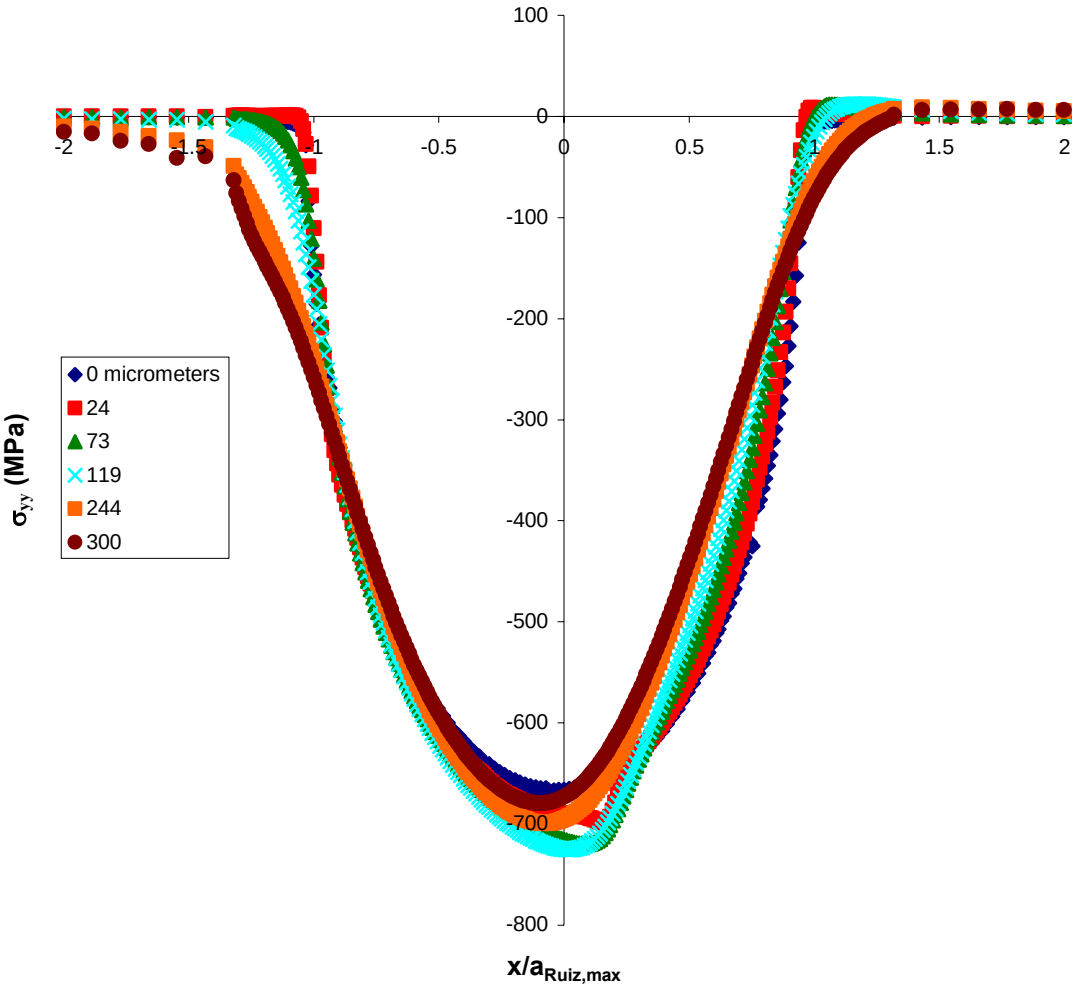

Figure 32. σ_{yy} Profile at Different Depths with 100%R (0% Residual Stress) (Test #9)

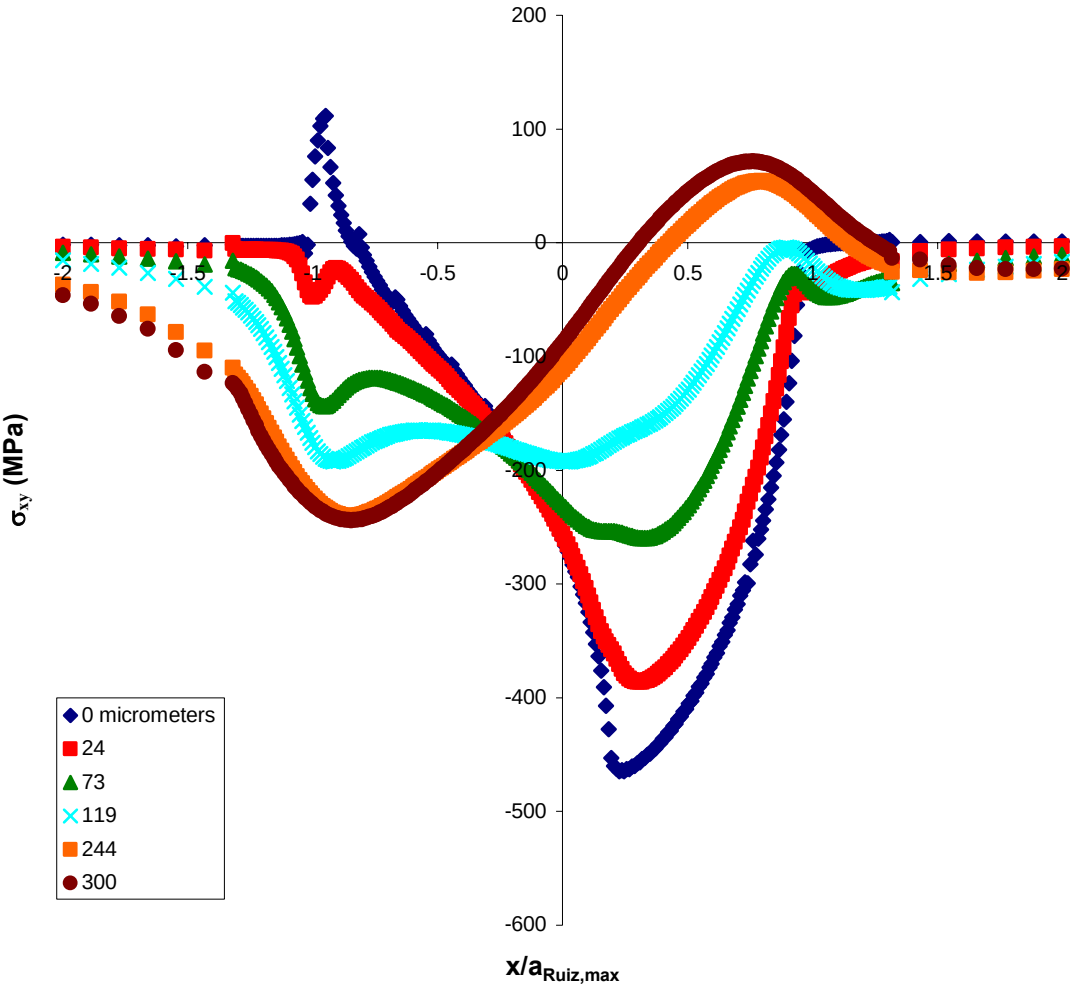

Figure 33. σ_{xy} Profile at Different Depths with 100%R (0% Residual Stress) (Test #9)

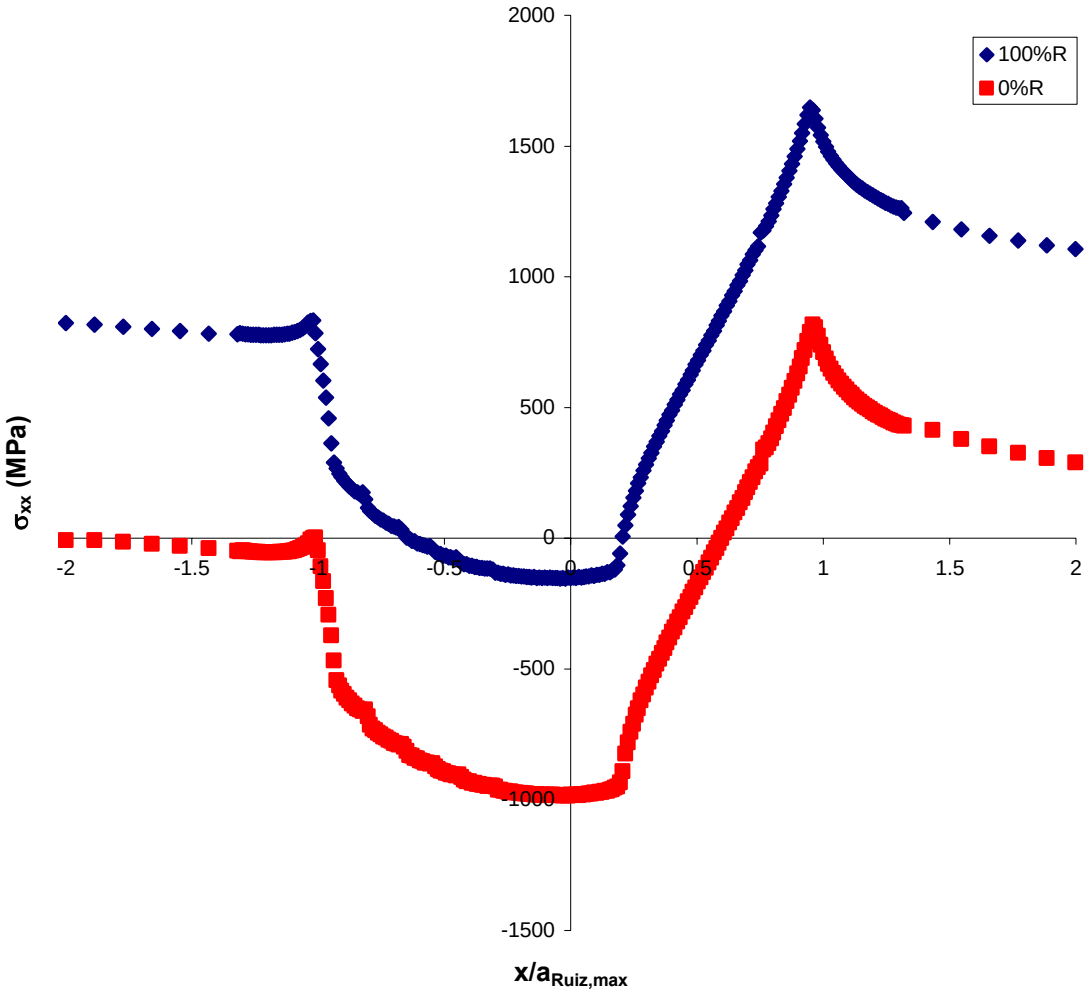

Figure 34. σ_{xx} Profile on Contact Surface with Different Amounts of Residual Stress (Test #9)

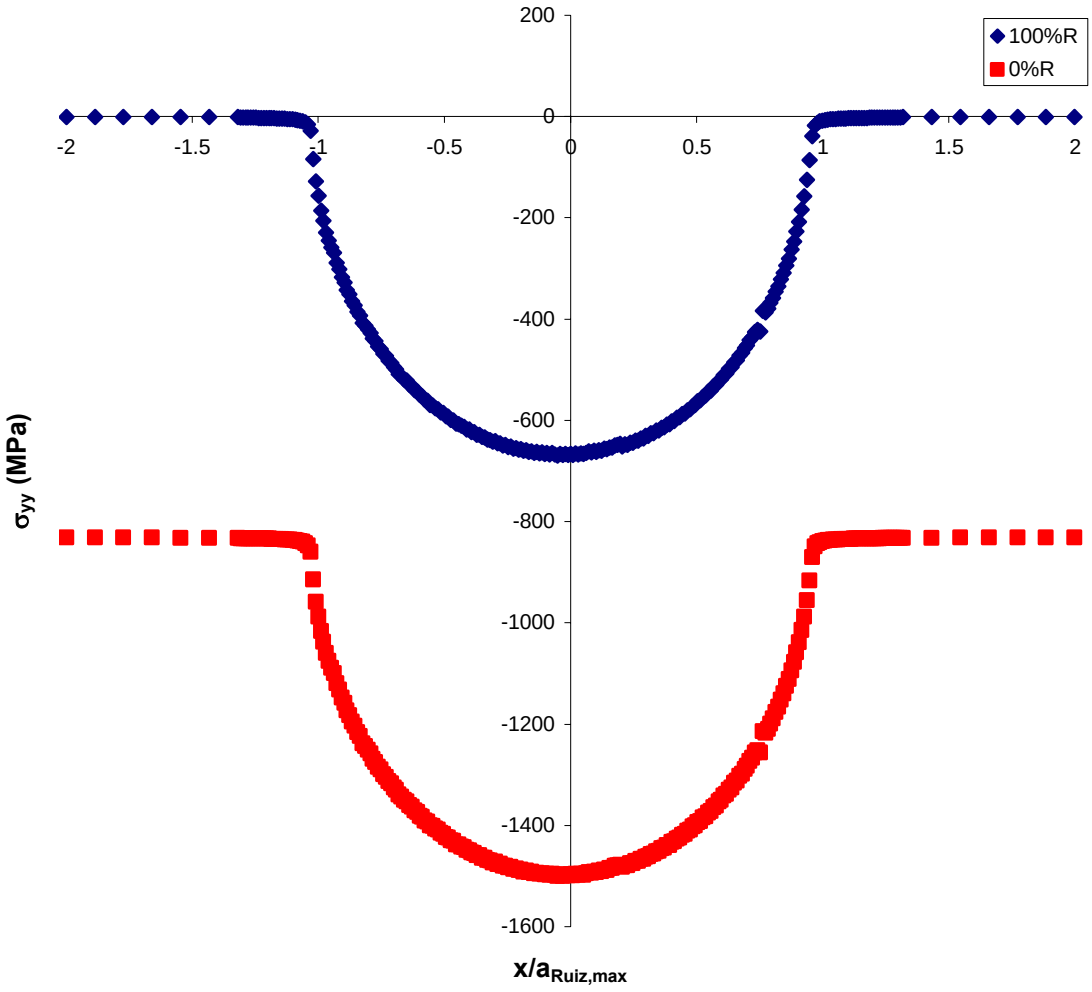

Figure 35. σ_{yy} Profile on Contact Surface with Different Amounts of Residual Stress (Test #9)

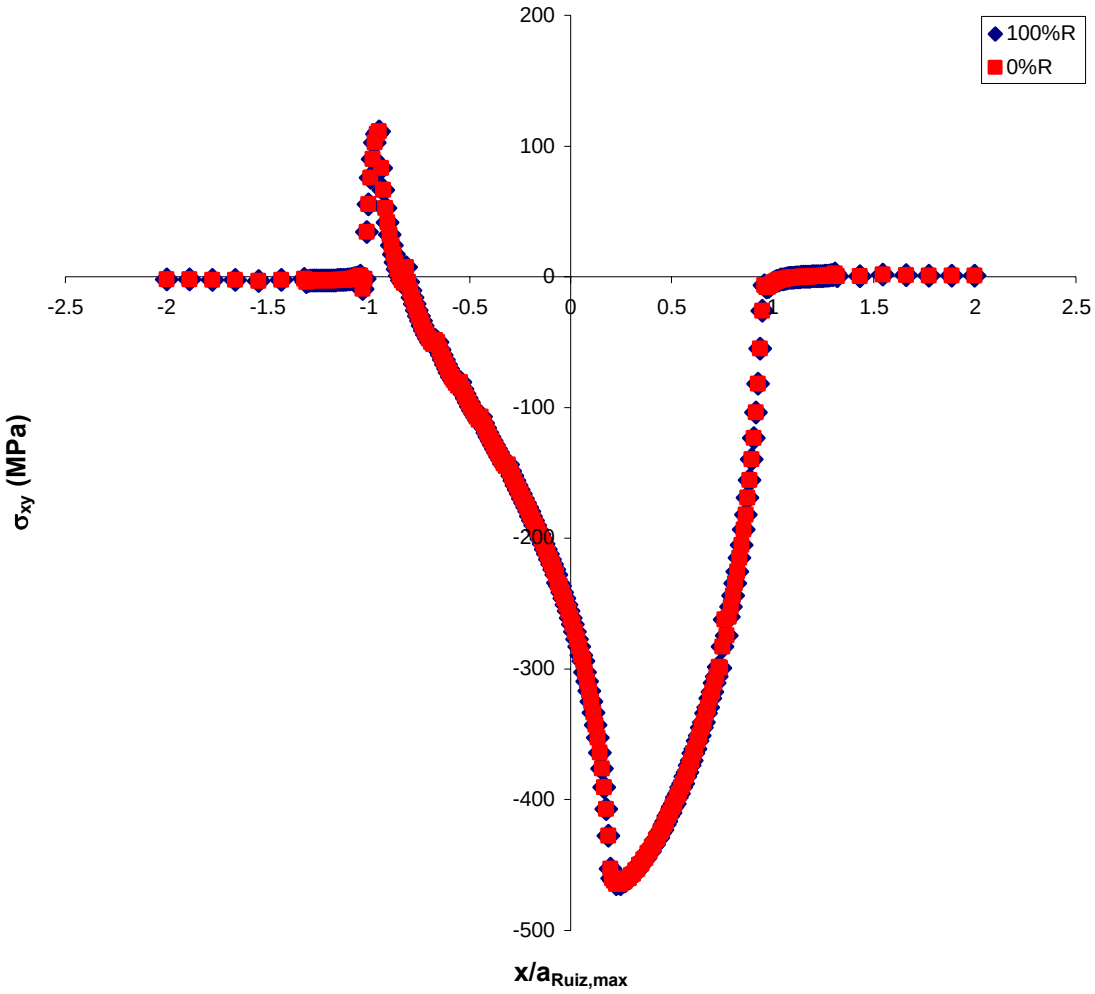

Figure 36. σ_{xy} Profile on Contact Surface with Different Amounts of Residual Stress (Test #9)

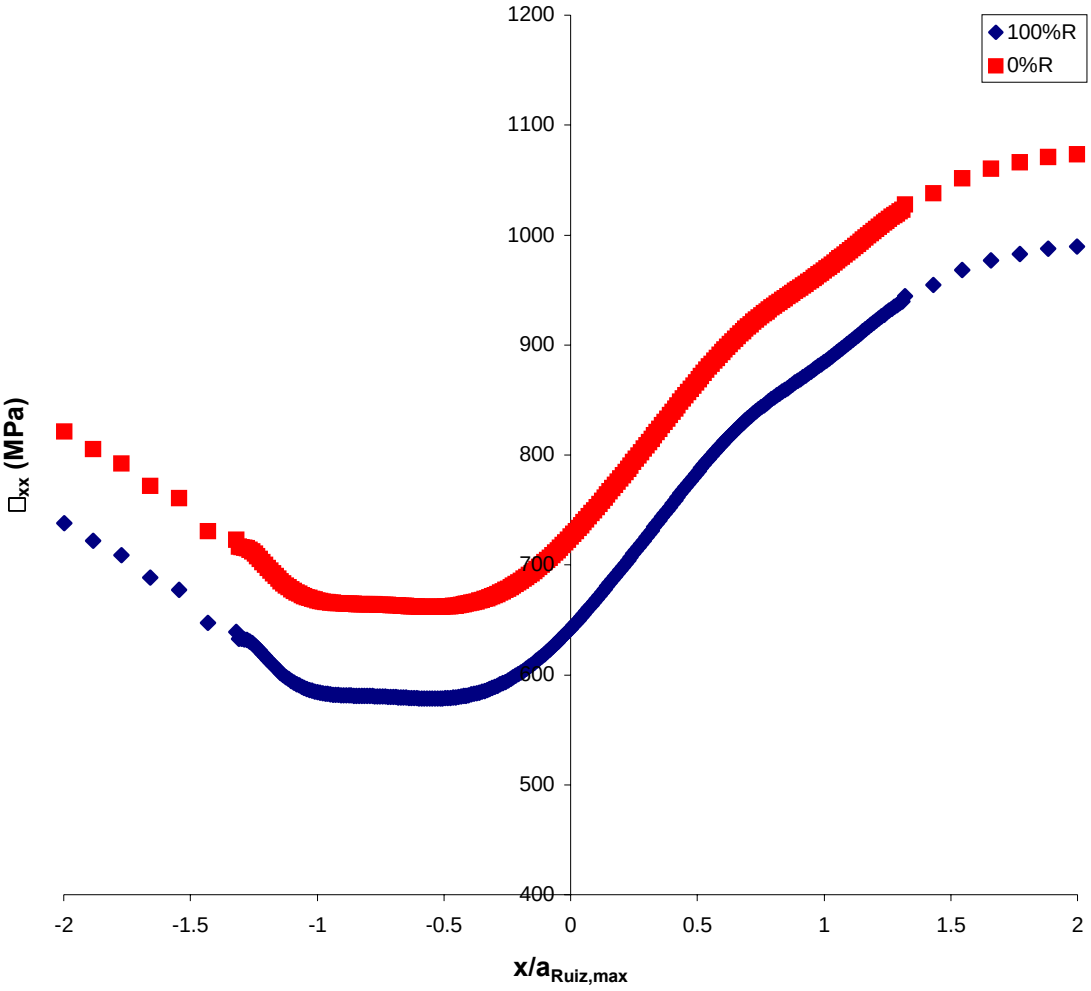

Figure 37. σ_{xx} Profile at Depth = 300 μm with Different Amounts of Residual Stress (Test #9)

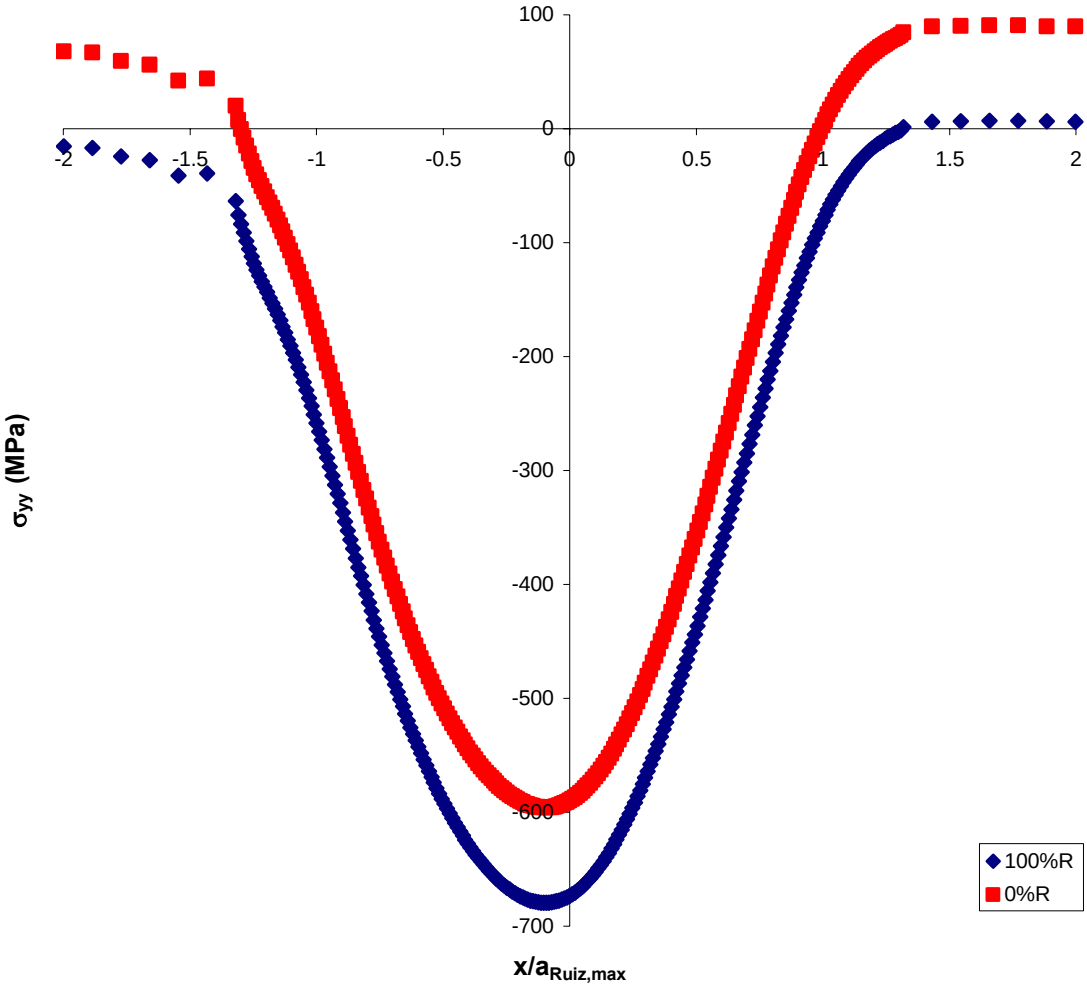

Figure 38. σ_{yy} Profile at Depth = 300 μm with Different Amounts of Residual Stress (Test #9)

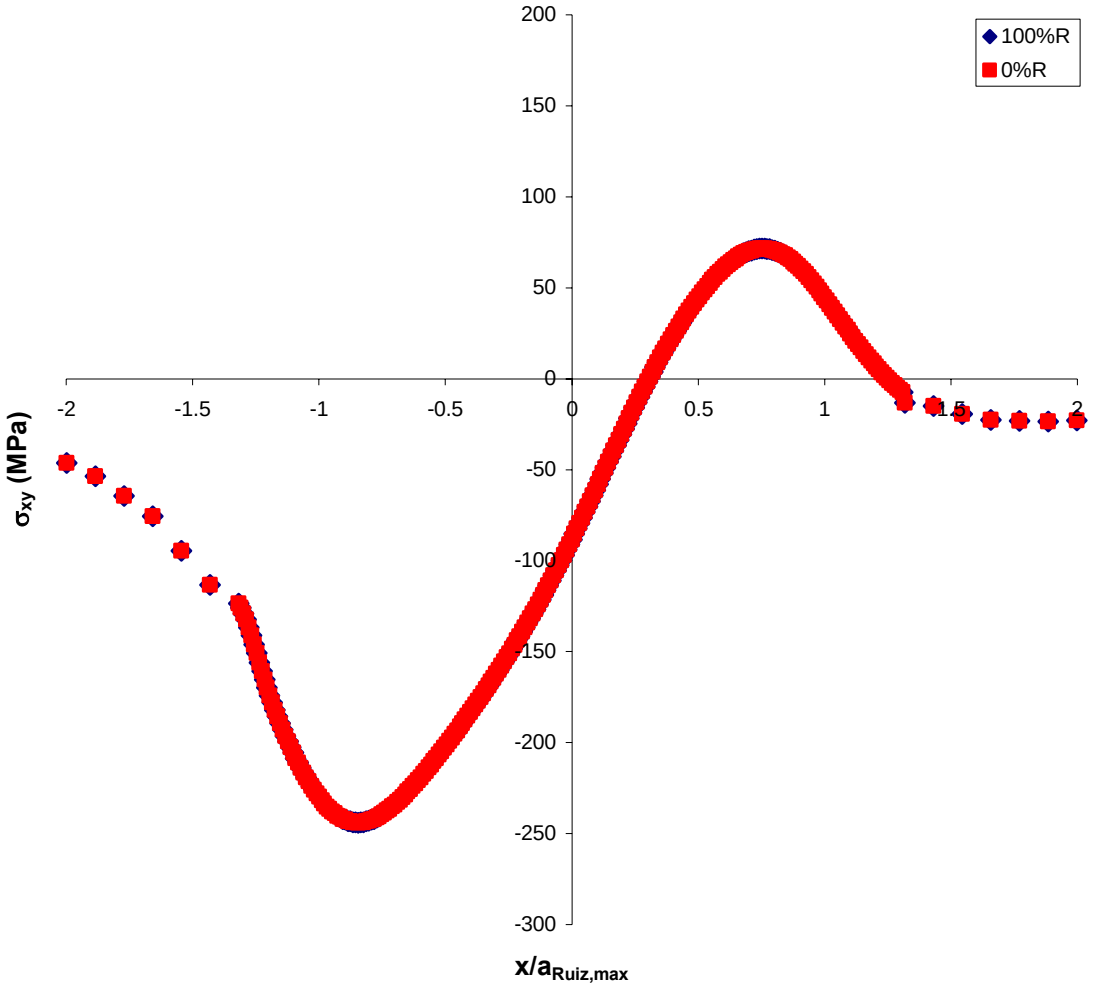

Figure 39. σ_{xy} Profile at a Depth = 300 µm with Different Amounts of Residual Stress (Test #9)

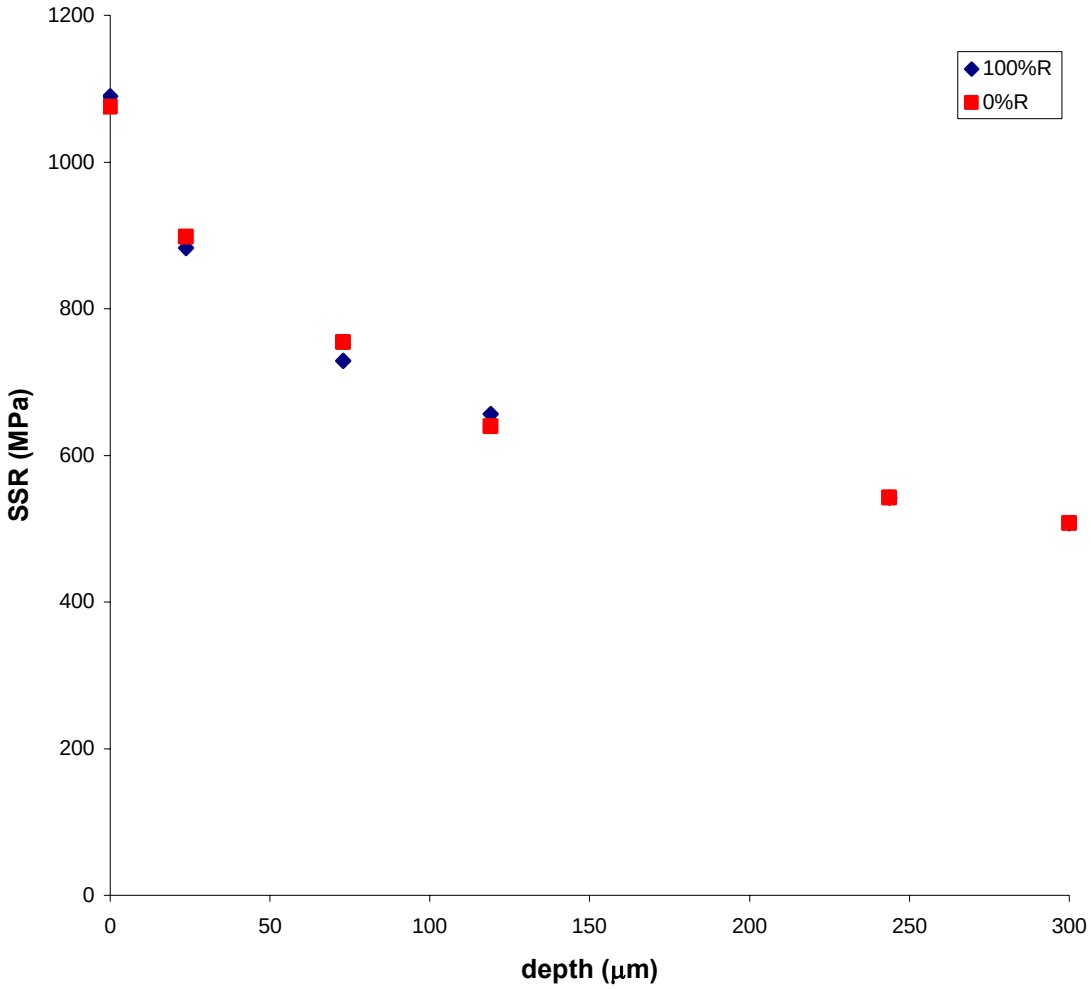

Figure 40. SSR under Influence of Residual Stress at Different Depths for 7A specimen (Test #1)

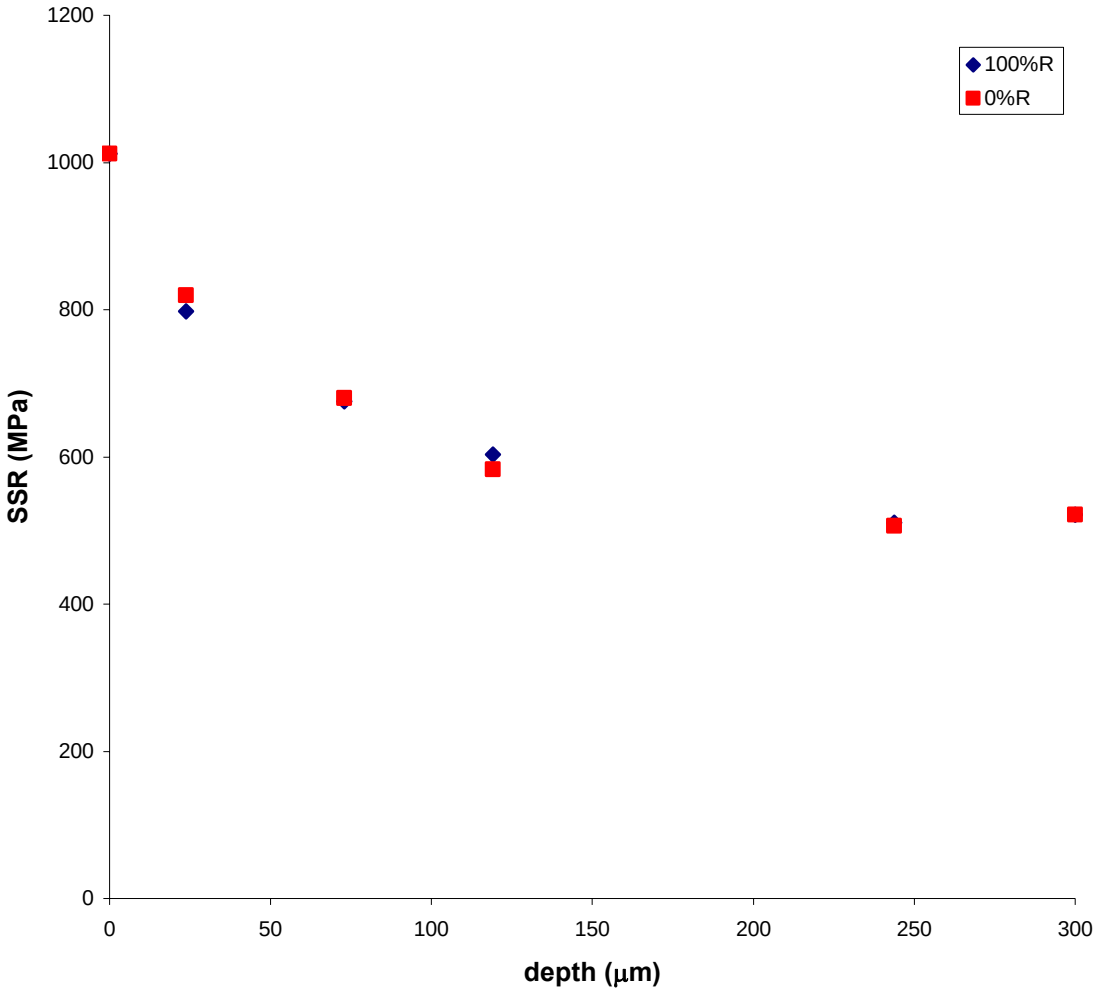

Figure 41. SSR under Influence of Residual Stress at Different Depths for 12A specimen (Test #9)

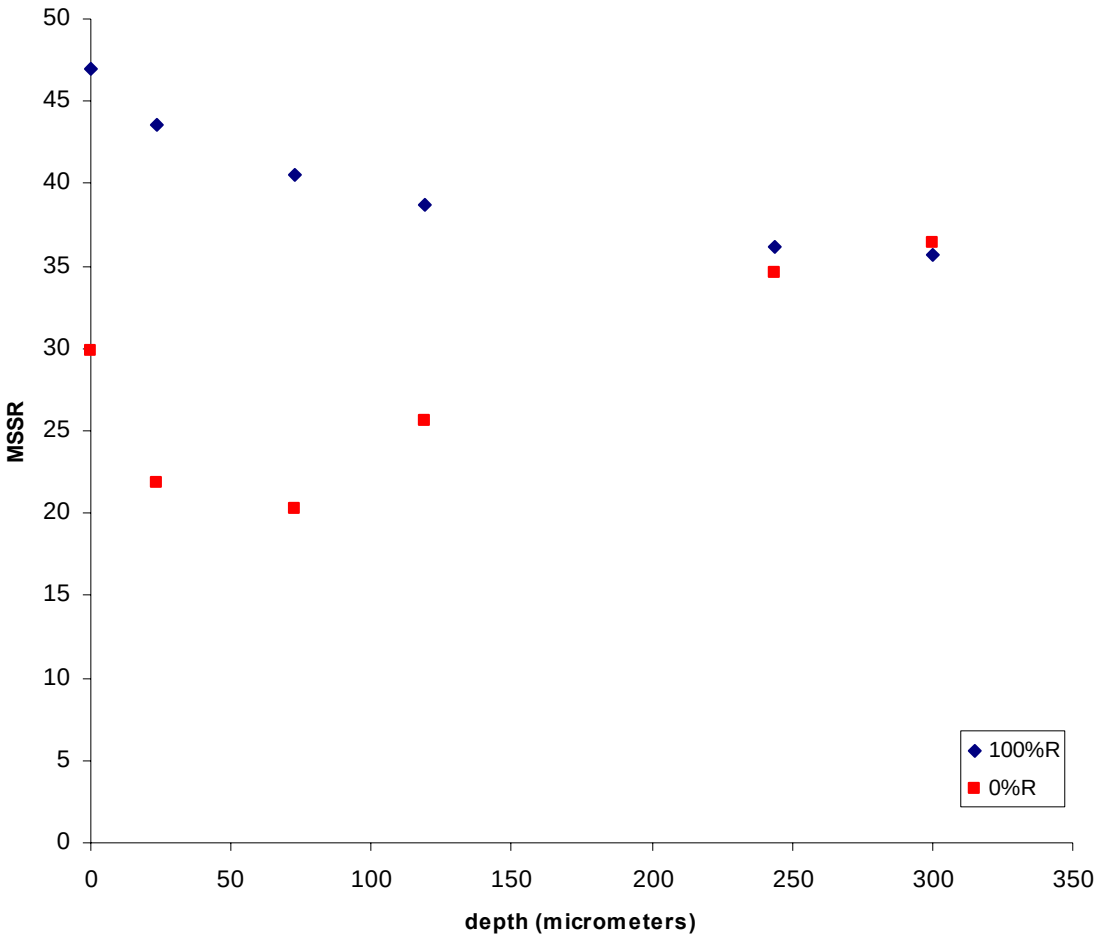

Figure 42. MSSR under Influence of Residual Stress at Different Depths for 7A specimen (Test #1)

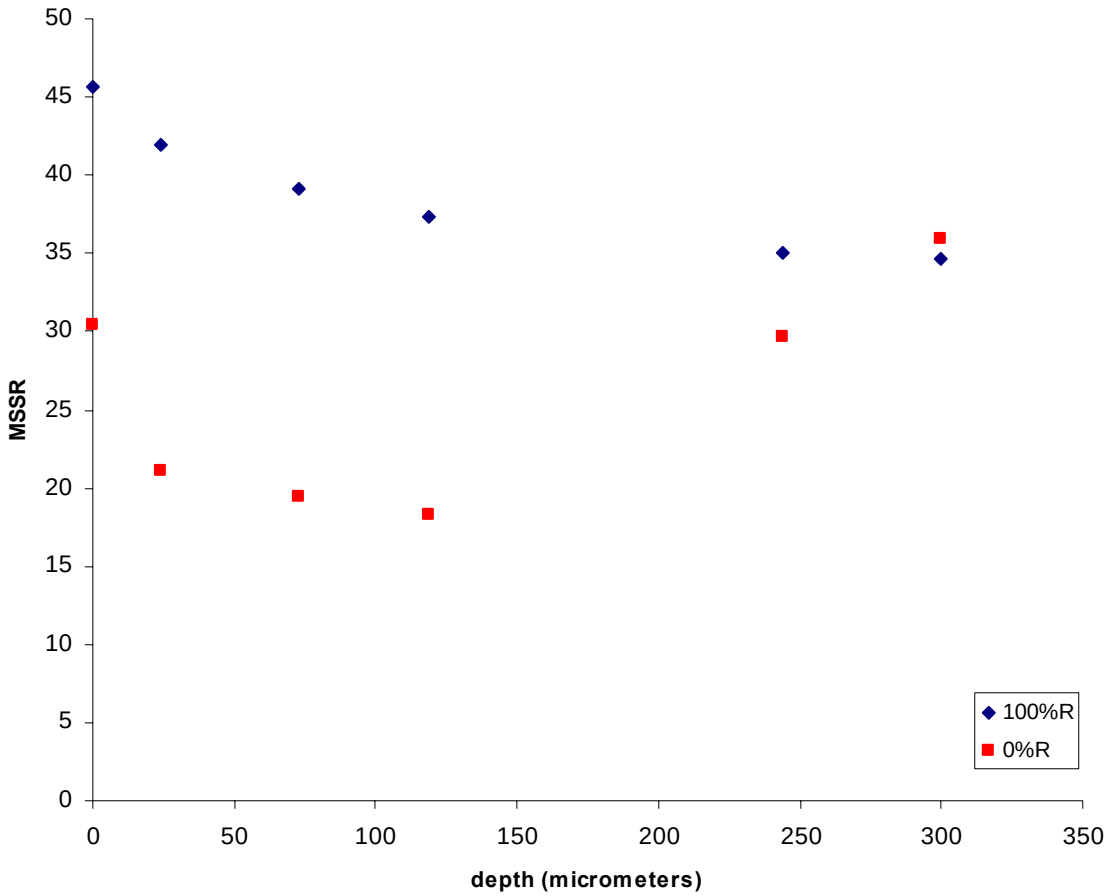

Figure 43. MSSR under Influence of Residual Stress at Different Depths for 12A specimen (Test #9)

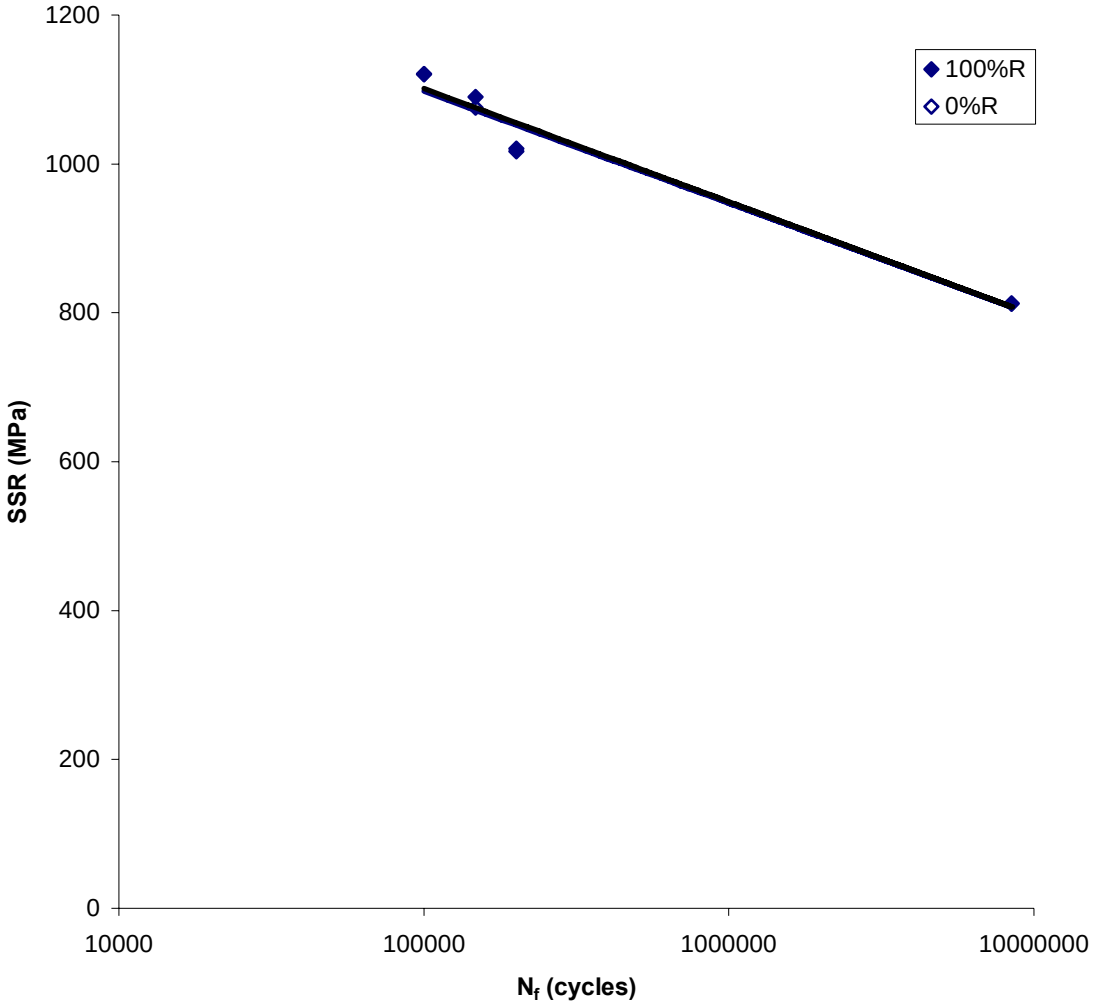

Figure 44. SSR versus N_f for 7A Specimens with 100%R and 0%R

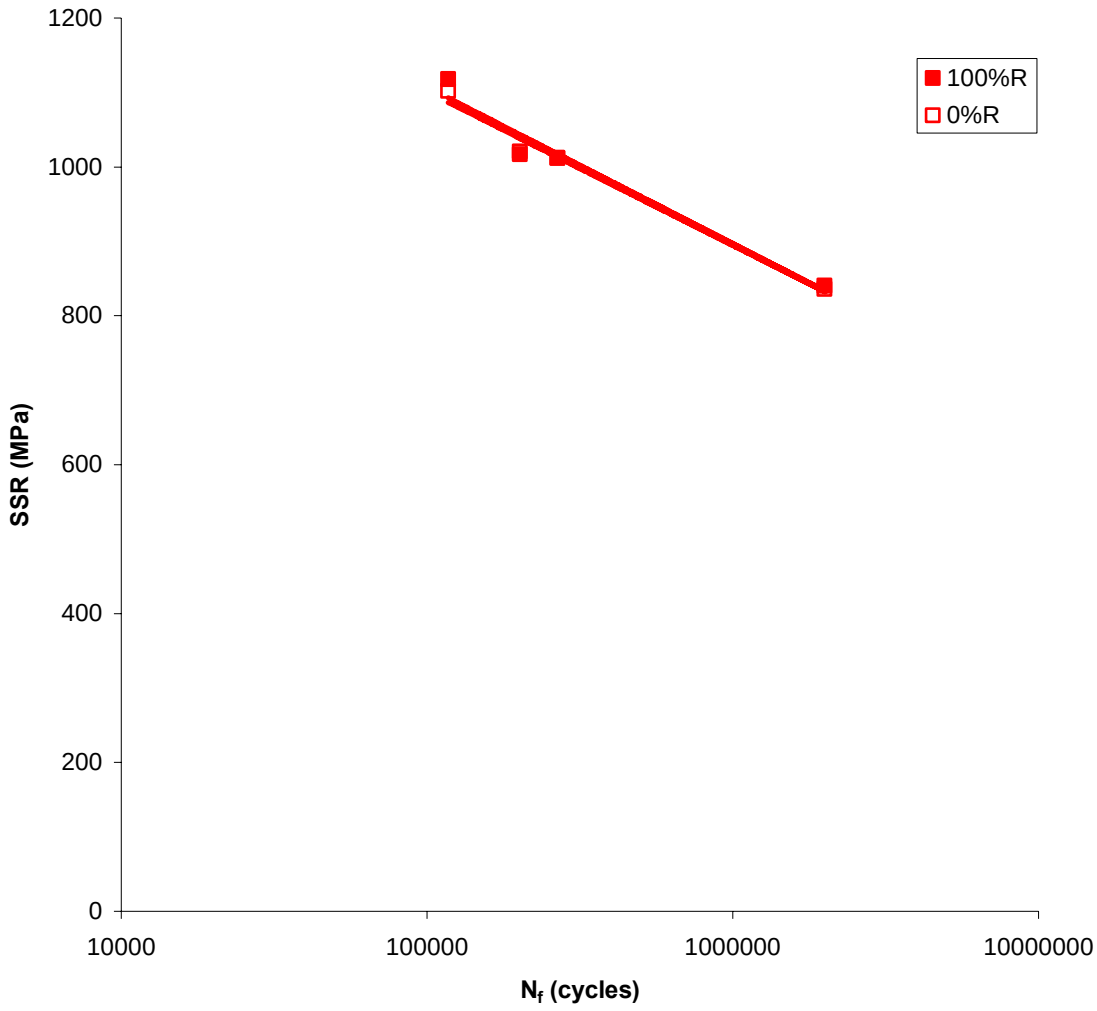

Figure 45. SSR versus N_f for 12A Specimens with 100%R and 0%R

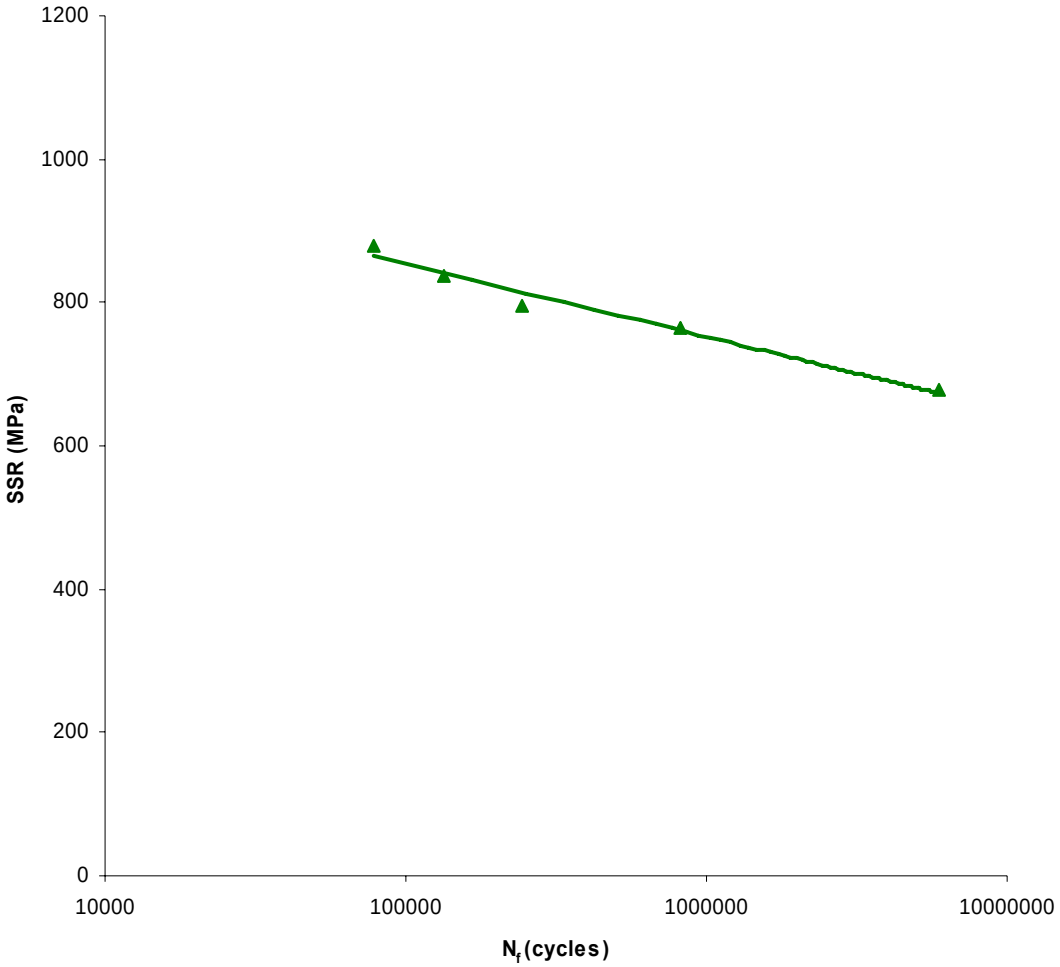

Figure 46. SSR versus N_f for Unpeened Specimens

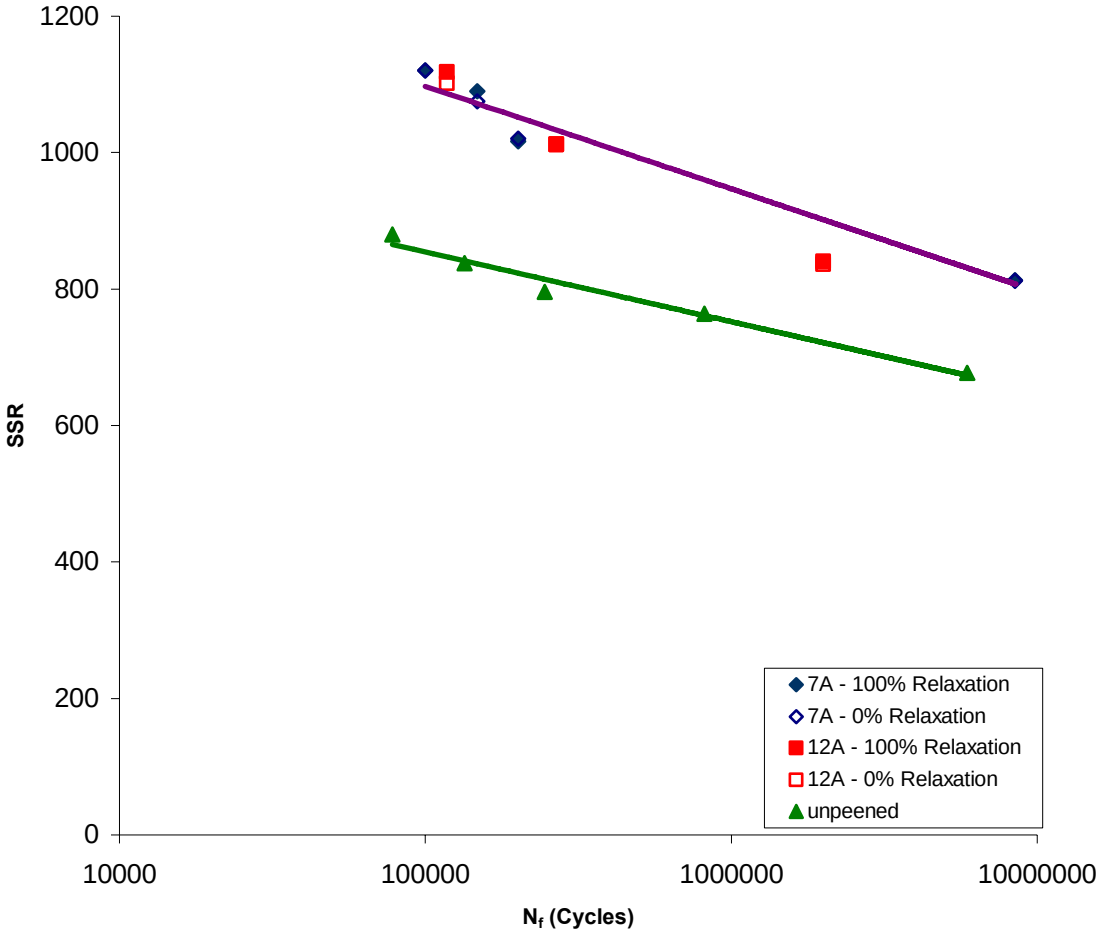

Figure 47. SSR versus N_f for All Cases

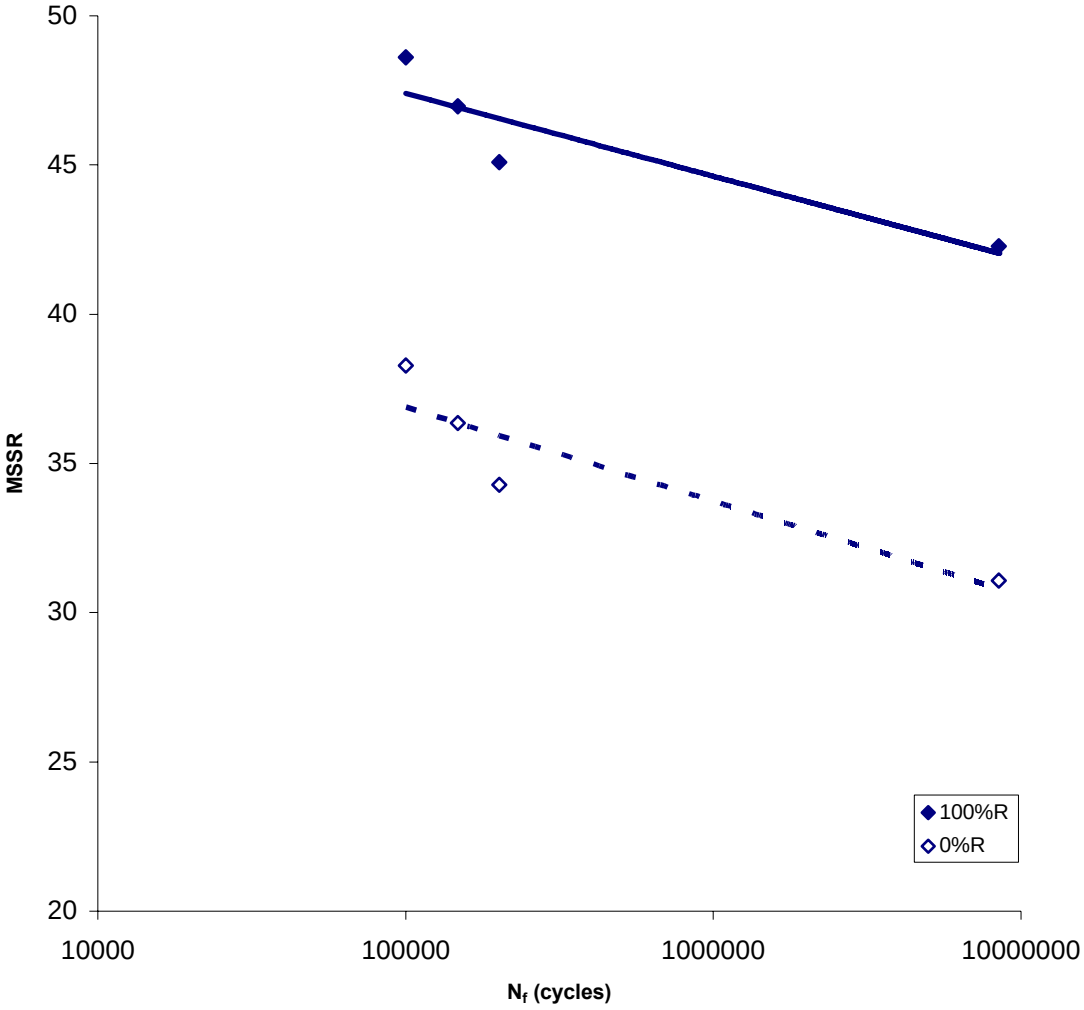

Figure 48. MSSR versus N_f for 7A Specimens with 100%R and 0%R

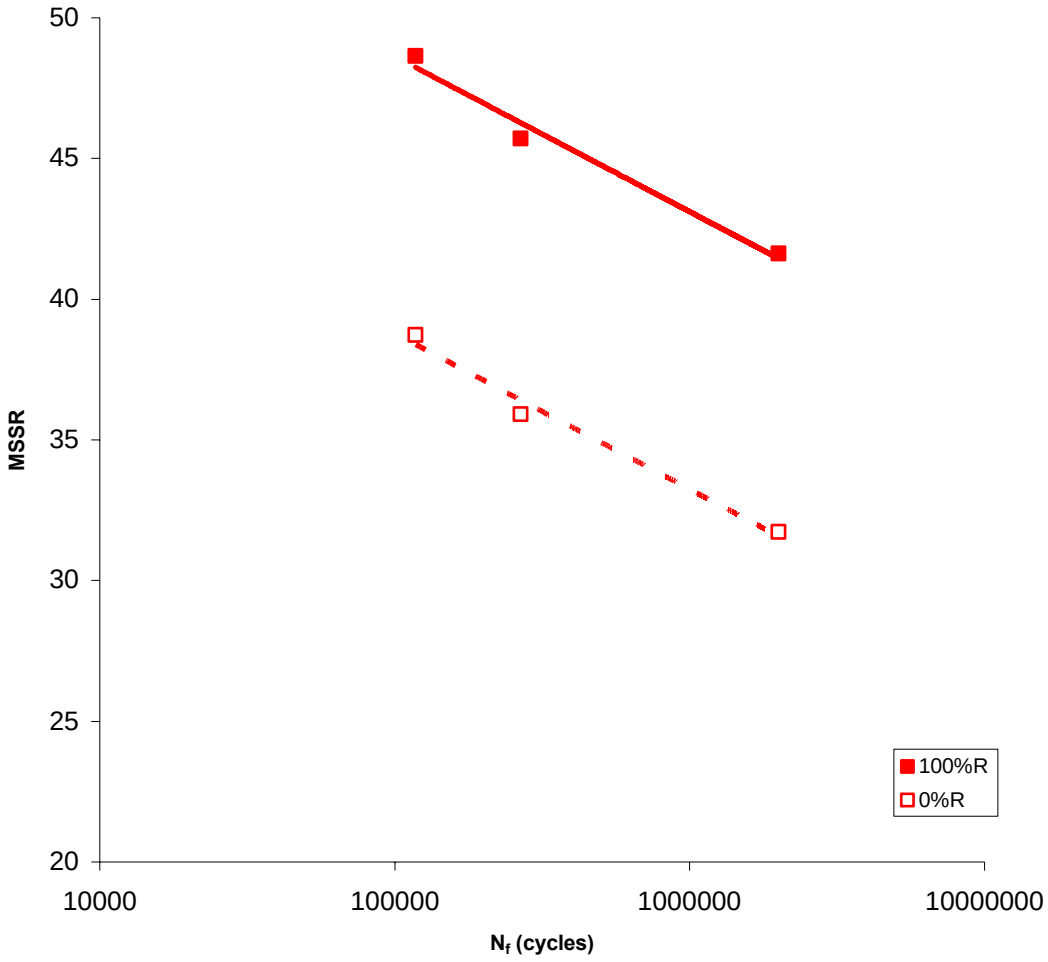

Figure 49. MSSR versus N_f for 12A Specimens with 100%R and 0%R

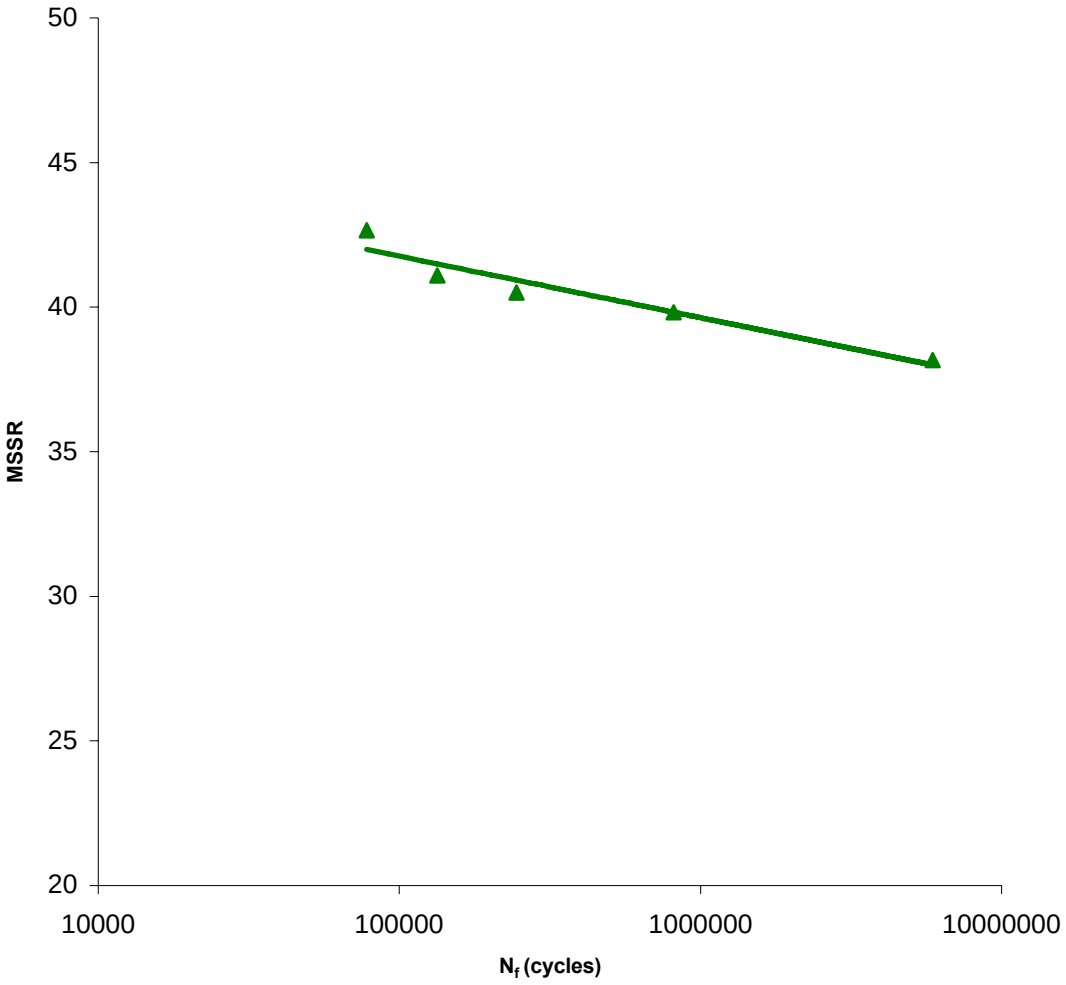

Figure 50. MSSR versus N_f for Unpeened Specimens

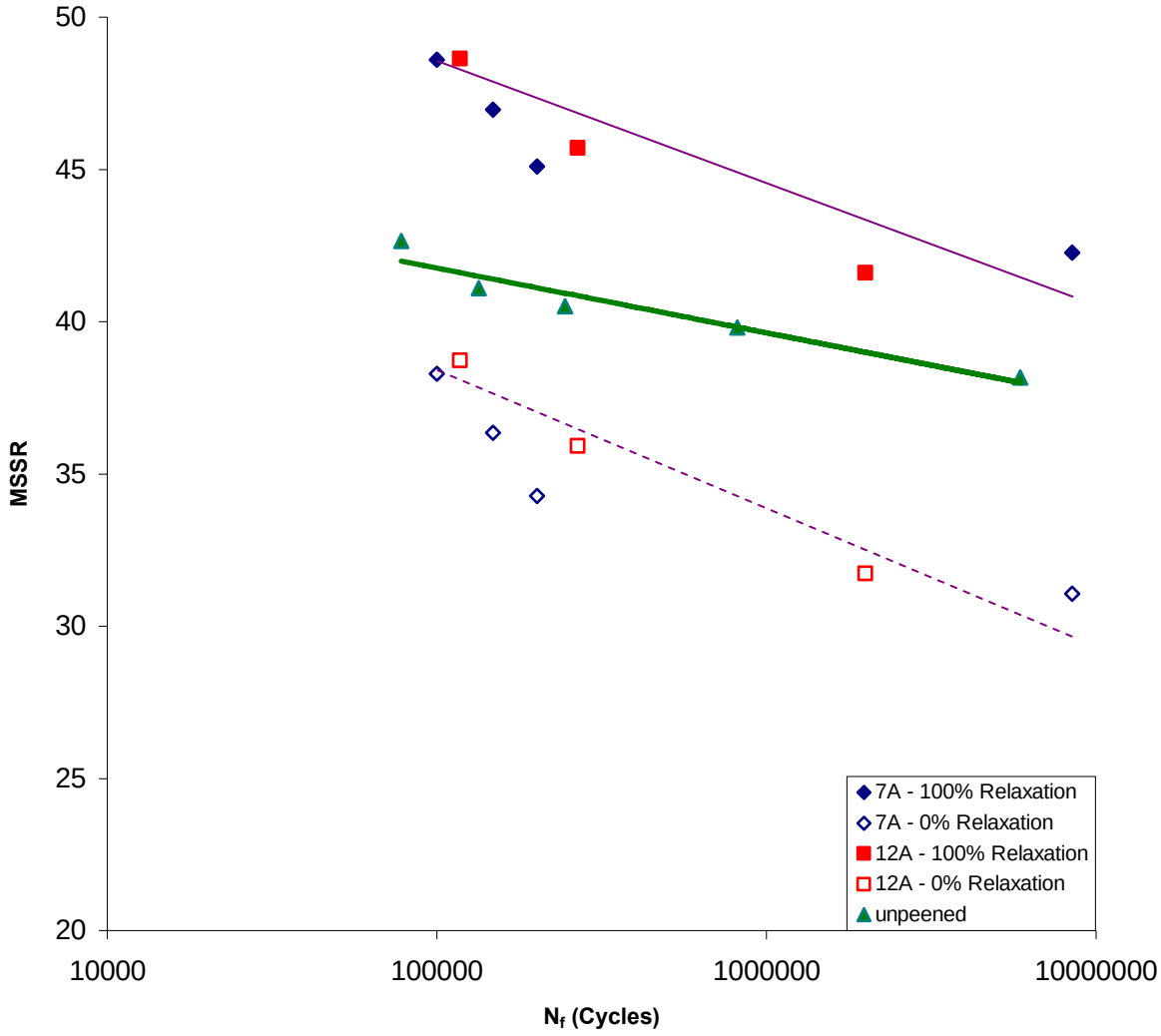

Figure 51. MSSR versus N_f for All Cases

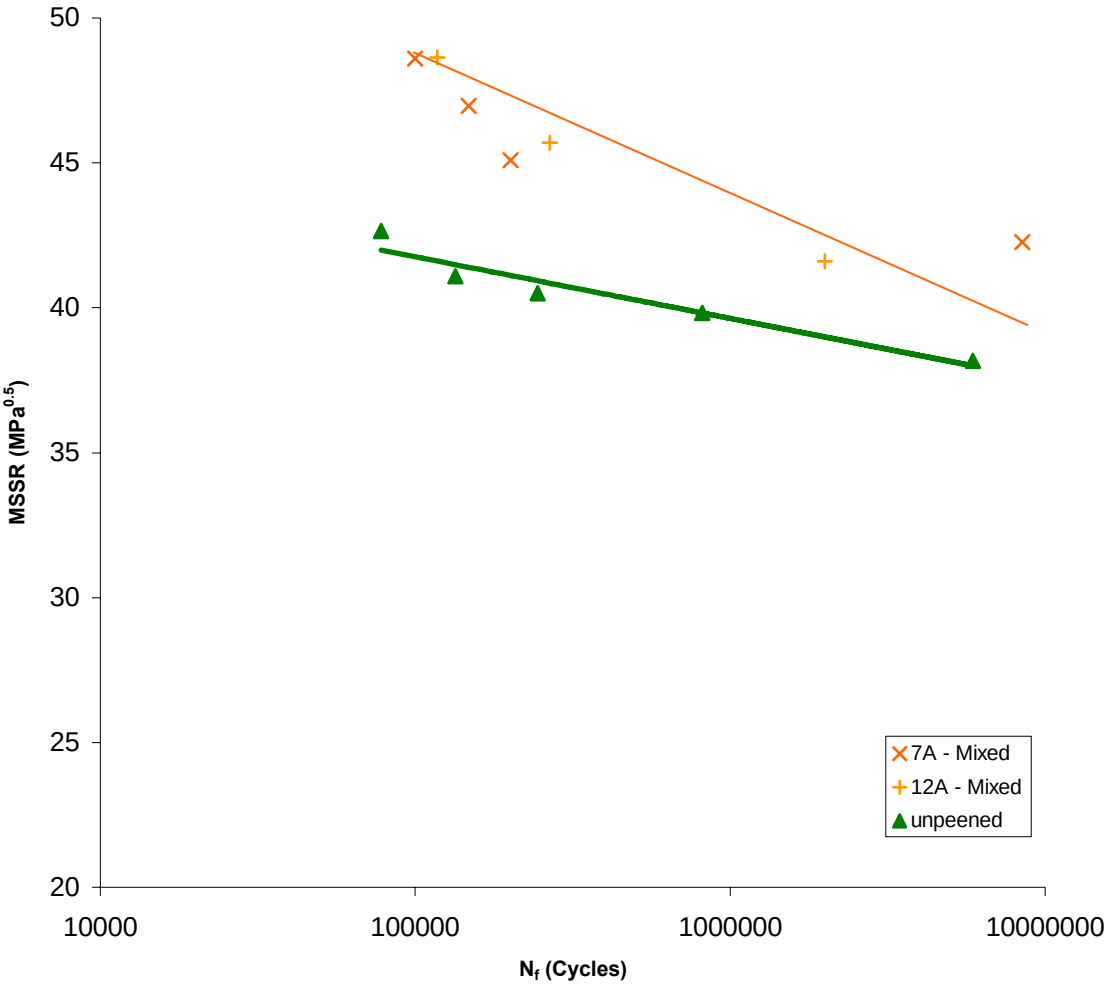

Figure 52. MSSR versus N_f for Mixed Relaxation Case and Unpeened Case

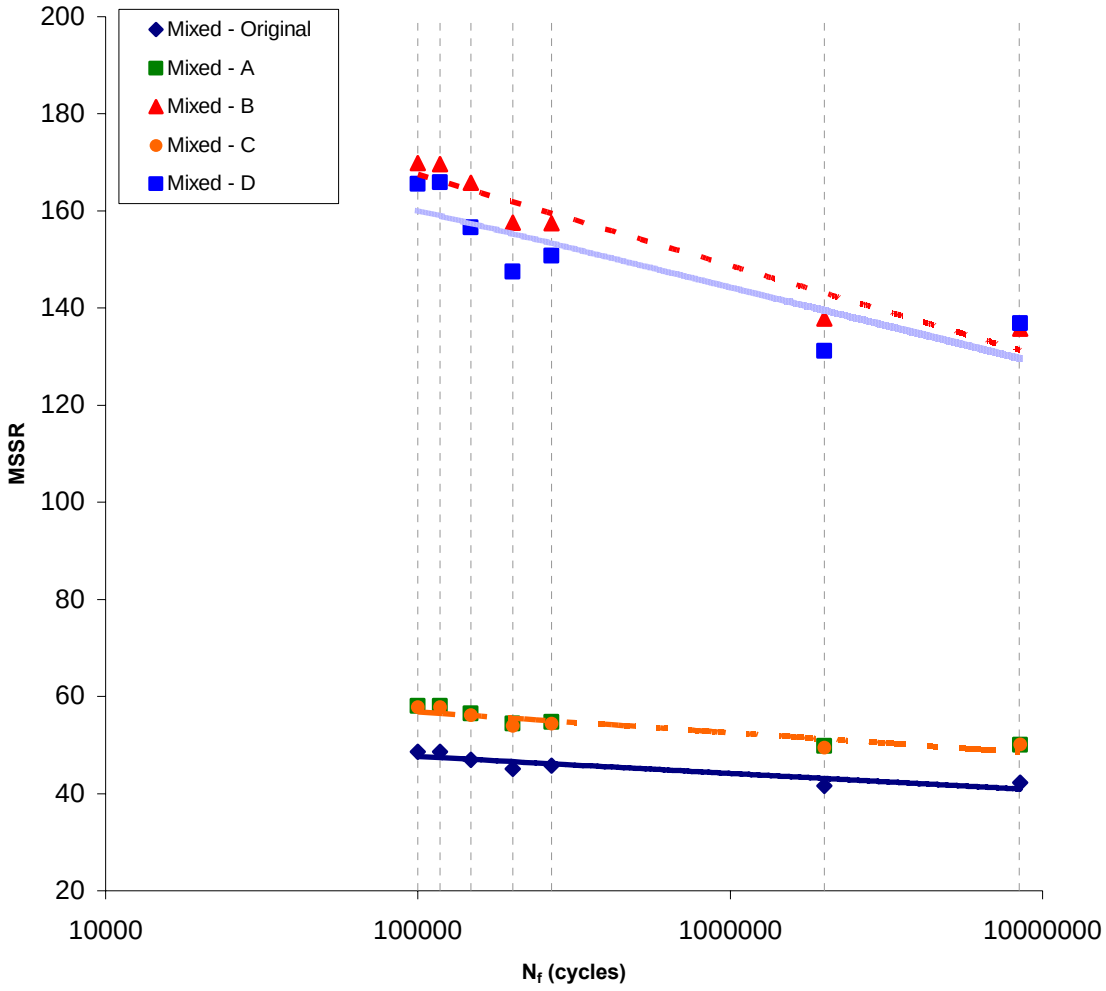

Figure 53. Effect of changing the MSSR coefficients (A,B,C,D) on MSSR versus N_f

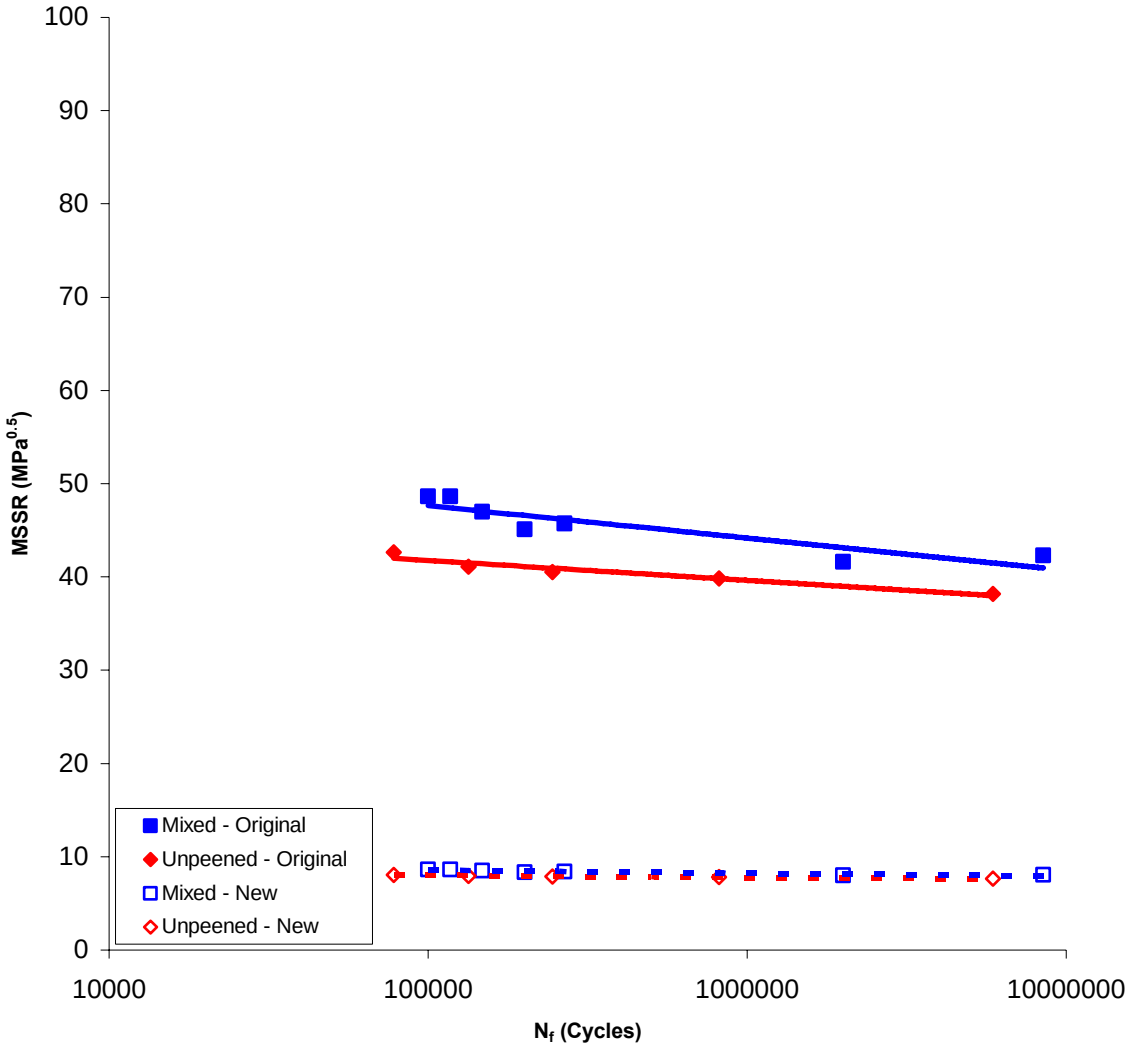

Figure 54. MSSR versus N_f for Mixed Relaxation Case and Unpeened Case (Iteration A)

Note:

	Original	New
A	0.75	0.75
B	0.50	0.25
C	0.75	0.75
D	0.50	0.25

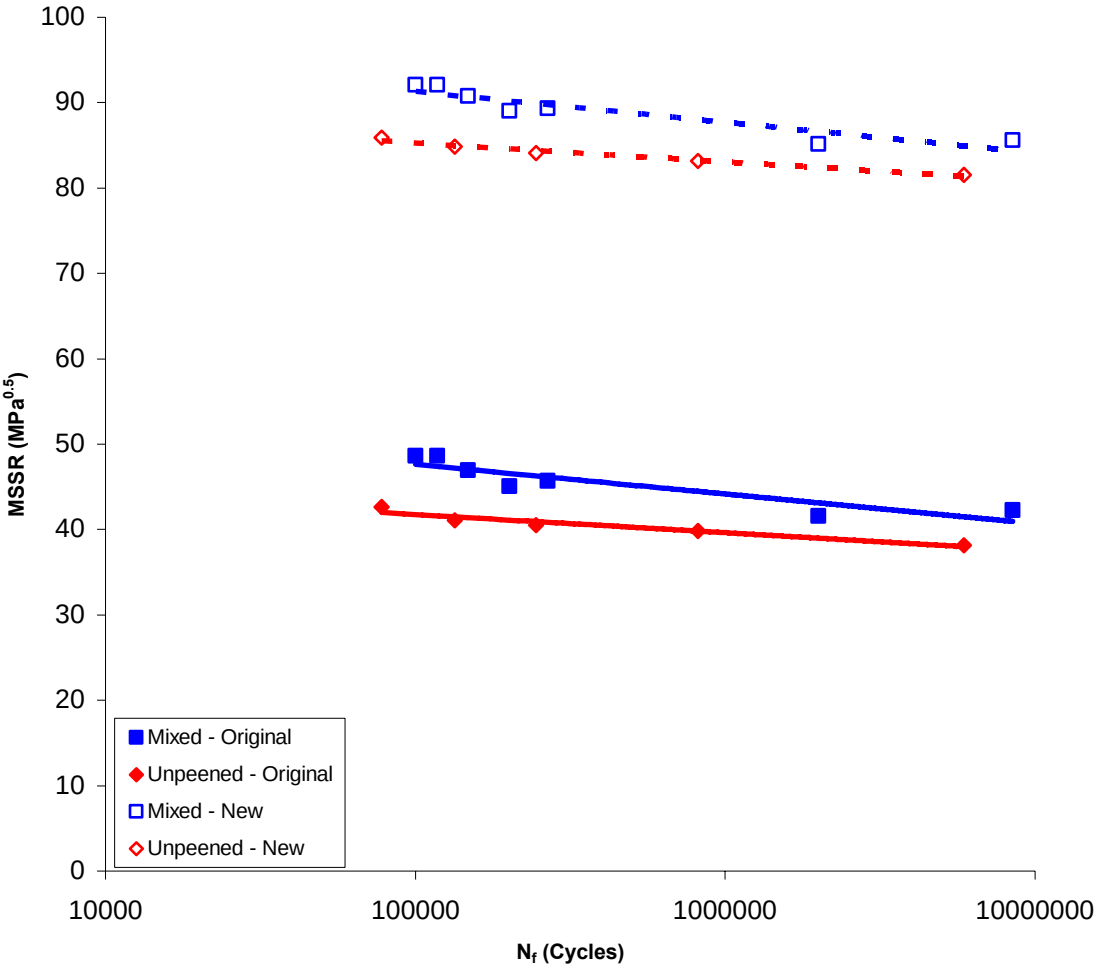

Figure 55. MSSR versus N_f for Mixed Relaxation Case and Unpeened Case (Iteration B)

Note:

	Original	New
A	0.75	8.00
B	0.50	0.25
C	0.75	8.00
D	0.50	0.25

Table 1. Summary of Experimental Results

Test #	*Shot Peened (Almen)*	σ_{max} *(MPa)*	σ_{min} *(MPa)*	$\Delta\sigma$ *(MPa)*	σ_{eff} *(MPa)*	Q_{max} *(N)*	Q_{min} *(N)*	N_f *(cycles)*	f_{FEA}
1	7A	900	27	873	887.75	2403.95	-1369.75	147907	0.75
2	7A	800	24	776	789.11	2017.86	-1277.86	201093	0.75
3	7A	1000	30	970	986.39	2868.04	-1215.46	100504	0.75
4	7A	650	19.5	630.5	641.15	1884.04	-679.384	8,400,000+	0.75
6	12A	800	24	776	789.11	1993.22	-1216.25	358,252	0.75
9	12A	900	27	873	887.75	1623.62	-1050.83	267,474	0.75
10	12A	700	21	679	690.47	1098.67	-758.014	2,000,399	0.75
11	12A	1000	30	970	986.39	2891.34	-1201.02	117,562	0.75
@13	Unpeened	950	28.5	921.5	937.07	898.63	-706.73	77,937	0.45
@14	Unpeened	850	25.5	824.5	838.43	1 225.67	- 1 028.96	134,103	0.45
@15	Unpeened	800	24	776	789.11	1 139.75	-1 081.67	245,000	0.45
@16	Unpeened	750	22.5	727.5	739.79	788.98	- 773.46	815,449	0.45
@17	Unpeened	650	19.5	630.5	641.15	543.86	- 643.44	5,900,000+	0.6

Note:
@ Data from Madhi's Tests [19]

Table 2. Summary of Maximum MSSR with Full (100%R) Relaxation (0% Residual Stress)

Test #	*MSSR ($MPa^{0.5}$)*	*SSR =$\Delta\tau$ (MPa)*	*τ_{eff} (MPa)*	*θ (deg)*	*$R_{\Delta\tau}$*	*σ_{max} (MPa)*	*σ_{min} (MPa)*	*Crack initiation depth (μm)*	*Crack initiation location (x/a_{max})*
1	46.97	1089.76	975.76	38.30	-0.22	984.94	-260.77	0	0.96
2	45.09	1016.72	903.78	38.30	-0.24	903.45	-255.09	0	0.95
3	48.60	1120.57	1028.48	38.50	-0.17	1071.54	-217.86	0	0.92
4	42.27	812.75	764.01	38.40	-0.12	825.05	-124.39	0	0.95
6	45.09	1016.72	903.78	38.30	-0.24	903.45	-255.09	0	0.95
9	45.71	1012.06	921.32	39.00	-0.19	935.83	-208.36	0	0.94
10	41.61	840.05	770.77	38.40	-0.17	768.45	-159.31	0	0.93
11	48.63	1117.84	1027.33	38.50	-0.17	1075.39	-214.66	0	0.92
[@]13	42.66	880.24	834.60	49.70	-0.10	783.17	-199.36	0	0.92
[@]14	41.09	837.90	756.56	46.40	-0.20	744.40	-148.20	0	0.99
[@]15	40.50	796.12	756.44	47.90	-0.19	733.68	-166.83	0	0.98
[@]16	39.82	764.14	711.63	48.80	-0.14	697.60	-191.75	0	0.97
[@]17	38.16	677.31	624.92	48.00	-0.16	670.16	-156.47	0	0.97

Note:
[@] Data from Madhi's Tests [19]

Table 3. Summary of Maximum MSSR with Mixed Relaxation

Test #	*MSSR* ($MPa^{0.5}$)	*SSR=*$\Delta\tau$ *(MPa)*	τ_{eff} *(MPa)*	θ *(deg)*	$R_{\Delta\tau}$	σ_{max} *(MPa)*	σ_{min} *(MPa)*	*Crack initiation depth* (μm)	*Crack initiation location* (x/a_{max})
1	46.97	1089.76	975.76	38.30	-0.22	984.94	-260.77	0	0.93
2	45.09	1016.72	903.78	38.30	-0.24	903.45	-255.09	0	0.94
3	48.60	1120.57	1028.48	38.50	-0.17	1071.54	-217.86	0	0.92
4	42.27	812.75	764.01	38.40	-0.12	825.05	-124.39	0	0.95
6	45.09	1016.72	903.78	38.30	-0.24	903.45	-255.09	0	0.94
9	45.71	1012.06	921.32	39.00	-0.19	935.83	-208.36	0	0.95
10	41.61	840.05	770.77	38.40	-0.17	768.45	-159.31	0	0.96
11	48.63	1117.84	1027.33	38.50	-0.17	1075.39	-214.66	0	0.92

7 Summary Conclusions, and Recommendations

7.1 Summary

Fretting fatigue is an important phenomenon to consider in the development of components which undergo high-cycle fatigue, like turbine engines. It is important to study other alloys and metals in efforts to make improvements on the present designs. Currently, not much work has been done on testing the fretting fatigue of IN 100, or the possible benefits of shot-peening on its fretting fatigue life. Therefore, a better understanding of fretting fatigue of shot-peened IN100 and how varying shot-peening intensity affects the fretting fatigue behavior is needed. This, in turn, can help engineers to better account for its effects. The main objective of this study was to investigate the effects of shot-peening intensity on fretting fatigue behavior of IN100.

Eleven fretting fatigue tests on specimens shot-peened with 7A and 12A intensities were conducted. The thickness for all specimens was 6.35 mm. X-ray diffraction method was used to measure residual stress values for fretting fatigue tests. Fretting fatigue tests were conducted over a wide range of maximum stresses σ_{max} = 650 to 1000 MPa with stress ration of R = 0.03. These stresses were applied by a computer-controlled uni-axial servo-hydraulic test machine, using a peak valley compensator to reduce the variation between control and feedback signals. Applied load outputs were monitored and recorded continuously until specimens fractured into two pieces, and induced tangential loads were determined as the half of difference between lower axial load and upper axial load. These experimental load outputs were then utilized as the load inputs for FEA modeling.

The determination of crack initiation location for the specimens was then utilized for the appropriate superimposing of residual stress into SSR and MSSR calculations. Also, the crack initiation locations and orientations were used to verify the applicability of SSR and MSSR predictions on crack initiation mechanism.

Since the infinite half space assumption was violated in this study, analytical solutions were no longer valid, and FEA, a numerical method that does not require the infinite half-space assumption to be satisfied, was necessary. The commercially available software, ABAQUS, was used for computing FEA in this study. For all simulations, the experimental contact load was always applied as the first step to prohibit the event of gross slip conditions. This was followed by the application of the measured maximum axial load as the second step. After step 2, the load sequence was applied based on the experimental peak/valley values and frequencies. The static coefficient of friction was chosen as a constant, 0.75, for all tests. The validation of the FEA model was accomplished by comparison with the Ruiz solutions for contact half-width, stress profiles and Hertzian peak pressure value.

A shot-peening process introduced residual stresses into peened specimens. These stresses were compressive near the peened surface and tensile after some depth within the interior. 7A and 12A specimens had relatively close compressive residual stress value at the surface, but location and value of the maximum tensile residual stress was different, the 7A specimen had a greater tensile residual stress than the 12A specimen. However, the 12A specimen did have a deeper effect, in that the compressive residual stresses remained higher for a greater depth. During fretting cycles, residual stress was subjected to relaxation, which was 0% before applying fretting fatigue cycles

and 100% after a specimen broke into two pieces at failure location. This relaxation could occur uniformly across a given depth. However, the correlation between relaxation rates and fretting fatigue life is still unclear.

Four fatigue parameters: the stress range, effective stress, SSR and MSSR were investigated for their effectiveness on predictions on fatigue life and crack initiation mechanisms. The stress range and the effective stress parameters were formulated based on global applied axial loads and did not take into account the effect of residual stress as well as local stress distribution. The critical plane-based fatigue parameter, SSR, incorporates the influence from residual stress and contact stress. However, SSR was not greatly affected when accounting for residual stresses. SSR was discussed about its fretting fatigue mechanism predictions including fatigue life, crack initiation location, and orientation. The critical plane-based fatigue parameter, MSSR, incorporates the influence from residual stress and contact stress, which is more fitting, since fretting fatigue configuration introduced a non-uniform stress distribution near a contact region. MSSR was greatly affected by the influence of residual stresses. It was for this reason that MSSR was determined to be the better parameter for fretting fatigue life predictions. MSSR was also discussed about its fretting fatigue mechanism predictions including fatigue life, crack initiation location, and orientation.

A mixed relaxation case for MSSR was also discussed. This constituted of the levels between the contact surface and a depth = 75μm to have 100%R and levels deeper than 75μm to have 0%R. This relaxation case was the actual representation to what residual stresses were.

The effects of adjusting the MSSR fitting constants were also investigated. It was found that this change did not have an adverse effect on the MSSR versus N_f trends. Therefore, it would be possible to adjust the constants to fit unpeened and peened samples together on one trend. However, after much iteration, no progress could be made to unify the two trends. This may be due to peened specimens having been plastically-deformed on the surface and unpeened specimens remaining unchanged, and hence they were two different types of material which did not act in the same way under fretting fatigue conditions.

7.2 Conclusions

1. Shot-peening had minimal effects, in this study, on the fretting fatigue life of IN100. Shot-peening intensity also had minimal effects on fretting fatigue life.
2. The residual stresses induced by shot-peening were probably negated early in the fatigue life.
3. Based on the effective stress and stress range values, there was no difference between shot-peening intensities or shot-peened versus unpeened specimens for fatigue life. However, since these parameters do not take into account the shear stresses that occur in fretting fatigue, they are not the best parameters for predicting fretting fatigue life.
4. Based on SSR and MSSR, there was an increase in life for shot-peened specimens when compared to unpeened. However, there was minimal difference between the two shot-peening intensities.
5. Based on the SSR and MSSR calculations, cracks initiated near the trailing edge in all fretting fatigue tests. For all cases, cracks occurred at the contact surface.

6. Residual stresses had a significant effect on the MSSR values for the different relaxation states.
7. Under fretting fatigue configuration with alternating axial loads applied, the maximum stress concentration for σ_{xx} was noticed to occur near the trailing edge, and the σ_{yy} stress distribution was no longer symmetric with respect to the center of a contact zone.
8. Even though MSSR fitting constants can be safely adjusted to fit peened and unpeened cases to one trend without any adverse effects to the trends, they cannot be unified. This may be because the plastically-deformed peened is now different from the untainted specimens.

7.3 Recommendations for Future Work

This study investigated the effect of shot-peening on the fretting fatigue life of the nickel alloy IN 100. Since 7A and 12A shot-peening did not seem to have a significant effect on the fatigue life of IN100, a stronger intensity might be considered to improve performance. Also, other surface treatments, such as laser-peening, might be employed to try to improve the fatigue life.

Also, fractured specimens should be further inspected using microscopy to determine the experimental crack orientations and locations. Since IN100 has magnetic properties, an alternative to scanning-electron-microscopy must be found, or to discover a way to negate the magnetic properties of IN100 to use SEM.

MSSR is not a good parameter for predicting fretting fatigue life for both peened and unpeened specimens simultaneously under a unified trend. Therefore, other parameters and their potential applicability in this field should be studied.

Bibliography

1. Albinali, S. "Effects of Temperature and Shot-Peening Intensity on Fretting Fatigue Behavior of Titanium Alloy Ti-6Al-4V." MS Thesis AFIT/GAE/ENY/05-M25. Air Force Institute of Technology (AU), Wright-Patterson AFB OH, March 2005.

2. Allen, W.Y. "Fretting Fatigue Behavior of Shot-peened Titanium Alloy Ti-6Al-4V under Seawater Conditions," MS Thesis, AFIT/GAE/ENY/04-J01, Air Force Institute of Technology (AU), Wright-Patterson AFB OH, June 2004.

3. Bhadeshia, H.K.D.H. "Nickel Based Superalloys." Cambridge, UK: University of Cambridge, 2003. http://www.msm.cam.ac.uk/phase-trans/2003/Superalloys/superalloys.html. 14 February 2006.

4. Chan, K. and Lee, Y. Ruiz Program, South West Research Institute, Personal Communication, 1998.

5. Fellows, L., Nowell, D., and Hills, D. "Contact Stresses in a Moderately Thin Strip," Wear, 185: 235-238 (1995).

6. Fellows, L.J., Nowell, D., D.A. Hills. Wear 185: 235-8 (1995).

7. Findley, W.N."Fatigue of Metals under Combination of Stresses," Trans ASME, 79: 1337-48 (1975).

8. Hills, D. and Nowell, D. Mechanics of Fretting Fatigue, Kluwer Academic Publishers, Netherlands, 1994.

9. Hills, D.A. and Nowell, D. "A Discussion of: Peak Contact Pressure, Cyclic Stress Amplitude, Contact Semi-width and Slip Amplitude: Relative Effects on Fatigue Life", International Journal of Fatigue, 23: 747-748 (2001).

10. Iyer, K. "Peak Contact Pressure, Cyclic Stress Amplitudes, Contact Semi-width and Slip Amplitude: Relative Effects on Fretting Fatigue Life," International Journal of Fatigue, 23:193-206 (2001).

11. Iyer, K. and Mall, S. "Analysis of Contact Pressure and Stress Amplitude Effects on Fretting Fatigue Life," Journal of Engineering Materials and Technology, 123:85-93 (January 2001).

12. Iyer, K. and Mall, S. "Effects of Cyclic Frequency and Contact Pressure on Fretting Fatigue under Two-level Block Loading," Fatigue Fract. Engng. Mater.

Struct., 23: 335-346 (2000).

13. Jutte, A.J. ”Effect of a Variable Contact Load on Fretting Fatigue Behavior of Ti-6Al-4V,” Thesis, Air Force Institute of Technology, Wright-Patterson Air Force Base, Ohio, 2004.

14. Lee, C. “Effects of Variable Contact Load on Fretting Fatigue Behavior of Shot-peened and Un-peened Titanium Alloy,” MS Thesis AFIT/GAE/ENY/04-D01. Air Force Institute of Technology, Wright-Patterson AFB OH, December 2004.

15. Lee, H., Mall, S.. “Stress Relaxation Behavior of Shot-peened Ti-6Al-4V under Fretting Fatigue at Elevated Temperature,” Materials Science and Engineering A366: 412-420 (2004).

16. Lee, H.,Jin, O., and Mall, S.. “Fretting Fatigue Behavior of Shot-peened Ti-6Al-4V at Room and Elevated Temperature,” Fatigue Fract Engng Master Struct, 26: 1-12 (2003).

17. Lykins, C.D., Mall, S., and Douglas. “An Investigation of Fretting Fatigue Crack Initiation Behavior of the Titanium Alloy Ti-6Al-4V,” PhD. dissertation, University of Dayton, December 1999.

18. Lykins, C.D., Mall, S., and Jain, V.K. “An Evaluation of Parameters for Predicting Fretting Fatigue Initiation,” Int J fatigue, 22: 703-16 (2000).

19. Madhi, E. “Effects Fretting Pad Radius on Fretting Fatigue Behavior of IN 100,” MS Thesis AFIT/GAE/ENY/06-M22. Air Force Institute of Technology (AU), Wright-Patterson AFB OH, March 2006.

20. Mall, S., Jain, V.K., Namjoshi, S., and Lykins, C.D. ”Fretting Fatigue Crack Initiation Behavior of Ti-6Al-4V,” Standard Technical publication 1425, ASTM International (2003).

21. Martinez, S. A., Sathish, S., Blodgett, M. P., Namjoshi, S. and Mall, S. “Residual Stress Relaxation due to Fretting Fatigue in Shot-peened Surfaces of Ti-6Al-4V,” American Institute of Physics, 1531-1537 (2003).

22. Martinez, S.A. “Quantitative Characterization of Fretting Fatigue Damage in Shot-peened Ti-6Al-4V,” Thesis, University of Dayton, Dayton, Ohio (August 2004).

23. Namjoshi, S., Jain, V. K., Mall, S. “Effects of Shot-peening on Fretting Fatigue Behavior of Ti-6Al-4V,” Transactions of the ASME, 124: 222-228 (April 2002).

24. Namjoshi, S.A., Mall, S., Jain, V.K., and Jin, O. “Effects of Process Variables on Fretting Fatigue Crack Initiation in Ti-6Al-4V,” Journal of Strain Analysis, 37, No.6: 535-542 (2002).

25. Namjoshi, S.A., Mall, S., Jain, V.K., and Jin, O. “Fretting Fatigue Crack Initiation Mechanism in Ti-6Al-4V,” Fatigue Fract Engng Master Struct, 25: 955-964 (2002).

26. Neu, R., Pape, J., and Swalla-Michaud, D. “Methodologies for Linking Nucleation and Propagation Approaches for Predicting Life under Fretting Fatigue”, Fretting Fatigue: Current Technology and Practices, ASTM 1367, D. Hoeppner, V. Chandrasekaran and C. Elliot, Eds. American Society for Testing and Materials.

27. "Nickel and Cobalt Alloys." Aerospace Specification Metals, Inc. n. pag. http://www.aerospacemetals.com/nickel_alloy.html. 14 February 2006.

28. "Nickel and Nickel Alloys." *Key to Metals*. n. pag. http://www.key-to-metals.com/Article9.htm. 14 February 2006.

29. Sabelkin, V., Martinez S.A., Mall, S., Sathish, S., and Blodgett, M.P. “Effects of Shot peening Intensity on Fretting Fatigue Crack Initiation Behavior of Ti-6Al-4V,” Department of Aeronautics and Astronautics, Air Force Institute of Technology, Wright Pattern Air Force Base, Ohio, in press.

30. Smith, K., Watson, P., and Topper, T. “A Stress Strain Function for the Fatigue of Metals,” Journal of Materials, JMLSA, 5, No. 4: 767-778 (1970).

31. Szolwinski, M., and Farris, T. “Mechanics of Fretting Fatigue Crack Formation”, Wear, 93-107 (1996).

32. Walker, K. “The Effect of Stress Relation during Crack Propagation and Fatigue for 2024-T3 and 7075-T6 Aluminum,” Presented to subcommittee E-9V Winter Meeting (Feb 1969).

33. Walker, K. “The Effective Stress Ratio during Crack Propagation and Fatigue for 2024-T3 and 7075-T6 Aluminum,” In: Effects on Environment and Complex Load History on Fatigue Life. Philadelphia (PA): American Society for Testing and Materials, 1-14 (1970).

34. Waterhouse, R.B. “Fretting Fatigue,” International Materials review, 37: 77-97 (1992).

35. Wharton, M.H., and Waterhouse, R.B. “Environmental Effects in the Fretting Fatigue of Ti-6Al-4V,” Wear, 62:287-297 (1980).

36. Yuksel, H. I. “Effects of Shot-peening on High Cycle Fretting Fatigue Behavior of Ti-6Al-4V,” MS Thesis AFIT/GAE/ENY/02-12. Air Force Institute of Technology (AU), Wright-Patterson AFB OH, December 2002.

Vita

2d Lt Jonathan Ng graduated with honors from River Dell Regional High School in Oradell, New Jersey. He attended Carnegie Mellon University, in Pittsburgh, Pennsylvania, for his undergraduate studies, where he graduated with honors with a double major in Chemical Engineering and Engineering and Public Policy in 2004. He was commissioned as a second lieutenant in the United States Air Force through Detachment 730 AFROTC, University of Pittsburgh.

His first assignment was at the National Air and Space Intelligence Center (NASIC) at Wright-Patterson Air Force Base, Ohio, as a developmental engineer. Almost immediately after arriving at NASIC, he was selected to attend the Graduate School of Engineering and Management, Air Force Institute of Technology, under the Watson Scholar Initiative. Upon graduating with a Master of Science degree in Aeronautical Engineering, he will triumphantly return to NASIC to resume his position as developmental engineer for a three-year tour of duty.

REPORT DOCUMENTATION PAGE

Form Approved
OMB No. 074-0188

1. REPORT DATE *(DD-MM-YYYY)*	**2. REPORT TYPE**	**3. DATES COVERED** *(From – To)*
23-03-2006	**Master's Thesis**	Sep 2004 – Mar 2006

4. TITLE AND SUBTITLE

Fretting Fatigue Behavior of Shot-Peened IN 100

5a. CONTRACT NUMBER

5b. GRANT NUMBER

5c. PROGRAM ELEMENT NUMBER

6. AUTHOR(S)

Ng, Jonathan, L., Second Lieutenant, USAF

5d. PROJECT NUMBER

5e. TASK NUMBER

5f. WORK UNIT NUMBER

7. PERFORMING ORGANIZATION NAMES(S) AND ADDRESS(S)
Air Force Institute of Technology
Graduate School of Engineering and Management (AFIT/EN)
2950 Hobson Way
WPAFB OH 45433-7765

8. PERFORMING ORGANIZATION REPORT NUMBER

AFIT/GMS/ENY/06-M01

9. SPONSORING/MONITORING AGENCY NAME(S) AND ADDRESS(ES)
AFRL/MLLP
Attn: Mr. Mark P. Blodgett
2230 Tenth St. Suite 1, Bldg 655
WPAFB, OH DSN: 785-9799

10. SPONSOR/MONITOR'S ACRONYM(S)

11. SPONSOR/MONITOR'S REPORT NUMBER(S)

12. DISTRIBUTION/AVAILABILITY STATEMENT
APPROVED FOR PUBLIC RELEASE; DISTRIBUTION UNLIMITED.

13. SUPPLEMENTARY NOTES

14. ABSTRACT

The fretting fatigue behavior of shot-peened of IN 100 was investigated in this study. S-N curves were obtained for two different shot-peened intensities (7A and 12A) and were compared to those of unpeened specimens. Stress relaxation behavior under fretting fatigue was also investigated after their measurements were obtained using the X-ray diffraction method. The crack initiation location and the crack angle orientation along the surface were determined using optical and scanning electron microscopy (SEM). Cracks initiated near the trailing edge and on the contact surface for both 7A and 12A shot-peened specimens. Finite element analysis was performed using commercially available software, ABAQUS, to obtain contact region state variables such as stress, strain and displacement. These state variables were needed for the computation of fretting fatigue parameters, such as stress range, effective stress, shear stress range (SSR) and modified shear stress range (MSSR), which were further analyzed. It was found that there was relaxation of residual compressive stress during fretting fatigue up to a certain depth. The effects of shot-peening were negated relatively early in the fretting fatigue life. There was little difference in fretting fatigue life between the two intensities of shot-peening, but there was an improvement in relation to unpeened specimens. Also, the MSSR parameter, a critical plane based fatigue parameter, was effective in characterizing the fretting fatigue behavior in terms of fatigue life, crack initiation location and orientation. However, it is not applicable to both shot-peened and unpeened cases simultaneously to yield a single trend. This may be due to the peened specimens having been plastically-deformed on the surface and the unpeened specimens remain unchanged, and hence they were two different types of material which did not to act the same way under fretting fatigue conditions.

15. SUBJECT TERMS
Fatigue Tests (Mechanics), Fretting, Shot peening, Nickel Alloys, Finite Element Analysis, Residual Stress

16. SECURITY CLASSIFICATION OF:			**17. LIMITATION OF ABSTRACT**	**18. NUMBER OF PAGES**	**19a. NAME OF RESPONSIBLE PERSON**
REPORT	ABSTRACT	c. THIS PAGE			Shankar Mall, Civ, USAF (ENY)
U	**U**	**U**	**UU**	134	**19b. TELEPHONE NUMBER** *(Include area code)* (937) 255-3636, ext. 4587; e-mail: Shankar.Mall@afit.edu

Standard Form 298 (Rev: 8-98)
Prescribed by ANSI Std. Z39-18